Journal of Drug Delivery Science and Technology 67 (2022) 102956

Contents lists available at ScienceDirect

Journal of Drug Delivery Science and Technology

journal homepage: www.elsevier.com/locate/jddst

Bentonite clay incorporated topical film formulation for delivery of trimetazidine: Control of ocular pressure and in vitro-in vivo correlation

Rakesh Swain [a], Souvik Nandi [a], Rudra Narayan Sahoo [a,b], Shasank Sekhar Swain [c], Sujata Mohapatra [a], Subrata Mallick [a,*]

[a] Department of Pharmaceutics, School of Pharmaceutical Sciences, Siksha 'O' Anusandhan (Deemed to be University), Bhubaneswar, 751003, Odisha, India
[b] Centurion University of Technology and Management, Odisha, India
[c] Division of Microbiology & NCDs, ICMR-Regional Medical Research Centre, Chandrasekharpur, Bhubaneswar, 751023, Odisha, India

ARTICLE INFO

Keywords:
Trimetazidine
Bentonite clay-based film
Topical delivery
In vitro-In vivo correlation
Molecular docking

ABSTRACT

Bentonite clay based film formulation has been prepared for topical delivery of trimetazidine (TZ) for the control of ocular pressure. Trimetazidine ophthalmic film formulation has been prepared incorporating bentonite at 1: 0.0001 to 1: 0.00005 ratio in hydroxylpropyl methylcellulose (HPMC) matrix by solvent casting method. Film formulation showed controlled release of drug and thereby extending the ophthalmic permeation for more than 6 h. Permeation has been extended with the decrease of bentonite amount in the film. Sustained trimetazidine delivery has been characterized by the area under the decreased intraocular pressure (IOP) versus time curve after topical administered film formulation. In rabbits treated with film formulation TB3, the peak IOP dropped of almost 30% from the baseline at 240 min and persisted until 360 min and a good in vitro-in vivo correlation has also been established. The matrix formulation containing bentonite has shown higher negative biding energy values compared to the formulation without containing bentonite indicating stable interaction with improved bioavailability and sustained effect. Bentonite incorporated trimetazidine film formulation could be utilised in the control and management of intraocular pressure in rabbit.

1. Introduction

Open angle glaucoma is associated with increased intraocular pressure (IOP), resulting in retinal ganglionic cell loss and visual field damage [1]. Endothelin −1 (Et-1) is synthesized and secreted in a three to four times higher in the aqueous humour compared to healthy human plasma [2]. ET-1 participates in IOP regulation by constricting the trabecular meshwork contractility. Thus, elevated intraocular pressure due to increased level of ET-1 in aqueous humour is the most common cause of glaucoma [3]. Glucocorticoids increased the release of Endothelin −1 resulting in the increased ocular hypertension due to amplified level in the humour of the eye [4,5]. In another experiment increased IOP was observed in rabbit model by laser trabeculoplasty [6]. Endothelin −1 receptor antagonist (Avosentan) was found to cause some sort of ocular side effects after topical application [7]. Trimetazidine, comes under a class of metabolic modulator and is commonly used as anti-anginal agent [8]. Trimetazidine has been reported to improve vascular endothelial function in a patient with chronic heart failure [9] and microvascular angina [10] by significantly decreasing the serum ET-1 level. The inhibition of ET-1 by trimetazidine may be possible due to the protection of endothelial cells. The effect of topical administration of trimetazidine ocular film on IOP has not been reported yet.

The normotensive rabbit model is the most often used preclinical animal model for demonstrating medication effectiveness in reducing IOP prior to regulatory approval [11]. Trimetazidine dihydrochloride has a short elimination half life of 3–4 h which leads to repeated administration (2–3 times daily) leading to lesser patient compliance [12,13].

Mucoadhesive polymeric hydrogel is gaining very importance in the ocular drug delivery system nowadays [14]. Hydroxypropyl methylcellulose (HPMC) is a biocompatible, non-toxic and biodegradable polymer that forms hydrogels and is widely utilised in mucoadhesive ocular drug delivery [15].

Bentonite is a phyllosilicate group of mineral containing principally montmorillonite. Na pre-treated bentonite has high swelling and gelling properties [16] and is suitable for cell attachment [17,18]. Because of

* Corresponding author. School of Pharmaceutical Sciences, Siksha O Anusandhan (Deemed to be University), Bhubaneswar, 751003, Odisha, India.,
E-mail addresses: profsmallick@gmail.com, subratamallick@soa.ac.in (S. Mallick).

https://doi.org/10.1016/j.jddst.2021.102956
Received 30 July 2021; Received in revised form 23 October 2021; Accepted 29 October 2021
Available online 7 November 2021
1773-2247/

the tortuous diffusion routes of silicate based polymer nanocomposites, they have high barrier characteristics and can be used to apply to produce sustained drug release application [19]. Na-bentonite incorporated trimetazidine ocular film has been developed for the control of ocular pressure on normotensive rabbit eye model.

2. Materials and methods

2.1. Animal

Nine white New Zealand rabbits (1.5–2.5 Kg) free from ocular abnormalities, including glaucoma, were used in this study. This study was approved by IAEC (Institutional animal ethics committee) with protocol no IAEC/SPS/SOA/21/2019. Animals were housed in the animal house of the School of pharmaceutical sciences Redg no.1171/PO/RE/S/08/CPSEA under-maintained standardized condition (12 h light-dark cycle), regulated air temperature (15–21 °C) and good ventilation. The animals were fed standard feed and had free access to water.

2.2. Materials

The active compound trimetazidine dihydrochloride was collected from Medley Research Center (Mumbai, Maharashtra), Hydroxylpropyl methylcellulose (HPMC K 15 M) was purchased from Burgoyne and Co (Mumbai, India). Bentonite, triethanolamine and NaCl were purchased from HIMEDIA (Mumbai, India), SRL Pvt. Ltd. Mumbai, Merck Pvt Ltd (Maharashtra India) respectively. Other reagents used were of analytical grade.

2.3. Fabrication of trimetazidine ocular film

2.3.1. Treatment of bentonite

Pre-treatment of the bentonite was performed after dispersing bentonite (100 gm/L: solid/liquid ratio) into 0.2 mol/L NaCl solution and shaking at 200 rpm for 12–15 h. Bentonite was washed 5–6 times with double distilled water through centrifugation for removing excess chloride ions. Removal of chloride in the washings was confirmed by silver nitrate testing. Remaining bentonite slurry was dried immediately in a hot air oven at 60 °C and the dried sodium bentonite was preserved in a closed container till used for film preparation [20–22].

2.3.2. Ocular film formulation

Bentonite was dispersed (1% wt/vol) in double distilled water and continuously stirred at room temperature for 24 h. The bentonite dispersion was transferred in a separating funnel and allowed to stand for overnight period for settling of larger particles. The upper layer dispersion was collected carefully and centrifuged (2500 rpm) for 30 min. Then the upper thin dispersion was cautiously removed and used to prepare the film [23]. The film was prepared by casting and solvent evaporation method. Swelling of HPMC K 15 M was done in presence of little amount of water and placing in the refrigerator for overnight period of about 12 h. The swelled gel was stirred magnetically for about 3 h and the thin bentonite dispersion was added into it with continuous stirring for another 24 h. Trimetazidine and triethanolamine were dissolved in a tiny quantity of water and added to the bentonite-HPMC dispersion and stirred for about 2 h. Then the prepared hydrogel was poured uniformly on a petri plate (Tarsons, diameter: 90 mm) and left for drying at 40 °C in an incubator for 24 h until constant weight was achieved. Folding endurance was conducted by folding a peace of film repeatedly at the same position up to 200 times or till it was broken. The surface pH of the film was measured by dipping the pH meter's glass electrode inside the swelled portion of the film formulation.

2.4. FTIR

The KBr disk technique was used to perform FTIR analysis on pure drug, bentonite, and produced films in an FTIR spectrophotometer (JASCO FTIR-4100, Japan).

2.5. Calorimetry analysis

DSC analysis of trimetazidine and the films were carried out by differential calorimeter (DSC-1, Mettler Toledo; Software- Star E, SNR-18289) within a range of 30–300 °C in a constant heating rate of 10 °C/min under continuous nitrogen purge (50 ml/min).

2.6. X-ray diffraction

Diffraction patterns of pure trimetazidine, bentonite and the prepared films were performed by X-ray powder diffraction (Model: Rigaku, Ultima IV). For X-ray source, K-Alpha anode has been used with a voltage of 40Kv and 15 mA current. The scanning was done in the 2Θ range of 5–70° with a scanning speed of 1° per min.

Scanning electron microscopy.

For surface morphology visualization, SEM analysis has been done. Pure powdered drug and films were sputter coated with platinum for 60 s in a vacuum chamber followed by SEM analysis by applying a voltage of 5–15 kv (Model: JEOL JSM-6510).

2.7. In-vitro release study

Prepared trimetazidine films were cut into suitable pieces (2–4 cm^2), weighed and glued to the glass slides by using cyanoacrylate adhesive and dipped into the dissolution vessels containing phosphate buffer (200 ml, pH 7.4) in a USP type II dissolution tester (Electrolab, TDT06L, India). The paddle agitation was fixed to 50 rpm with the temperature at 34.0 ± 2 °C. Samples were withdrawn at a preset time interval and estimated spectrophotometrically at λ_{max} 269 nm after filtering through a 0.45 μm syringe driven filter.

2.8. Ex vivo corneal permeation study

Fresh goat eye balls were procured from slaughter house within an hour after sacrifice and washed properly with distilled H_2O followed by phosphate buffer pH 7.4. The cornea along with an attached 5–6 mm broad sclera ring were removed from the whole goat eye. After placing a pre-weighed circular film to the centre of the epithelial cornea and positioning it in the diffusion chamber with an effective surface area of 1.56 cm^2 facing the donor compartment. The diffusion media (phosphate buffer, pH 7.4, 200 ml) was put in the receptor compartment. The corneal permeation was kept going for 6 h at 34 ± 2 °C under steady agitation of 50 rpm 10 ml of samples were withdrawn as predetermined time and filtered through a 0.45 μm membrane filter and assayed by Ultra-Violet visible spectrophotometer (JASCO V-630 spectrophotometer, Software: Spectra Manager) at 269 nm. The experiment was performed triplicate and mean ± sd were calculated.

2.9. Kinetics

There were different kinetics models were used in previous reports to understand the mechanism of drug release and permeation [14,15] from polymeric formulations. The Higuchi and Korsmeyer-Peppas equation was used to calculate the kinetics of percentage release and quantity penetration of trimetazidine dihydrochloride in the presence of bentonite.

Higuchi:

$$Q = K_H \times \sqrt{t}$$

Korsmeyer–Peppas

$$\frac{M_t}{M_\infty} = K_P\, t^n$$

Q = Cumulative amount of drug release, K_H = Higuchi release rate constant/permeation rate constant, M_t = Amount of trimetazidine release/permeation at time t, M_∞ = maximum amount of trimetazidine available to release/permeation, K_P = parameter reflecting the structural and geometrical characteristics of the delivery device, or Peppas release/permeation rate constant, n = power law exponent, or release/permeation exponent.

The n value reflects drug release/permeation as regulated by Fick's laws and confirmed by Higuchi model. Both the Higuchi and Korsmeyer-Peppas equations were used to calculate the rate constants (K_H and Kp) of dissolution and permeation, as well as the coefficient of determination (r^2).

The differences in permeability coefficients between the control category of film without bentonite and the other categories of film with bentonite were investigated using one-way analysis of variance (ANOVA) in XLSTAT 2021 and the statistical significance was determined by a p value of less than 0.05. A double-sided Dunnett's analysis was used to compare the control (TB0) to the other films (TB1, TB2, TB3, TB4, TB5).

2.10. IOP experimental protocol

The rabbits were allocated into three groups (3 rabbits each) for studying the effect of topically applied trimetazidine drop, TZ film formulation with bentonite (TB3) and without bentonite (TB0) on the normal IOP, respectively. The rabbits were kept in a restriction cage for IOP measurements. 30 min before starting the experiment, rabbits were anaesthetized with 0.5% tetracaine HCl (0.75 mg in 150 μl) and a control or zero time value of IOP was recorded. One drop of freshly prepared TZ was instilled in the middle of the inferior conjunctival sac, followed by lid closure. In another two groups, TZ films (TB0 and TB3) were

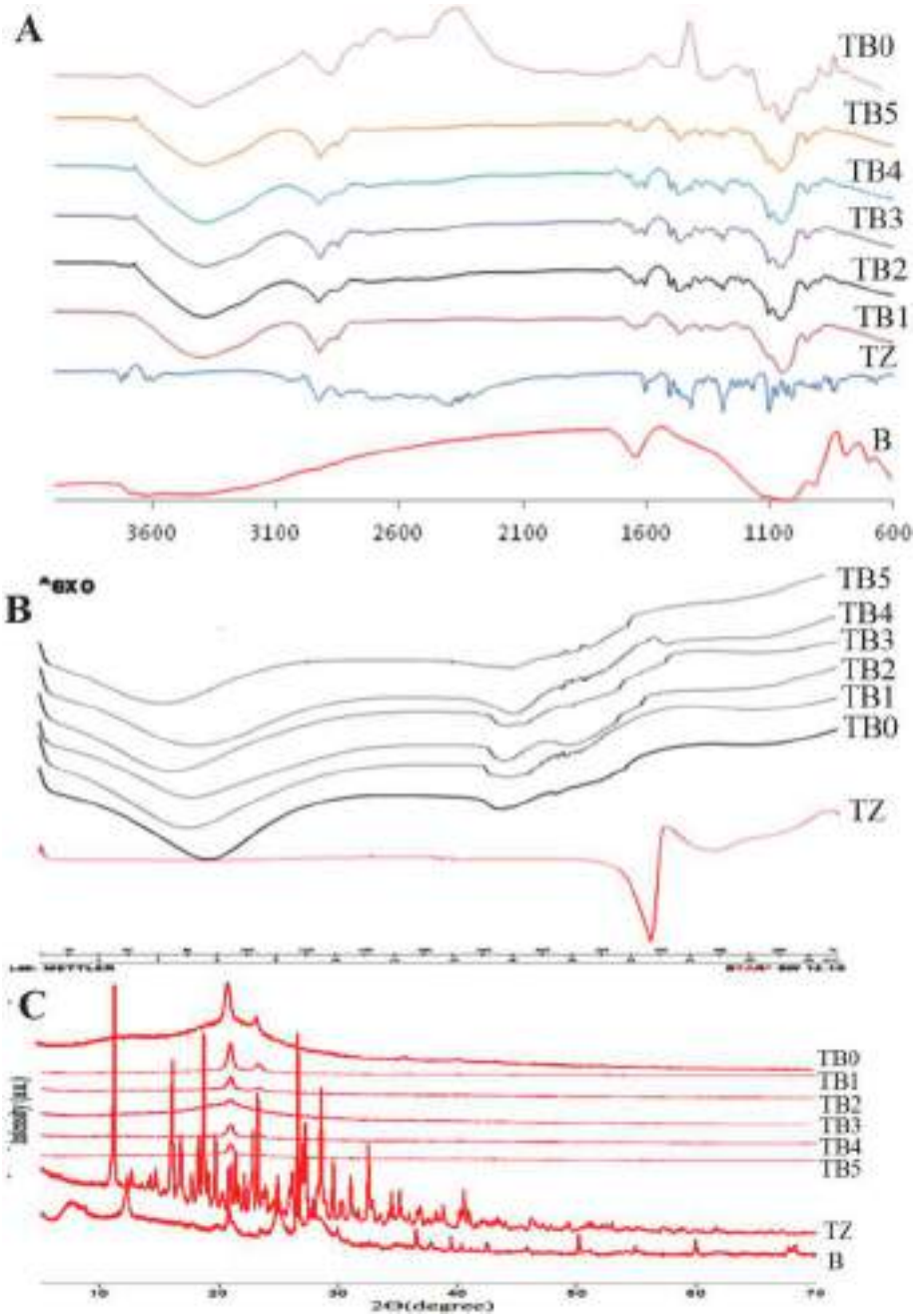

Fig. 1. (A) FTIR spectrograms (B) DSC thermogram (C) XRD pattern of trimetazidine dihydrochloride and film formulation.

applied into the cul-de-sac region of the rabbit eye shown in Fig. 4 (A) IOP was measured using a Schiotz Tonometer (Riester, Germany) is placed on the cornea shown in Fig. 4 (B) Conversion of the scale value into table value provided by the manufacturer calculates the IOP in mmHg units. All values repeated thrice and are presented as mean ± SE. After completion of the experiment, eyes were washed properly with normal saline followed by moxifloxacin eye drop [24].

2.11. Computational analysis

The computational research work was carried out in Linux-Ubuntu 16.04 LTS system. As per the requirements, the HPMC and Montmorillonite unit cell were designed using the software MarvinSketch (ChemAxon, Budapest, Europe) from the previously published papers [14,25] and the drug, trimetazidine was retrieved from PubChem (CID: 83201) for this study. Further, all chemical structures were converted to pdb (.pdb) format with clean geometry using BIOVIA Discovery Studio Visualizer software (BIOVIA DSV). The software, AutoDock 4.1, was used for molecular docking study. The molecular interactions of single and double docking complexes were visualized using BIOVIA DSV [26].

3. Results and discussion

3.1. Properties of formulated film

Surface pH found (7.0–7.2) was very much compatible with the eye and supposed to produce no irritation. Film have also demonstrated good folding endurance and not brittle rather strong and plastic in nature to produce sufficient flexibility upon placing in the cul-de-sac due to the presence of triethalonamine.

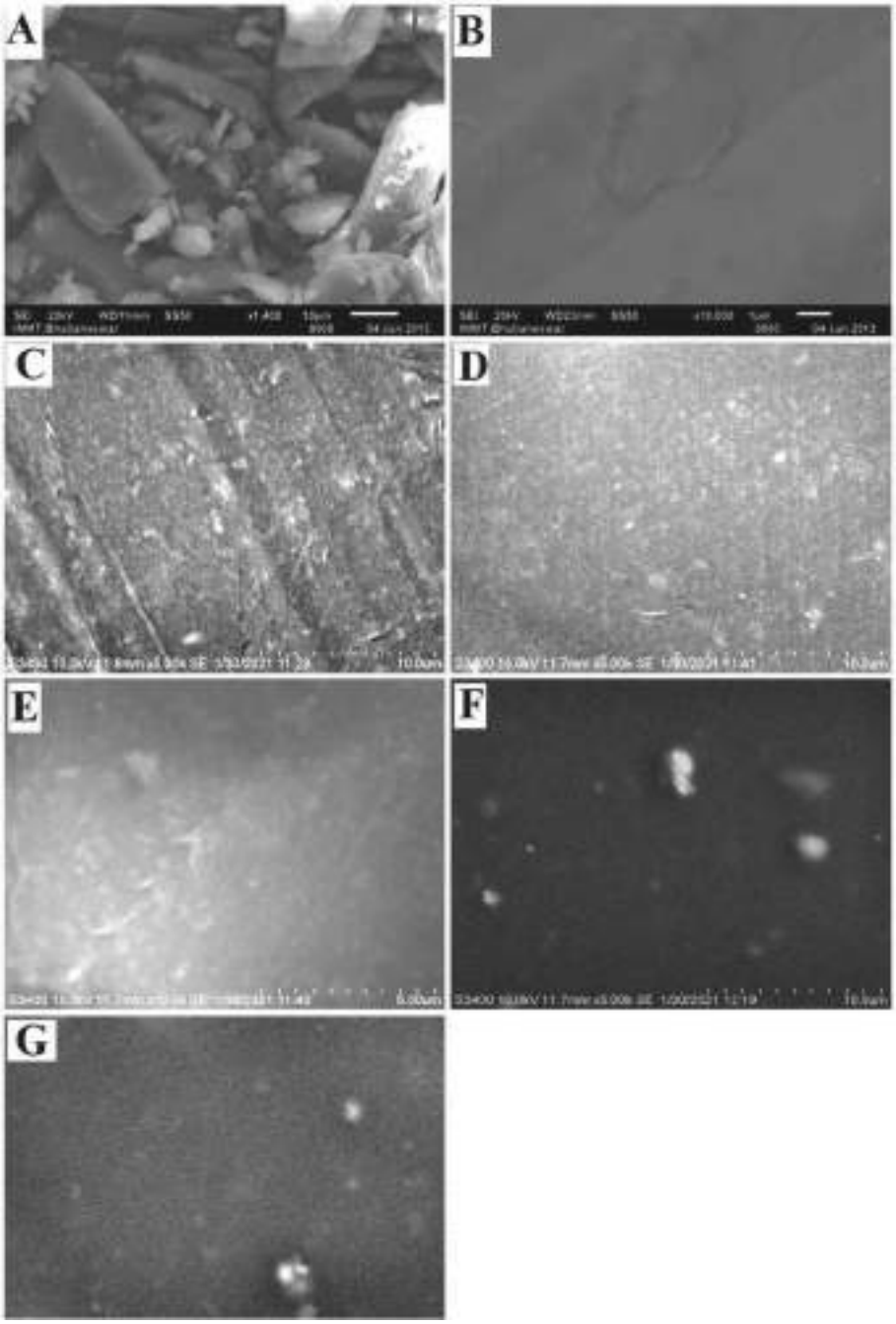

Fig. 2. Scanning electron micrographs of pure drug crystals (A) and film formulations in HPMC K15 matrix TB0 (B), TB1 (C), TB2 (D), TB3 (E), TB4 (F), TB5 (G).

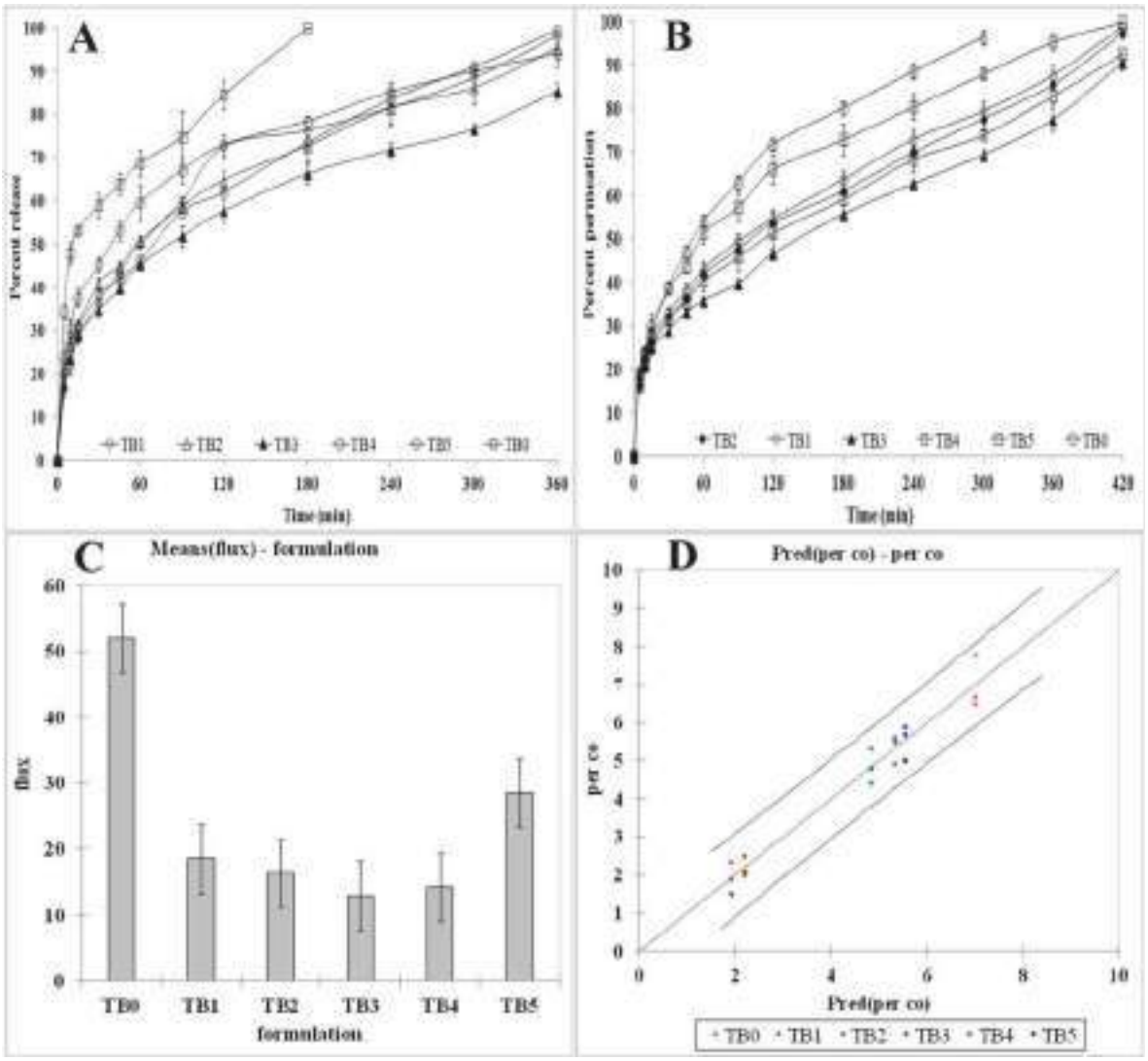

Fig. 3. Dissolution (A) and Permeation profiles; (B) of trimetazidine dihydrochloride and film formulations across cornea at 34 °C; (C) Js (flux) as a function of bentonite content; (D) mean chart of observed vs. predicted permeation coefficient.

3.2. FTIR

Fig. 1 (A) shows IR spectra of trimetazidine, bentonite and film containing different amount of bentonite. The IR spectrum of Trimetazidine showed the characteristic bands of –CH stretching, $–NH_2$ bending, –OH stretching, –CH bending, -C-O stretching at 2923, 1600, 3489, 1415, and 1099 cm^{-1} respectively [27,28]. The spectrum of pure bentonite Fig. 1 (A) exhibited a broad band at 3420 cm^{-1} attributed to the –OH stretching mode of interlayer water. The characteristic band at 1638 and 1108 cm^{-1} indicate the bending vibration of physically adsorbed water and longitudinal Si–O stretching vibration respectively. The observed absorption band at 3622 cm^{-1} and 915 cm^{-1} associated with Al–OH and Mg–OH stretching and Al–Al–OH bending vibration are distinctive for dioctahedral smectite [29]. The principal absorption bands appeared at 1033 cm^{-1} and 782 cm^{-1} due to Si–O stretching of smectite and quartz, respectively. The bands at 534 and 789 cm^{-1} originated due to Fe–O–Si and Mg–Al-Oh respectively [22,30].

For all formulations with trimetazidine, the characteristic vibration of –CH stretching was clearly observed around 2923 cm^{-1}. The relatively weak absorption around 1415 and 1600 cm^{-1} was assigned to the C–H bending and $–NH_2$ bending respectively. The absorption band at 1638 and 1108 cm^{-1}, due to OH deformational mode of water and the longitudinal Si–O stretching vibration for bentonite nanoclay also appeared in the spectra of the formulations. This is indicating the presence of trimetazidine and bentonite in clay containing complex. The broadening of absorption band in the range 3400–3200 cm^{-1} was observed due to the presence of polymer. Moreover, the band of at 1638 and 1033 cm-1 was broadened in the spectra of all formulations. These changes suggested to the interactions between the functional group of trimetazidine (amide) and the bentonite nanoclay [31,32].

3.3. Differential scanning calorimetry

In Fig. 1 (B) the calorimetry of pure trimetazidine showed a sharp melting endothermal peak at 236.13 °C with an onset of melting, 228.48 °C confirming its crystalline characteristics. Shifting of the endothermic melting peak with weaker enthalpy in the film formulations is a sign of nearly full amorphization of the drug crystals [33]. It happens probably due to arresting of drug amorphous state in to the polymer-clay matrix [34]. A broad endothermic peak in the range of 80–100 C has been found in all film formulations due to water evaporation in the HPMC matrix. A broad endothermic peak in the range of 80–100 °C has been found in all film formulations due to water evaporation in the HPMC matrix.

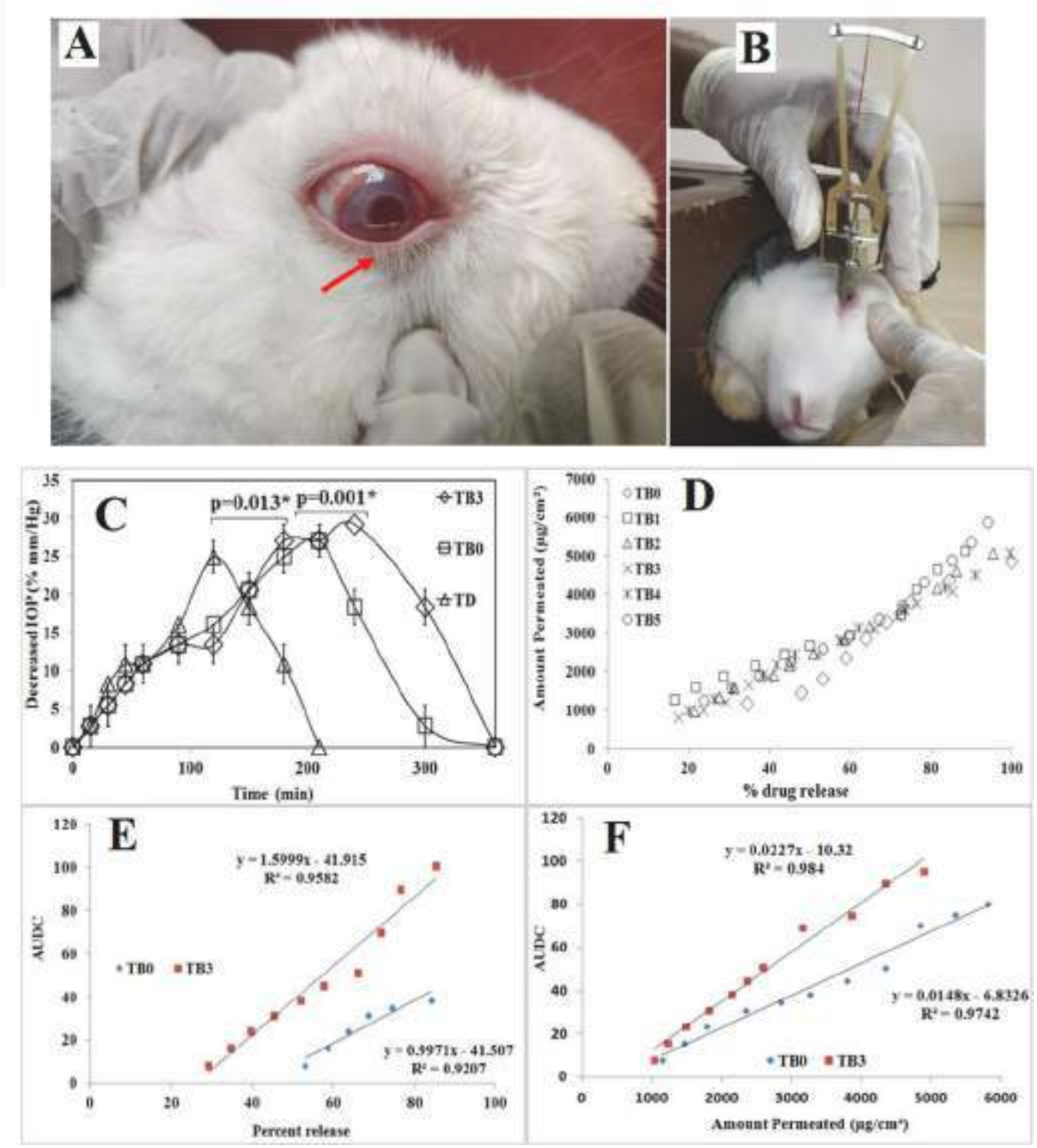

Fig. 4. TZ film administred into the rabbit cul-de-sac region (A), Measuring of intra ocular pressure (IOP) by using Schiotz Tonometer (B), Area under decreased IOP curve (AUDC) on normotensive rabbits the effects of different formulations of TZ on IOP in normotensive rabbits (trimetazidine drop (TD), TB0, TB3) has shown in Figure (C) in both cases, e.g. area under decreased IOP value of the formulation TB3 is significantly higher from the ocular drop of trimetazidine ($p = 0.013$) and TBO ($p = 0.001$) at the bracketed significant level, correlation between drug release in vitro and permeability ex vivo of the film (D), Correlation between in vitro drug release and area under decreased IOP (E); Ex vivo permeation and area under decreased IOP (F).

3.4. X-ray difractometry

In Fig. 1 (C) the diffraction spectrum of Na-bentonite exhibited characterization peak at 2Θ 6.78 (001) and 20.5 (110) peak of pure montmorillonite [21,31]. The deffractogram of pure drug showed the characteristic peak at 11.4, 15.5, and 18.9 (2Θ) indicating the crystalline pattern of trimetazidine [28] The majority of diffraction peak was disappeared may be due to the electrostatic attraction of the positively

charged drug with the negatively charged surface of the clay and the –OH group of HPMC [31]. However, no diffraction peaks of trimetazidine were observed in the XRD profile of trimetazidine-loaded composites. It is supposed to be the drug was dispersed in the composites in molecular form, may be due to the electrostatic attraction of the positively charged drug with the negatively charged surface of the clay and the –OH group of HPMC. It was also observed that in presence of bentonite drug becomes more amorphised. The disappearance of characteristic peaks of the bentonite in film formulations suggested that, bentonite was amorphously distributed in the polymeric matrix [31,35].

3.5. SEM

SEM images were utilised to study the surface morphology of pure trimetazidine, and films containing bentonite and without bentonite in Fig. 2. The geometric nature of the trimetazidine crystal is distinctly noticed in Fig. 2 (A). The crystal geometry of drug has almost been lost in the SEM of the film formulation in the presence and absence of the nano sized bentonite particles. SEM indicates that the high degree of dispersion of clay in the HPMC matrix was obtained at nano level of clay content when low concentration of clay content in Fig. 2 (F-G). In increasing Bentonite concentration, dispersion becomes more difficult and more particles are agglomerates can be evidenced by Fig. 2 (C, D, E). It should be emphasised that such behaviour is typical; due to the greater concentration of nanoparticles, dispersion in the polymer matrix becomes problematic, even under high shear force mixing conditions [36].

3.6. Drug dissolution testing

Drug dissolution experiment of TZ from bentonite incorporated HPMC films in simulated tear fluid (34 °C, pH 7.4) is shown in Fig. 3 (A). When bentonite is not present in the film (TB0), the entire release of TZ is seen in 180 min. The drug release was extended up to 6 h along with the decreased bentonite amount. This finding can be attributed to TZ adsorption on the bentonite surface, which enabled cation exchange and hydrogen bonding between the surface –OH and –NH of TZ. The adsorption of atenolol on to Ca-montmorillonite surface has already been proved by cation exchange and hydrogen bonding via the NH group, benzene ring, COH groups of the atenolol molecule [37]. Doxorubicin was found to be adsorbed effectively on the surface of bentonite nanoclay by forming electrostatic interaction and hydrogen bonding between NH group of doxorubicin and surface hydroxyl group of bentonite [38]. Because of their tortuous diffusion paths, silicate-based polymer nanocomposites have strong barrier characteristics and can be utilised in the development of applications for sustained drug release [19]. For TZ sustained release from the HPMC k15 M matrix, the following sequence was observed: TB0 > TB5 > TB1 > TB2 > TB4 > TB3. This observation demonstrates that the decreasing amount of bentonite should be in an appropriate ratio for optimal drug release. This suggests that a high concentration of bentonite would disrupt the production of a denser HPMC matrix film due to the –OH group in bentonite reacting with the hydrogen in the HPMC, disrupting the electrostatic connection between bentonite and TZ. As a result of these factors, TZ was released quickly from the film formulation [31,39]. To evaluate the release kinetics, the Higuchi and Korsmeyer-Peppas models were utilised. Estimated kinetic value of dissolution exponent (n), coefficient of regression (r^2), and rate constant (K) were depicted in Table 2. According to Peppas model, n < 0.5 indicates the pattern of Fickian release. For all the formulations the n value was residing between 0.260 and 0.414 indicated the release pattern as diffusion. Higuchi model fitting was also used to examine the diffusion-controlled release kinetics of all formulations (r^2 = 0.910–0.989).

3.7. Ex vivo corneal permeation

Ex vivo permeation was carried out for more than 6 h using fresh goat cornea, and the amount of TZ penetrated per unit area vs. time profiles are depicted in Fig. 2 (B). Reduced bentonite concentration in the film formulation resulted in a lower rate of penetration into goat corneal tissue. The following order was observed for TZ permeation from the formulations: TB0 > TB5 > TB1 > TB2 > TB4 > TB3. The permeation kinetics were studied using Higuchi and Korsmeyer-Peppas. Table 2 illustrates the parameters.

Table 1
Bentonite incorporated hydrogel film for trimetazidine ophthalmic delivery.

Formulation	HPMC (mg)	Drug/ Bentonite ratio	Triethalonamine (%)	Folding endurance (n = 6)
TB_0	1000	Bentonite-nil	15	>200
TB_1	1000	1: 10^{-4}	15	>200
TB_2	1000	1: $2*10^{-5}$	15	>200
TB_3	1000	1: 10^{-5}	15	>200
TB_4	1000	1: $5*10^{-6}$	15	>200
TB_5	1000	1: $2*10^{-6}$	15	>200

Peppas permeation exponent value (n) of all formulations were <0.5 (0.323–0.402) therefore, can be described as diffusion-controlled. The linearity of the Higuchi model also validated the formulation (0.980–0.984).

The quantity penetrated per cm^2 vs time profile plot was used to calculate the permeability coefficient (P) and flux (Js). Fig. 3 (C) shows the variability of flux according to the bentonite amount alteration. In Fig. 3 (D), the limitation of prediction was shown by a mean chart of observed vs. predicted permeation coefficients of films. The film formulation (TB0) devoid of bentonite has shown highest Pfilm and Js value where the lowest has been observed films containing bentonite (TB1, TB2, TB3, TB4, TB5).

Fig. 4 (D) depicts the relationships between in vitro release and film permeation. The correlation coefficient 0.960–0.997 and regression equation of the in vitro release against ex vivo permeation graph are shown in Table 1, revealing a good Level A correlation between in vitro release and ex vivo permeation. A good correlation ship ensures batch-to-batch consistency in ex vivo film performance.

The results revealed the influence of bentonite on the permeability coefficient. Dunnett's test study (Table 3) revealed that formulation permeation coefficients varied significantly from the control formulation (TB0) by comparing pair wise: TB0 vs TB1, TB0 vs TB2, TB0 vs TB3, TB0 vs TB4, TB0 vs TB5. The findings show that bentonite has a significant influence on the ex vivo penetration of films into ocular tissue. With decreasing bentonite ratios in formulations, the flux dropped from 60.022 to 11.045. The flux of permeation in films with different bentonite concentrations is depicted in Fig. 3 (C).

3.8. IOP Result

After instillation of several formulations, such as ocular trimetazidine drop (TD), film formulation without bentonite (TB0), and film formulation with bentonite the highest sustained release (TB3), the IOP reducing effects of TZ in normotensive rabbit eyes examined. The mean IOP value before the administration of TZ instillation (zero time) was (20.03 ± 0.9 mm Hg). It was observed that with 2 mg/kg (50 μl) TZ the IOP lowering effect reached the maximum value of 15.4 ± 0.7 mmHg within 120 min and the TB0 formulation reached the maximum value of 15.03 ± 0.75 mmHg within 240 min after instillation.

On the other hand the IOP-lowering impact diminished and was completely abolished within 210 min and 300 min for drop and TB0 formulation respectively. In contrast, the TB3 formulation resulted in a significant and persistent decrease in IOP. TB3 demonstrated an impact that lasted up to 6 h. The peak effect of TB3 was observed at 240 min with reduction of IOP value 14.6 ± 0.8 mmHg. The area under the decreased IOP versus time curve (AUDC) was carried out after administration of different TZ formulation Fig. 4 (C). The AUDC value for drop

Table 2
Kinetic of drug release and permeation.

Film code	Release				Permeation					
	Higuchi		peppas		Higuchi		Peppas		Js (μg/min)	$P_{Film*10^{-5}}$ (cm/min)
	K (% $min^{-½}$)	r^2	n	r^2	K (% $min^{-½}$)	r^2	n	r^2		
TB0	6.333	0.910	0.260	0.969	5.643	0.983	0.402	0.997	60.02	6.2
TB1	5.100	0.970	0.414	0.991	4.233	0.983	0.366	0.994	19.43	5.70
TB2	4.900	0.970	0.343	0.999	4.137	0.984	0.359	0.996	17.90	5.12
TB3	4.102	0.976	0.356	0.996	3.609	0.980	0.323	0.988	13.85	2.59
TB4	4.855	0.989	0.367	0.995	3.978	0.984	0.356	0.998	15.97	3.72
TB5	5.191	0.941	0.331	0.991	4.612	0.981	0.381	0.996	36.58	5.74

Table 3
Analysis of variance with Dunnett test comparing between control category (TB0) and the other film formulation.

Contrast	Difference	Standardized difference	Critical value	Critical difference	Pr > Diff	Significant
TB0 vs TB3	5.077	13.397	2.901	1.099	<0.0001	Yes
TB0 vs TB4	4.787	12.631	2.901	1.099	<0.0001	Yes
TB0 vs TB2	2.153	5.682	2.901	1.099	0.000	Yes
TB0 vs TB1	1.653	4.363	2.901	1.099	0.004	Yes
TB0 vs TB5	1.453	3.835	2.901	1.099	0.010	Yes

was 43.112 ± 5.06 mm Hg where as for TB0 and TB3 it was found 80.433 ± 4.816 mm Hg and 95.196 ± 5.3 mm Hg respectively. Due to the quick availability of TZ in high concentration in solution form, ocular drops of TZ had an immediate impact. But in case of TB0, TB3 was embedded or cross linked in polymer matrix, sufficient concentration of TZ was not attend to produce an immediate effect. The formulation's sustained effect could be attributable to HPMC's increased mucoadhesion in the formulation, and bentonite's synergistic effect on tissue binding in TB3. As a result, when compared to eye drops, the formulated TB3 was found to be more efficient in lowering IOP in eyes.

The correlations between amount permeated and AUDC of formulations are shown in Fig. 4 (E, F). The correlation coefficient (0.9742 for TB0 and 0.984 for TB3) and regression equation of the quantity permeated versus AUDC graph are shown in the figure, indicating a good Level A correlation between ex vivo permeation and AUDC.

3.9. Docking

Molecular docking is a type of artificial intelligence technique that can predict the molecular interaction of any biological substances. Docking can also confirm the fitting of a drug with a carrier with a stable configuration and a favourable energy. Therefore, we applied molecular modelling to illustrate the drug intercalated in Na-Montmorillonite. Based on the individual docking score (kcal/mol), HPMC-drug was comparability higher docking score −2.71 kcal/mol Fig. 5 (A) in comparison, the montmorillonite unit cell-drug produced −1.98 kcal/mol Fig. 5 (B). Concurrently, according to our objectives, 'HPMC-DRUG-UNIT CELL' obtained −5.74 kcal/mol, which indicates as a stable

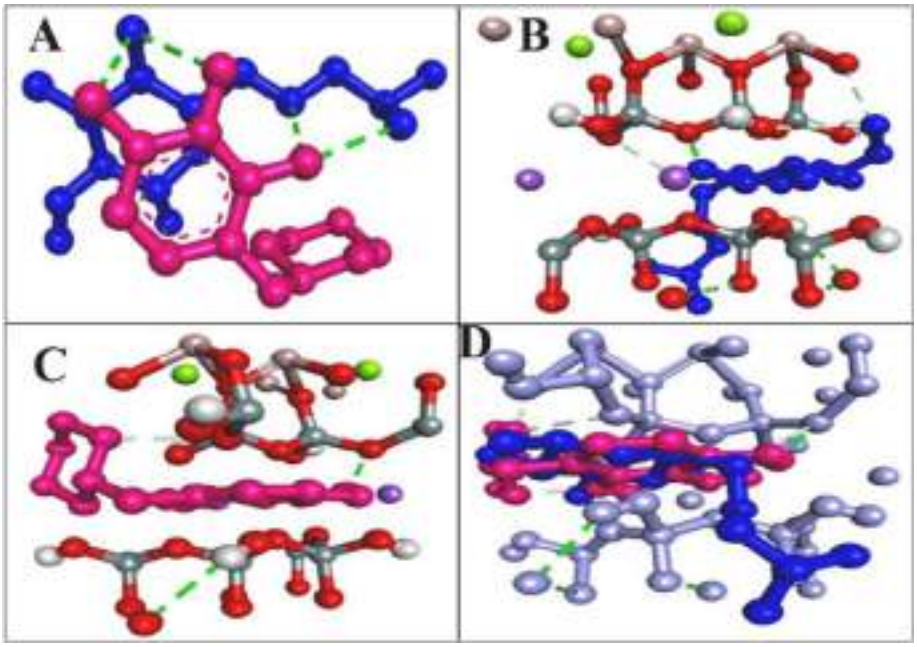

Fig. 5. Molecular Docking structure of HPMC-TZ (A), HPMC-Bentonite (B), Bentonite-TZ (C), Bentonite-TZ-HPMC (D) where HPMC (Polymer – dark blue) – trimetazidine (drug-dark peach)- unit cell (montmorillonite – lavender/light purple). (For interpretation of the references to colour in this figure legend, the reader is referred to the Web version of this article.)

interaction than from a single chemical docking complex in Fig. 5 (D). Thus, docking analysis can support the suitability of drug delivery and fitting of a drug with a stable configuration with favorable binding energy (van der Waals, ion-dipole, dipole-dipole interaction, H-bonding, etc.). Briefly, as per the theoretical chemistry point of view, there was an ideal embolism between polar organic molecules with hydroxyl groups of the Na-bentonite layer. The drug adsorption with Na-bentonite free surface and solidityfoundation of three-component layers with a polymer coat is expected to control the drug delivery as validated in the experimental section Fig. 5 (D). Our molecular modelling analysis revealed that trimetazidine intercalation was most likely caused by adsorption to the free surface as well as the creation of hydrogen bonds between the amine group hydrogen and the lamellar surface oxygen atom of Na-bentonite. The computational method illustrated the building blocks, binding energy and molecular interaction realistically as per our hypothesis. Moreover, bioinformatics tools were an indispensable part of early drug discovery, drug chemistry, and drug delivery analysis, theoretically [25,26].

4. Conclusion

Bentonite clay based film formulation has been prepared successfully for ophthalmic delivery of trimetazidine. Entrapment of TZ in the polymer-clay matrix was confirmed with the FTIR and DSC thermograms. Reduced crystal lattice was found in X-ray diffraction pattern. TB3 film containing drug to bentonite ratio of 1: 10^{-5} exhibited a most sustained drug release as well as corneal permeation up to 6 h compared to the TB0 film free of bentonite. The same TB3 film has shown reduced IOP in normotensive rabbit model promisingly. Estimation of area under response time curve revealed the significant improvement of bioavailability with sustained effect. molecular modelling analysis reveled that the trimetazidine intercalated bentonite based hydrogel matrix film indicated a durable interaction enhancing ocular bioavailability and long-term impact.

CRediT authorship contribution statement

Rakesh Swain: Methodology, Investigation, Formal analysis, Writing – original draft. **Souvik Nandi:** assisted during the in vivo, ex vivo studies. **Rudra Narayan Sahoo:** assisted during the in vitro, and ex vivo studies. **Shasank Sekhar Swain**: assisted in molecular docking study. **Sujata Mohapatra**: additional assistance in review & editing of the manuscript. **Subrata Mallick**: was in charge of the whole operation, rectification and approval of the manuscript.

Declaration of interests

The authors declare that they have no known competing financial interests or personal relationships that could have appeared to influence the work reported in this paper.

Acknowledgements

The authors are grateful to the Department of Science & Technology, Ministry of Science & Technology, New Delhi, India, for providing INSPIRE fellowship to Rakesh Swain (IF 180581). The authors are also very much grateful to the President, Siksha O Anusandhan (Deemed to be University) for providing other facilities. The authors are also grateful to Medley Pharmaceutical Ltd. for the gift sample of Trimetazidine Dihydrochloride.

References

[1] S. Li, A. Zhang, W. Cao, X. Sun, Elevated plasma endothelin-1 levels in normal tension glaucoma and primary open-angle glaucoma: a meta-analysis, J. Ophthalmol (2016), https://doi.org/10.1155/2016/2678017.

[2] R. Rosenthal, M. Fromm, Endothelin antagonism as an active principle for glaucoma therapy, Br. J. Pharmacol. (2011), https://doi.org/10.1111/j.1476-5381.2010.01103.x.

[3] L. Choritz, M. Machert, H. Thieme, Correlation of endothelin-1 concentration in aqueous humor with intraocular pressure in primary open angle and pseudoexfoliation glaucoma, Invest. Ophthalmol. Vis. Sci. (2012), https://doi.org/10.1167/iovs.12-10216.

[4] E. Rigosi, M. Ensini, D. Bottari, P. Leone, L. Galli-Resta, Loss of retinal capillary vasoconstrictor response to Endothelin-1 following pressure increments in living isolated rat retinas, Exp. Eye Res. (2010), https://doi.org/10.1016/j.exer.2009.09.006.

[5] X. Zhang, R.R. Krishnamoorthy, G. Prasanna, S. Narayan, A. Clark, T. Yorio, Dexamethasone regulates endothelin-1 and endothelin receptors in human non-pigmented ciliary epithelial (HNPE) cells, Exp. Eye Res. (2003), https://doi.org/10.1016/S0014-4835(02)00323-8.

[6] G. Holló, P. Lakatos, P. Vargha, Immediate increase in aqueous humour endothelin 1 concentration and intra-ocular pressure after argon laser trabeculoplasty in the rabbit, Ophthalmologica (2000), https://doi.org/10.1159/000027507.

[7] S.M. Podos, R.F. Wang, J.B. Serle, O.C. Baltatu, Effect of SPP 301, an endothelin antagonist, on intraocular pressure in glaucomatous monkey eyes, Invest. Ophthalmol. Vis. Sci. (2009).

[8] J. Zhang, M. Fu, M. Zhang, L. Xu, Y. Gao, Synthesis of oxidized glycerol monooleate-chitosan polymer and its hydrogel formation for sustained release of trimetazidine hydrochloride, Int. J. Pharm. (2014), https://doi.org/10.1016/j.ijpharm.2014.02.001.

[9] Y. Shaorui, T. Guizhou, Z. Yingjie, GW24-e1192 the effect of trimetazidine on endothelial function of patient with chronic heart failure, Heart (2013), https://doi.org/10.1136/heartjnl-2013-304613.624.

[10] I.A. Leonova, S. Boldueva, O. Zakharova, L. Gaykovaya, P887Trimetazidine improves symptoms and reduces microvascular dysfunction in patients with microvascular angina, Eur. Heart J. (2017), https://doi.org/10.1093/eurheartj/ehx501.P887.

[11] M. Shah, S. Cabrera-Ghayouri, L.A. Christie, K.S. Held, V. Viswanath, Translational preclinical pharmacologic disease models for ophthalmic drug development, Pharm. Res. (2019), https://doi.org/10.1007/s11095-019-2588-5.

[12] L. Wang, R. Feng, J. Gao, Y. Xi, G. Huang, Generic sustained release tablets of trimetazidine hydrochloride: preparation and in vitro–in vivo correlation studies, Asian J. Pharm. Sci. (2016), https://doi.org/10.1016/j.ajps.2015.10.001.

[13] T.M. Aminabhavi, M.N. Nadagouda, S.D. Joshi, U.A. More, Guar gum as platform for the oral controlled release of therapeutics, Expet Opin. Drug Deliv. (2014), https://doi.org/10.1517/17425247.2014.897326.

[14] R. Mohapatra, S. Mallick, A. Nanda, R.N. Sahoo, A. Pramanik, A. Bose, D. Das, L. Pattnaik, Analysis of steady state and non-steady state corneal permeation of diclofenac, RSC Adv. (2016), https://doi.org/10.1039/C6RA03604J.

[15] A. Nanda, R.N. Sahoo, A. Pramanik, R. Mohapatra, S.K. Pradhan, A. Thirumurugan, D. Das, S. Mallick, Drug-in-mucoadhesive type film for ocular anti-inflammatory potential of amlodipine: effect of sulphobutyl-ether-beta-cyclodextrin on permeation and molecular docking characterization, Colloid. Surface. B (2018), https://doi.org/10.1016/j.colsurfb.2018.09.011.

[16] L.A. Shah, N.S. Khattak, M. Valenzuela, A. Manan, F.V. Díaz, Preparation and characterization of purified Na-activated bentonite from Karak (Pakistan) for pharmaceutical use, Clay Miner. (2013), https://doi.org/10.1180/claymin.2013.048.4.03.

[17] J. Dziadkowiec, R. Mansa, A. Quintela, F. Rocha, C. Detellier, Preparation, characterization and application in controlled release of ibuprofen-loaded guar gum/montmorillonite bionanocomposites, Appl. Clay Sci. (2017), https://doi.org/10.1016/j.clay.2016.09.003.

[18] V. Ambrogi, D. Pietrella, M. Nocchetti, S. Casagrande, V. Moretti, S. De Marco, M. Ricci, Montmorillonite–chitosan–chlorhexidine composite films with antibiofilm activity and improved cytotoxicity for wound dressing, J. colloid interf. sci. (2017), https://doi.org/10.1016/j.jcis.2016.12.058.

[19] K. Yano, A. Usuki, A. Okada, Synthesis and properties of polyimide-clay hybrid films, Polym. Sci. A Polym. Chem. (1997), 19, https://doi.org/10.1002/(SICI)1099-0518(199708)35:11<2289::AID-POLA20>3.0.CO;2-9.

[20] M. Boufatit, H. Ait-Amar, Removal of N, N-dimethylaniline from a dilute aqueous solution by Na+/K+ saturated montmorillonite, Desalination (2007), https://doi.org/10.1016/j.desal.2006.04.058.

[21] J. Lin, B. Jiang, Y. Zhan, Effect of pre-treatment of bentonite with sodium and calcium ions on phosphate adsorption onto zirconium-modified bentonite, J. Environ. Manag. (2018), https://doi.org/10.1016/j.jenvman.2018.03.079.

[22] M. Alshabanat, A. Al-Arrash, W. Mekhamer, Polystyrene/montmorillonite nanocomposites: study of the morphology and effects of sonication time on thermal stability, J. Nanomater. (2013), https://doi.org/10.1155/2013/650725.

[23] A Pramanik, R.N. Sahoo, A Nanda, R Mohapatra, R Singh, S Mallick, Ocular permeation and sustained anti-inflammatory activity of dexamethasone from kaolin nanodispersion hydrogel system, Curr. Eye Res. (2018). https://doi.org/10.1080/02713683.2018.1446534.

[24] S. Natesan, S. Pandian, C. Ponnusamy, R. Palanichamy, S. Muthusamy, R. Kandasamy, Co-encapsulated resveratrol and quercetin in chitosan and peg modified chitosan nanoparticles: for efficient intra ocular pressure reduction, Int. J. Biol. Macromol. (2017), https://doi.org/10.1016/j.ijbiomac.2017.04.117.

[25] E.H. Fini, B. Høgsaa, J.D.C. Christiansen, C.G. Sanporean, E.A. Jensen, M. Mousavi, F. Pahlavan, Multiscale investigation of a bioresidue as a novel intercalant for sodium montmorillonite, J. Phys. Chem. C (2017), https://doi.org/10.1021/acs.jpcc.6b11966.

[26] S.S. Swain, S.K. Paidesetty, B. Dehury, M. Das, S.C. Vedithi, R.N. Padhy, Computer-aided synthesis of dapsone-phytochemical conjugates against dapsone-resistant Mycobacterium leprae, Sci. Rep. (2020), https://doi.org/10.1038/s41598-020-63913-9.
[27] A. Chiș, I. Kacsó, G. Borodi, I. Bratu, Complexul de incluziune al trimetazidinei cu β-cyclodextrina, Clujul Med. (2011).
[28] S. Mandal, S.S. Kumar, B. Krishnamoorthy, S.K. Basu, Development and evaluation of calcium alginate beads prepared by sequential and simultaneous methods, Braz. J. Pharm. Sci. (2010), https://doi.org/10.1590/S1984-82502010000400021.
[29] V.T Farmer, J.D. Russell, The infra-red spectra of layer silicates, Spectrochim. Acta A Mol. Biomol. Spectrosc (1964). https://doi.org/10.1016/0371-1951(64)80165-Xd.
[30] S. Yang, M. Guo, E. Yang, H. Zhang, Study on preparation and performance of high swelling bentonite, MATERIA-BRAZIL (2018), https://doi.org/10.1590/S1517-707620180003.0522.
[31] H. Zhang, Y. Shi, X. Xu, M. Zhang, L. Ma, Structure regulation of bentonite-alginate nanocomposites for controlled release of imidacloprid, ACS Omega (2020), https://doi.org/10.1021/acsomega.0c00610.
[32] A. Pramanik, R.N. Sahoo, A. Nanda, K.P. Pattnaik, S. Mallick, Swelling kinetics and corneal hydration level of Kaolinin-HPMC hydrogel film, Indian J. Pharmaceut. Sci. (2020), https://doi.org/10.36468/pharmaceutical-sciences.651.
[33] H.M. El-Nahas, K.M. Hosny, Chitosan-based floating microspheres of trimetazidin dihydrochloride; preparation and in vitro characterization, Indian J. Pharmaceut. Sci. (2011), https://doi.org/10.4103/0250-474X.95619.
[34] B. Panda, A.S. Parihar, S. Mallick, Effect of plasticizer on drug crystallinity of hydroxypropyl methylcellulose matrix film, Int. J. Biol. Macromol. (2014), https://doi.org/10.1016/j.ijbiomac.2014.03.033.
[35] Y. Dong, S.S. Feng, Poly (d, l-lactide-co-glycolide)/montmorillonite nanoparticles for oral delivery of anticancer drugs, Biomaterials (2005), https://doi.org/10.1016/j.biomaterials.2005.03.021.
[36] L.A. Savas, M. Hancer, Montmorillonite reinforced polymer nanocomposite antibacterial film, Appl. Clay Sci. (2015), https://doi.org/10.1016/j.clay.2015.02.021.
[37] P.H. Chang, W.T. Jiang, B. Sarkar, W. Wang, Z. Li, The triple mechanisms of atenolol adsorption on ca-montmorillonite: implication in pharmaceutical wastewater treatment, Materials (2019), https://doi.org/10.3390/ma12182858.
[38] F. Hosseini, F. Hosseini, S.M. Jafari, A. Taheri, Bentonite nanoclay-based drug-delivery systems for treating melanoma, Clay Miner. (2018), https://doi.org/10.1180/clm.2018.4.
[39] D. Hou, R. Gui, S. Hu, Y. Huang, Z. Feng, Q. Ping, Preparation and characterization of novel drug-inserted-montmorillonite chitosan carriers for ocular drug delivery, Adv. Nanoparticles (2015), https://doi.org/10.4236/anp.2015.43009.

International Journal of Biological Macromolecules 242 (2023) 124628

Contents lists available at ScienceDirect

International Journal of Biological Macromolecules

journal homepage: www.elsevier.com/locate/ijbiomac

Bentonite-in hypromellose-poloxamer sol-gel for corneal application of trimetazidine: Study of rheology and ocular anti inflammatory potential

Rakesh Swain [a], Souvik Nandi [a], Shasank Sekhar Swain [b], Krushna Prasad Pattanaik [a], Sujata Mohapatra [a], Dhananjay Panigrahi [a], Subrata Mallick [a,*]

[a] Department of Pharmaceutics, School of Pharmaceutical Sciences, Siksha 'O' Anusandhan (Deemed to be University), Bhubaneswar 751003, Odisha, India
[b] Division of Microbiology & NCDs, ICMR Regional Medical Research Centre, Chandrasekharpur, Bhubaneswar 751023, Odisha, India

ARTICLE INFO

Keywords:
Sol-gel transformation
Bentonite
Ocular delivery
Trimetazidine
Anti inflammatory potential

ABSTRACT

Bentonite is reported to be used for extending ocular drug delivery safely in a controlled manner. Bentonite combined hydroxypropyl methylcellulose (HPMC)-poloxamer based sol-to-gel formulation has been developed for the prophylactic ocular anti-inflammatory effect of trimetazidine after corneal application. HPMC-poloxamer sol formulation was prepared incorporating trimetazidine to bentonite at 1: $2*10^{-5}$ to 1:$5*10^{-6}$ ratios using cold method, and investigations were carried out in carrageenan-induced rabbit eye model. Pseudoplastic shear thinning behavior without any yield value and high viscosity at low shear rate were the positive attribute of the tolerability of the sol formulation after ocular instillation. Presence of bentonite nanoplatelets revealed more sustained in vitro release (~79–97 %) and corneal permeation (~79–83 %) over a period of 6 h in comparison to its absence. Prominent acute inflammation has been produced in the carrageenan-induced untreated eye, whereas the absence of ocular inflammation has been noticed in the previously sol-treated eye even after carrageenan injection. HPMC-poloxamer-based formulation exhibited stronger binding affinity (5.13 kcal/mol) in the presence of bentonite rather than its absence (3.99 kcal/mol), resulting in a stable and sustained effect. HPMC-poloxamer in-situ gel of trimetazidine containing bentonite could be utilized for sustained ocular delivery and the control of ophthalmic inflammation prophylactically.

1. Introduction

Trimetazidine (TRZ) is a metabolic modulator traditionally used as an anti-anginal medication. Previous studies demonstrated that TRZ protects against smoking-induced left ventricular remodeling and inflammation [1]. In addition, TRZ reduces the release of serum inflammatory mediators and also decreases the production of inflammatory cytokines during ischemia and inflammation [1,2]. Anti-inflammatory activity of TRZ has been observed in patients with coronary artery disease due to a drop of IL-2 (interleukin-2) concentration and prevention of augmented concentration of IL-8, IL-1, and IL-6 [3]. TRZ inhibits the neutrophil accumulation in the myocardium when administered orally [4]. TRZ moreover, prevents the calcium penetration into mitochondria, inhibiting swelling and cell death [5]. This results in anti-inflammatory activity, including cytoprotective role in various other tissues like myocardium, kidney, intestine, and liver [4,6–9]. TRZ has also been reported to protect rat retina after administration of oral [10] and intra-peritoneal [11]. Neutrophil infiltration and degranulation also occur on the ocular surface in the pathogenesis of ocular inflammation and dry eye condition [12]. Hence, TRZ ocular delivery could be more beneficial therapeutic option for acute ocular inflammation.

Using an eye drop, only 1–10 % of the drug is absorbed when the majority is removed from the precorneal region. Short precorneal residence time, tear turnover, and reflex blinking are among the major causes of poor ocular bioavailability [13,14]. In-situ forming hydrogels are free-flowing liquids that jellify under specified physiological conditions. In-situ gelling polymers usually exhibit pseudoplastic behavior at ocular surface temperatures, tear pH, and the electrolyte present in the tear. Thermo-sensitive polymer, poloxamer 407 (POL) is a synthetic non-ionic compound with a poly (ethylene oxide)-poly (propylene oxide)-poly (ethylene oxide) type triblock copolymer structure. POL has numerous pharmaceutical applications, such as transdermal, ophthalmic, and injectable sustained drug delivery formulations

* Corresponding author at: School of Pharmaceutical Sciences, Siksha O Anusandhan (Deemed to be University), Bhubaneswar 751003, Odisha, India.
E-mail addresses: subratamallick@soa.ac.in, profsmallick@gmail.com (S. Mallick).

https://doi.org/10.1016/j.ijbiomac.2023.124628
Received 24 January 2023; Received in revised form 11 April 2023; Accepted 24 April 2023
Available online 27 April 2023

[15–17]. Even though POL forms a gel spontaneously above a particular lower critical solution temperature, its structural integrity is maintained only for a short term in the physiological system. Certain limitation of POL is associated with its insufficient mechanical strength resulting in premature hydrogel dissolution and rapid erosion [18]. Therefore, a relatively higher polymer concentration is required in order to maintain the gelation, which may include an ocular sensitivity reaction. The addition of different mucoadhesive type polymers such as carbopol [19], carboxymethylcellulose [20], and HPMC (hydroxypropyl methylcellulose) have been used to improve its properties [15].

Bentonite (B) is a natural aluminum phyllosilicate clay mineral holding montmorillonite as a main component and is categorized by lamellar structure. It is subjected to exfoliation into nanoplatelets in an aqueous environment because of the strong hydration of the interlayer. The nanoplatelets or nano-sheets are entirely separated when it is combined into the polymeric network within polymeric hydrogel may be due to the intercalation of polymer chains into the interlayer [21–24]. The extensive layer separation causes the structural break of the coherent layer resulting in a dispersion of loose nanoplatelets of bentonite in the polymer-clay matrix. Bentonite could be used in the fabrication of polymer-clay composite for extending ocular drug delivery in a controlled manner without any reported adverse effect [25] due to its good swelling, high specific surface area, and adsorption properties [26]. Behera et al., (2021) developed an ocular hydrogel (non in situ gel) system of ciprofloxacin incorporating bentonite in high concentration (1.0 to 4.0 %) for improved ocular delivery and antimicrobial efficacy only [27]. However, a high amount of bentonite may lead to sticky eyelids (http://www.capebentonite.co.za).

Bentonite incorporated HPMC-POL sol-to-gel formulation has been developed for the controlled ocular delivery of TRZ. Rheological studies of the formulation have been carried out for examining viscoelastic behavior, and understanding spreading and precorneal residence time. Prophylactic anti-inflammatory potential of TRZ has also been observed in the carrageenan-induced rabbit eye model. This research work was expected to assure the controlled delivery of such a soluble drug for a prolonged period. This type of study probably has not yet been reported.

2. Materials and methods

2.1. Materials

The API sample trimetazidine was gifted by Medley Research Centre (Mumbai, India). Poloxamer 407 and Hydroxypropyl methylcellulose (HPMC K15M) were kindly provided by Ready's Laboratory (Hyderabad, India). Bentonite was purchased from HIMEDIA Laboratories Pvt. Ltd. Mumbai, India (CAS No.: 1302-78-9). All other chemicals and solvents were analytical grade and commercially procured.

2.2. Animals

For animal experiment, the procedure complied with the ARRIVE guidelines (Animal Research: Reporting of in vivo experiments) scrutinizing the research adequately for evaluating methodological rigor to get reproducible findings. The approval has been obtained from IAEC (Institutional animal ethics committee) approval no. IAEC/SPS/SOA/21/2019. New Zealand albino rabbits weighed between 2.0 and 2.5 kg were individually housed in the laboratory (in properly light-controlled and air-conditioned rooms) maintained 25 ± 1 °C temperature at 70 ± 5 % RH with a standard pellet diet, and were provided with free water supply.

2.3. Preparation of sol

TRZ in-situ gel based on POL was prepared using a slightly modified cold method [28]. First, the required amount of HPMC and POL were dissolved in cold distilled water with continuous stirring for about 2 h.

Table 1
Bentonite containing aqueous in-situ gel formulation for ophthalmic delivery of trimetazidine.

Gel code	HPMC (% w/vol)	POL (% w/vol)	Drug: Bentonite	pH	$T_{sol\text{-}gel}$ (°C)
TgB_0	0.2	17	Bentonite nil	6.8	33
$TgB_{2.0}$	0.2	17	$1: 2*10^{-5}$	6.8	32
$TgB_{1.0}$	0.2	17	$1: 10^{-5}$	7.0	32
$TgB_{0.5}$	0.2	17	$1: 5*10^{-6}$	7.2	32

Then, thin dispersion of bentonite was added over the above mixture as per formulation tabulated in Table 1. Next, TRZ solution was added and stirred continuously for 1 h to get the homogenous sol preparation to make the final concentration of 20 mg per ml. Sol preparation of 5 ml was filled in a glass vial and well-closed (Aluminum cap sealed) vials were autoclaved at 121 °C for 20 min (15 psi) for final sterilization.

2.4. Characterization of the formulation

2.4.1. Gelling temperature, clarity, and pH

A test tube with about 1 ml of sol preparation was placed in a temperature-controlled water bath. A thermometer dipped in a second test tube containing 1 ml water was used as control for measuring gelling temperature. Temperature of the water bath was increased gradually, and the temperature at which the sol stopped flowing at its inverted state was recorded as sol-to-gel transformation (T1). Then gradually reduced the temperature and the temperature at which the gel began to flow again was recorded as gel-to-sol transformation (T2). The critical gelation temperature ($T_{sol\text{-}gel;}$ °C) was the average of T1 and T2. One of the major characteristics of ophthalmic preparations is clarity. Under a good light source and against a black-and-white background, the sol preparations were examined for their physical appearance and optical clarity. Calibrated pH meter (Systronics digital pH meter 335) was used to investigate the pH of the sol.

2.4.2. FTIR

The pure TRZ and sol formulations were scanned for IR transmission spectra to observe the drug-excipients interaction study. With an average of 80 scans and resolution of 4 cm^{-1}, the scans were performed in the range of 4000–600 cm^{-1}. In the FTIR spectrophotometer (JASCO FT/IR 4600) the samples were placed above diamond ATR (JASCO ATR PRO ONE) crystal [29].

2.4.3. DSC

DSC spectra were obtained by the Mettler Toledo instrument (DSC-1, Mettler Toledo; Software-Star E, SNR-1889) for studying the thermal behavior of TRZ and sol formulations. The temperature was increased at a rate of 10 °C/min from 30 to 300 °C in hermetically sealed flat-bottomed aluminum pans using nitrogen flow (50 ml/min).

2.4.4. XRD

X-ray crystallography of TRZ, bentonite, and formulations was carried out by XRD (Model: Rigaku Ultima IV). A K-Alpha anode with a voltage supply of 40 KV and a current of 15 mA was used as the X-ray source. The scanning was done at a speed of 1° per minute in the 2 Θ range of 5–70°.

2.4.5. Rheology

A parallel plate rheometer (Mars III, Thermo Fisher Scientific, Germany) was used to evaluate the rheological behavior of sol formulation. For all evaluations, parallel plate geometry was used, with a diameter of 40 mm. Two types of rheological testing were carried out.

2.4.6. Steady shear deformation

The shear rate (γ) was changed in logarithmic scale from 0.01 to

2000 s^{-1} for the determination of viscosity and stress.

2.4.7. Oscillatory deformation (Frequency sweep)

The storage modulus (G′) and loss moduli (G″) were determined by varying frequency from 0.01 to 100 Hz at a constant amplitude of deformation (γA ≈ 0.1 %).

2.4.8. SEM

The scanning electron microscopy was done for examining the morphological features at the surface of the formulations. It was done using ZEISS, EVO 18 model scanning electron microscope at different magnifications of 270 to 55,000.

2.5. In-vitro drug release

The drug diffusion study of the formulations was carried out using a modified Franz diffusion apparatus. The medium consisted of 200 ml of phosphate buffer saline (pH 7.4), and constant stirring speed was maintained at 50 rpm. at 34 ± 0.2 °C. Diffusion study was carried out for 6 h after placing the accurately weighed amount of sol formulation over the dialysis membrane in the donor compartment. Samples were withdrawn at predetermined time intervals and replenished with the blank medium to maintain the sink condition, and examined at fixed wavelength at 269.5 nm in the UV/visible spectrophotometer.

2.6. Ex vivo corneal permeation

The whole goat eyes were collected in a beaker containing saline from the butcher shop within 1 h after sacrifice and properly washed with distilled water followed by normal buffered saline (pH 7.4). The cornea was excised carefully with the help of scissors and forceps along the surrounding 5–6 mm of scleral tissue. It was then washed with sufficient phosphate buffer saline to get the washings free from proteins and the unrequired tissues. The process of permeation was carried out using the same modified Franz diffusion apparatus. The accurately weighed amount of sol formulation was placed in such a way that the epithelial surface faced the donor compartment for the permeation of drug into the medium with an effective surface area of 1.56 cm^2. The receiver compartment was filled with Phosphate buffer saline (pH 7.4, 200 ml) and was maintained at 34 ± 0.2 °C under constant stirring speed of 50 rpm. At the regular time interval (5, 15, 30, 45, 60, 90, 120, 180, 240, 300, and 360 min) the sample (10 ml) was withdrawn using a syringe driven filter (Nylon-66, hydrophilic membrane, pore size 0.45 μm, 25 mm diameter, HIMEDIA, India) and the same volume was replenished with fresh phosphate buffer solution. Collected samples were analyzed spectrophotometrically. A blank experiment was conducted to eliminate the occurrence of any interference from the tissue. The experiment was replicated three times or more using different ocular tissues from different animals and mean ± SD was recorded [29–32].

2.7. Kinetics

The release and permeation kinetics of the formulation have been explained using the Higuchi, Korsmeyer-Peppas and Peppas-Sahlin kinetic models using the equation as per below.

2.7.1. Higuchi model

$$C = k_h\sqrt{t}$$

C is the cumulative amount of drug released or permeated per unit area of formulation at time t; while, K_h denotes the Higuchi diffusion rate constant.

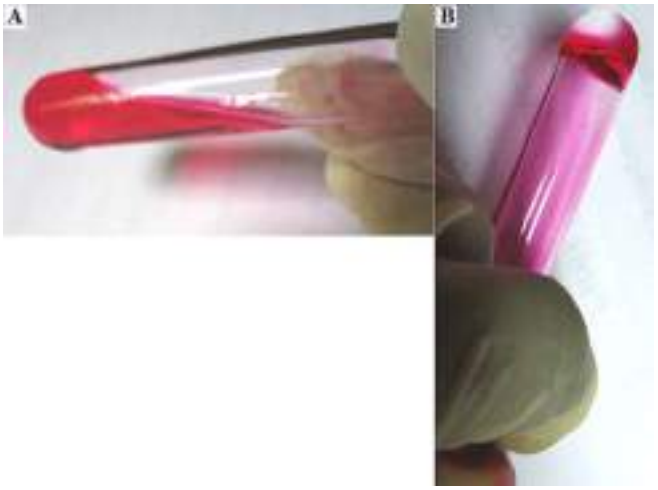

Fig. 1. Gelation process of thermosensitive in-situ gel. In room temperature when the temperature is below the gelation temperature, it is clear solution with low viscosity, upon heating it to gelation temperature; the solution is converted to the gel with high viscosity.

2.7.2. Korsmeyer-Peppas model

$$\frac{C_t}{C_\infty} = K_p t^n$$

C_t/C_∞ is the fraction of drug released or permeated at time t; K_p is the Peppas release or permeation rate constant; and n is the release or permeation exponent.

2.7.3. Peppas-Sahlin model

$$\frac{M_t}{M_\infty} = k_1 t^m + k_2 t^{2m}$$

M_t/M_∞ is the fraction dissolved; k_1 is a constant relating to the Fickian kinetics; k_2 is a constant relating to the Case II relaxation kinetics; and m represents Peppas-Sahlin diffusion exponent.

2.8. Anti-inflammation study

For evaluation of anti-inflammatory effect, the standard carrageenan-induced rabbit eye model was used without sacrifice [25,33]. Male New Zealand rabbits were separated into 3 groups containing three each. Group I was treated as the test group (with formulation), Group II was positive control group- (Carrageenan induced), and Group III was treated as negative control group. For anti-inflammation study, sol formulation was instilled in Group-I (50 μl; 1 mg/Kg) and 2 h after the same animals received carrageenan injection subconjunctivally (200 μl; 2 % *w/v*). Group-II rabbits received carrageenan injection (same dose). Photographs were taken of any signs of acute inflammation and reddening of the conjunctiva, followed by lachrymal secretions. After the completion of the experiment of about 4 h Moxifloxacin Eye Drop I·P (0.5 % w/v) was instilled in the eye for quick recovery.

2.9. Molecular docking study

Linux-Ubuntu 16.04 LTS system was used for the investigation of molecular docking studies. For computational analyses chemical structure of TRZ, HPMC, and POL, was collected from PubChem database, and a unit cell of bentonite clay ($Al_2H_2Na_2O_{13}Si_4$) has been developed as per chemical formula through the MarvinSketch software [34]. Structure of TRZ, HPMC, POL, and bentonite was converted to pdb (.pdb) file using BIOVIA Discovery Studio Visualizer software. Molecular docking

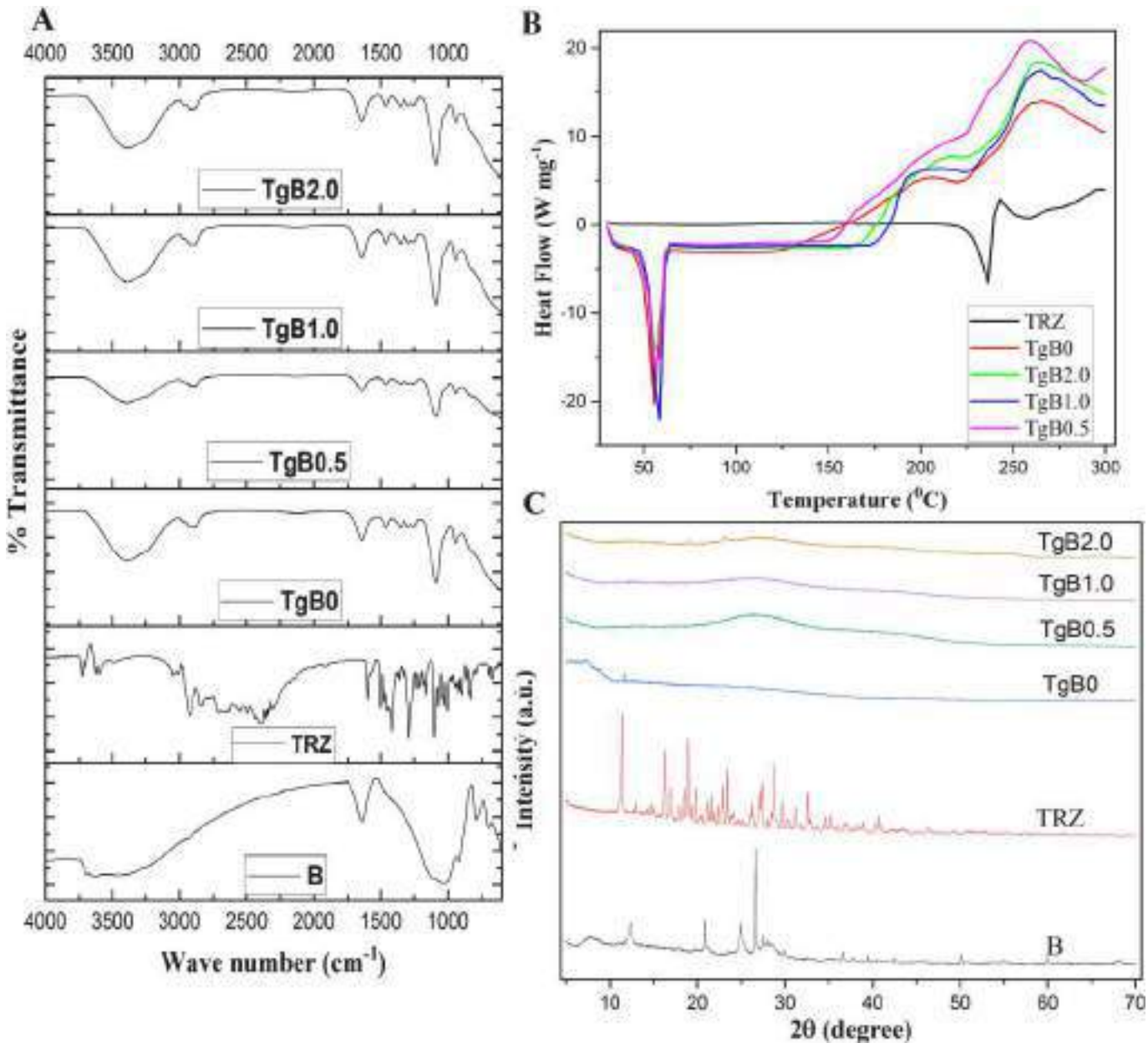

Fig. 2. FTIR spectroscopy (A) DSC thermogram (B) XRD patterns (C) of TRZ and in situ gel formulations.

study was performed with Auto Dock 4.2 using default AutoDock parameters with a user-defined grid (30x30x30) [35]. Multiple docking complex as complex_1 (HPMC-TMZ-B-POL) and complex_2 (HPMC-TMZ-POL) have been analyzed and the interaction of the docking complexes were imaged [35].

3. Results and discussion

3.1. Gelling temperature, clarity and pH

A thermo-responsive system is a free-flowing sol or solution, and it forms a gel at body temperature (upon instillation in the eyes). Critical gelation temperature as the average of sol-to-gel transformation and gel-to-sol transformation of all the formulations was recorded as in the range of 32–33 °C (Fig. 1) which is appropriate for in-situ-ocular gel formation upon instillation in the eye. HPMC is a suitable choice of mucoadhesive polymer for ocular delivery [29,33] and the addition of HPMC in the present formulation might have improved the gelling capacity [36]. Formulations were found clear, colorless, and transparent in appearance (Fig. 1). The pH value was within the tolerable physiological range (6.8–7.2) of the eye.

3.2. FTIR

The IR spectrum of pure TRZ, bentonite and in-situ gel containing a different ratio of bentonite is depicted in (Fig. 2A). Bands of TRZ at 2923, 1415, 1600, 3489, and 1099 cm^{-1} were due to stretching and bending of –CH, bending of $–NH_2$, stretching of -OH, and -C-O, respectively [37,38]. FTIR spectra of pure bentonite peaks at 3420 and 3622 cm^{-1} was attributed to the hydroxyl stretching vibration of adsorbed water associated with aluminum, magnesium, and silicon. Bending vibrations due to adsorbed water as well as stretching of Si—O represented the bands at 1638 and 1108 cm^{-1}. Bands at 1033 and 782 cm^{-1} signified the stretching of smectic and quartz Si—O respectively [39,40]. Characteristic stretching of -CH has been noticed at about 2923 cm^{-1} in all sol-gel formulations due to the presence of TRZ. C—H and $-NH_2$ bending

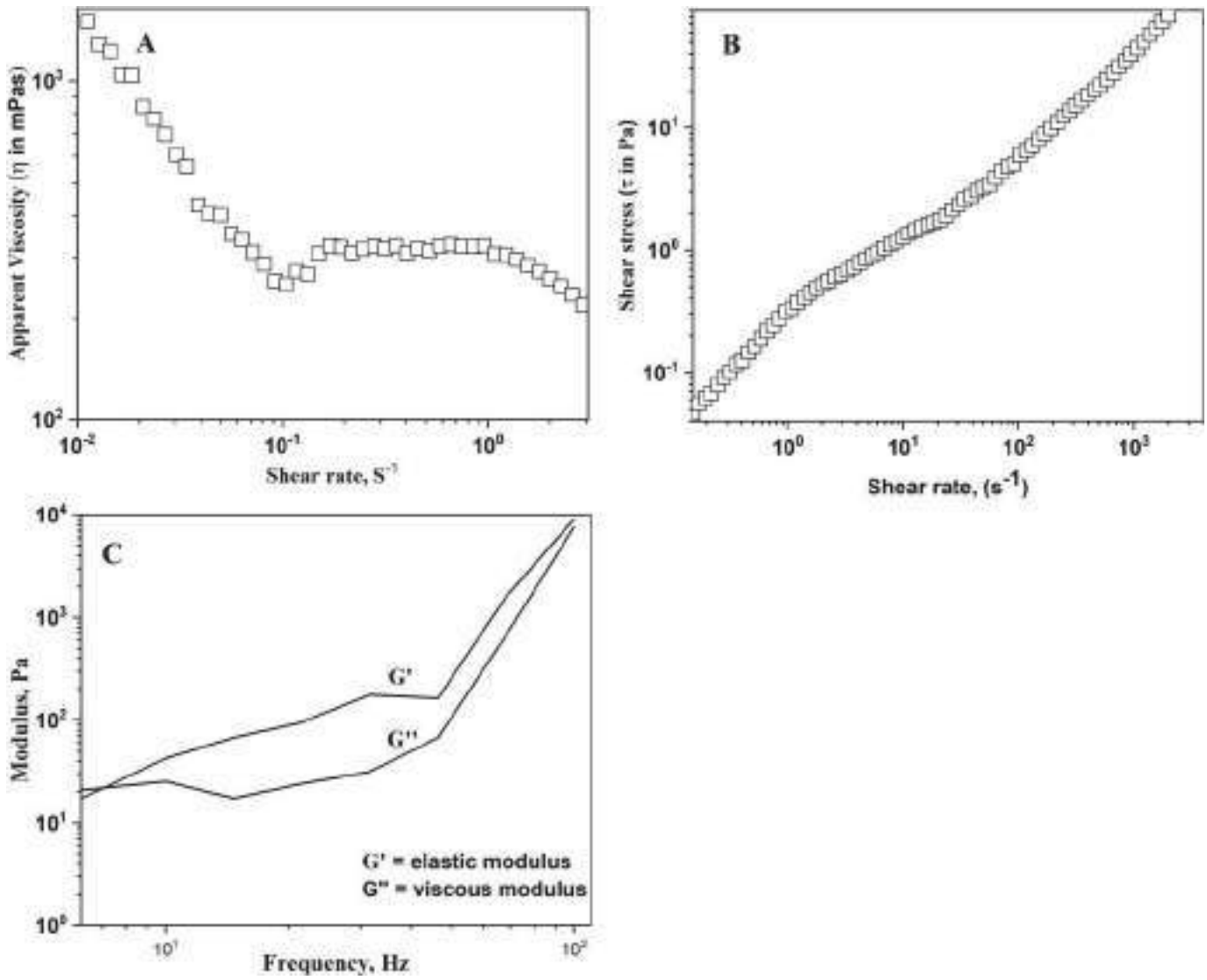

Fig. 3. Apparent viscosity as a function of shear rate for TRZ in situ gel (A), Shear stress vs. shear rate flow curve (B), Elastic and viscous moduli as a function of frequency of oscillation (C).

were attributed to about 1415 and 1600 cm^{-1} correspondingly. Absorption spectrum at 1108 and 1638 cm^{-1} indicated the presence of bentonite in all formulations. A broad band at 3400–3200 cm^{-1} indicates the presence of O—H stretching vibration. The bands at 1638 and 1033 cm^{-1} were widened in all the sol preparations. These modifications showed the intramolecular hydrogen bonding among bentonite and drug molecule.

3.3. DSC

Fig. 2B shows the DSC of pure TRZ and in-situ gel formulations. The thermogram of the pure TRZ exhibited an endothermic peak at 236 °C, indicating drug crystallinity [41]. Complete disappearance of the melting peak of the drug designates the drug dispersion in the prepared polymer-clay composite. Melting peak at about 55 °C confirmed the presence of POL in all formulations [42].

3.4. XRD

The XRD peaks of TRZ at 2Θ 11.4, 15.5, and 18.9 in X-ray crystallography (Fig. 2C), indicating crystallinity [38]. The patterned diffraction of pure bentonite showed the characteristic peak at 6.78 and 20.5 (2Θ) due to the presence of montmorillonite [22]. Diffraction peaks of TRZ have almost been disappeared in the polymer-clay composite due to the dispersion of the drug associated with electrostatic affinity between drug, bentonite and HPMC.

3.5. Rheology

Rheological studies were performed at a precorneal temperature of 35 °C to describe the rheological behavior of TRZ in-situ gel formulation ($TgB_{1.0}$). Apparent viscosity has been decreased with the increase of shear rate as depicted in Fig. 3A. Shear rate vs. Shear stress flow curve (Fig. 3B) also shows the same non-Newtonian pseudoplastic shear thinning behavior starting from zero without any yield value. High viscosity at low shear rate is the positive attribute of the tolerability of the sol formulation after instillation. The pseudoplastic behavior of the developed in-situ gel allows for smooth spreading on the epithelial surface and enhanced precorneal residence duration at the same time avoiding discomfort by blinking.

To investigate the viscoelastic properties of the prepared in-situ gel under a small deformation frequency variation test was performed and shown in Fig. 3C. Oscillatory measurements allow simulating behavior of the systems at low shear, investigating the native behavior of

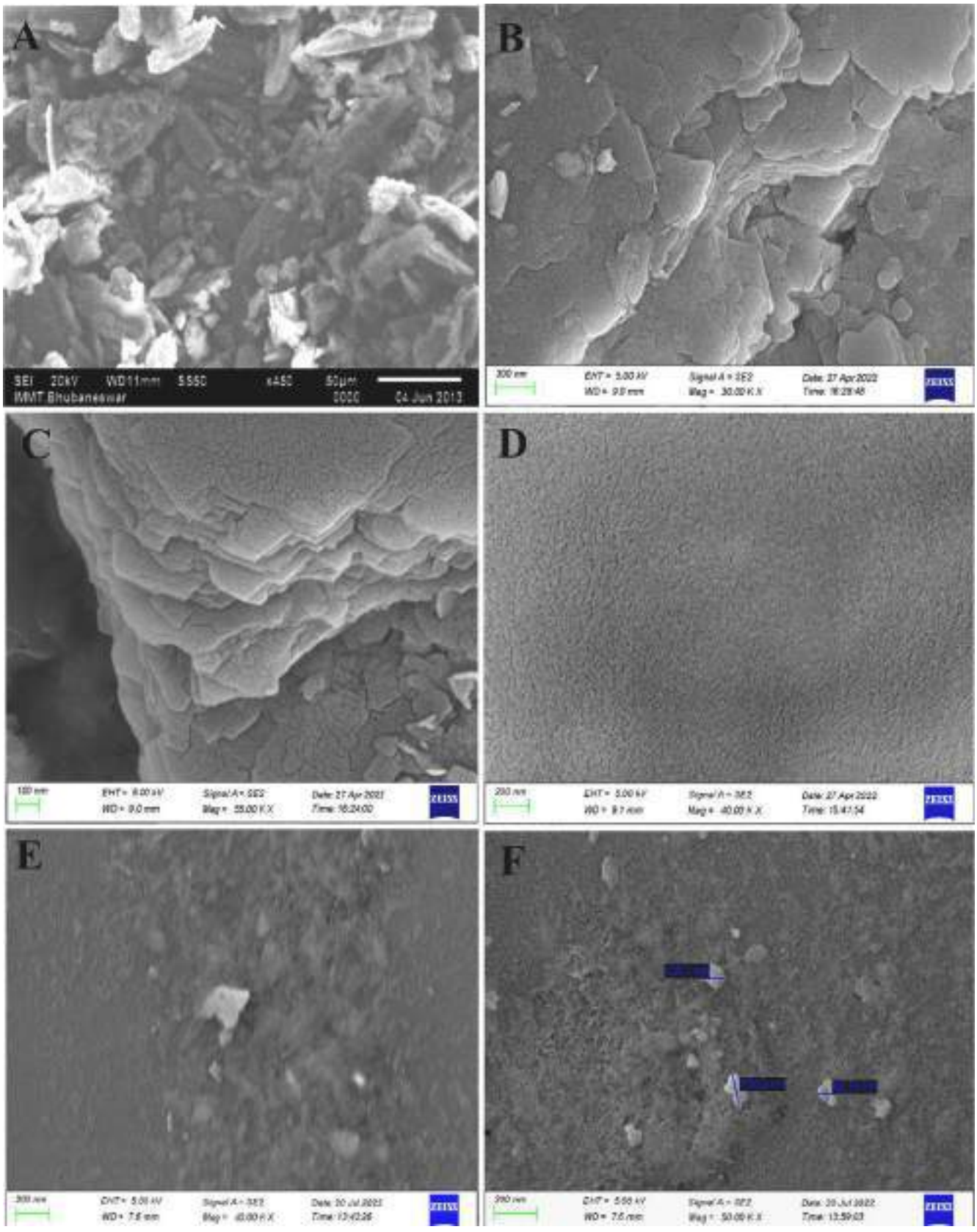

Fig. 4. Scanning electron microscope of pure TRZ (A) pure bentonite (B, C), in-situ gel formulation without bentonite (TgB_0) (D), with bentonite ($TgB_{1.0}$) (E, F).

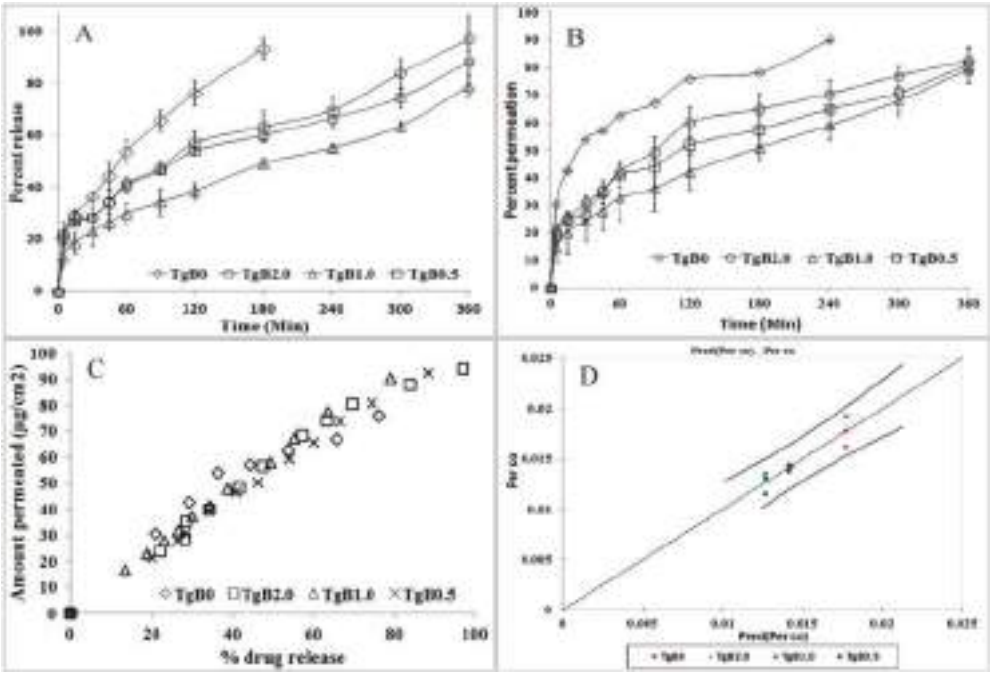

Fig. 5. In vitro diffusion (A); ex vivo Permeation profile (B) of TRZ and in-situ gel formulations across cornea at 34 °C; mean chart of observed vs. Predicted permeation coefficient (C); Correlation between in vitro drug release and ex vivo permeation of the in situ gel (D).

semisolids at physiologically relevant shears. The elastic modulus (G′) and viscous modulus (G″) measured by oscillatory rheometry are proportional to the energy stored and recovered respectively in each deformation cycle at a set frequency. The formulation has shown a higher G′ value compared to G″ in the higher frequency duration (above 40 Hz). A model-independent method for comparison is based on the determination of difference factor ($f1$) and similarity factor ($f2$) ($f1 > 15$, and $f2 < 50$ signify the difference). A significant difference in between G′ and G″ was observed when compared pairwise ($f1$ value as: 17 and $f2$ value as: 30) [33,43]. This result indicates that the formulation has viscoelastic behavior which may facilitate the retention at the target site providing prolonged drug release [44]. It was also observed that G′ and G″ prominently increased in response to an increase in oscillatory frequency above about 40 and 60 Hz, respectively.

3.6. SEM

Scanning electron microscopy images were used for the investigation of the surface morphology of the pure TRZ, and in-situ gel with and without bentonite (Fig. 4). Drug crystal geometry is clearly visible in Fig. 4A. Pure bentonite particles consisting of well-oriented layers of flat platelet having large surface area are clearly observed in Fig. 4B & C. Drug crystal growth in HPMC film containing triethanolamine (TgB_0) was almost lost in the appearance of SEM image (Fig. 4D) because of interfacial adhesion between TRZ and polymer, in accordance with XRD analysis. HPMC, a crystal habit modifier significantly prevented crystal formation [33]. Presence of bentonite particles in the sol formulation containing bentonite has been noticed (Fig. 4E & F). Appearance of rough surface proved the presence of clay platelets in the composite in relation to formulation without bentonite. POL-HPMC matrix polymer in the sol formulation reduced the bentonite clay particle size to about 20–150 nm. Exfoliation of interlayer spacing of the silicate layers of bentonite might have occurred due to the polymer chain insertion in between the gallery of the oriented layers of flat platelets [22]. Extensive layer separation possibly caused the structural break of the coherent layer resulting in a dispersion of loose nanoplatelets of bentonite in the polymer-clay matrix.

3.7. In-vitro drug release

In-vitro drug release from in-situ gel in the presence of bentonite exhibited a relatively more sustained effect over a period of 6 h (~79–97 %) in comparison to its absence (~93 % in 3 h) (Fig. 5A). The gel formulation, $TgB_{1.0}$ (TRZ to B: $1{:}10^{-5}$) showed most delayed-release (~49.12 % in 3 h) rather than others. TRZ adsorption on the surface of bentonite particles due to ion exchange and hydrogen bonding might have extended the drug release. Bentonite-polymer nanocomposites containing imidacloprid has been reported to be used in the development of sustained drug release product [22]. A remarkable increase in specific surface area of the nanoplatelets after exfoliation of interlayer of bentonite facilitated the intimate contact with the polymer, and sustained the release of drug [22,45]. An optimum level of bentonite nanoplatelets in $TgB_{1.0}$ extended the drug release to the highest extent compared to others [25]. Release of TRZ from the POL-bentonite hybrid

Table 2
Kinetic modelling parameters of TRZ in situ gel formulations.

Gel code	In-vitro drug release							Corneal permeation								
	Higuchi		Peppas		Peppas Sahlin			Higuchi		Peppas		Peppas Sahlin			Js (µg/min)	Pgel (cm/min)
	k	r^2	n	r^2	K1	K2	m	k	r^2	n	r^2	K1	K2	m		
TgB_0	6.943	0.986	0.486	0.989	7.696	0.609	0.405	6.255	0.901	0.199	0.991	22.4	6.56	0.148	162.42	0.0162
TgB_2	4.960	0.932	0.453	0.974	7.916	0.302	0.381	5.421	0.979	0.383	0.991	10.5	0.15	0.381	137.39	0.0137
$TgB_{1.0}$	3.810	0.982	0.485	0.983	4.710	0.468	0.362	4.615	0.970	0.476	0.989	6.0	0.64	0.355	115.72	0.0115
$TgB_{0.5}$	4.640	0.978	0.410	0.986	8.680	1.517	0.303	5.022	0.952	0.404	0.984	9.9	2.07	0.296	122.76	0.0122

Table 3
Analysis of the differences between the control category formulation-TgB_0 and the other categories ($TgB_{1.0}$, $TgB_{0.5}$, $TgB_{2.0}$) with a confidence interval of 95 % by two sided Dunnett.

Contrast	Difference	Standardized difference	Critical value	Critical difference	Pr > Diff	Significant
TgB_0 vs $TgB_{1.0}$	0.005	6.688	2.880	0.002	0.000	Yes
TgB_0 vs $TgB_{2.0}$	0.004	4.708	2.880	0.002	0.004	Yes
TgB_0 vs $TgB_{0.5}$	0.004	4.620	2.880	0.002	0.004	Yes

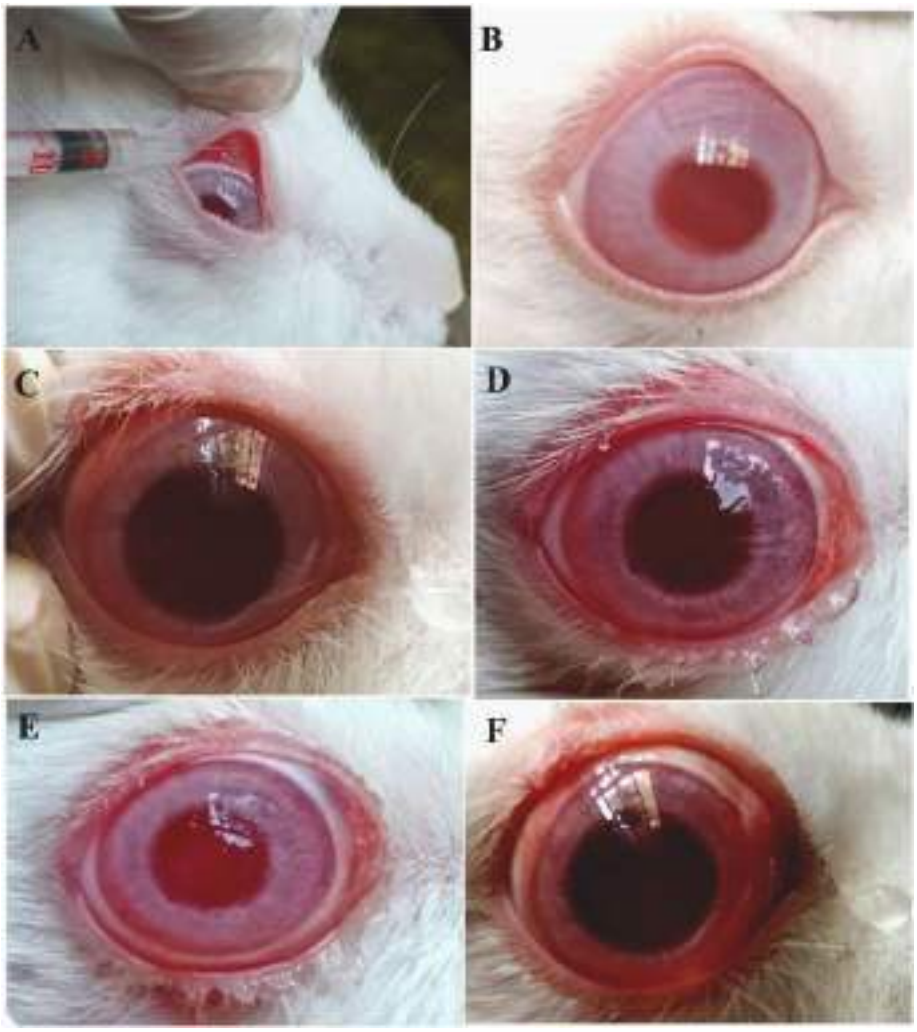

Fig. 6. Carrageenan injection into the subconjunctiva of rabbit eye (A); Normal rabbit eye (B); Conjunctival redness, swelling and watery eye developed after 30 min (C); TRZ in-situ gel was applied to the cul-de-sac prophylactically, mild inflammation observed initially (D); and after 30 min reduced inflammation (E); inflammation persisted after 2 h without applying in-situ gel (F).

system exhibited a sustained type of sequence as: $TgB_0 < TgB_{2.0} < TgB_{0.5} < TgB_{1.0}$.

3.8. Ex vivo corneal permeation

Goat cornea is the most commonly used ex-vivo model, because it is almost similar to human eye [33,46]. Corneal permeation study of in-situ gel was carried out for 6 h through goat cornea and presented as the percentage permeated vs. time curve in Fig. 5B. Ex vivo permeation study also extended more in the presence of bentonite (79–83 % in 6 h) rather than its absence in the formulation (TgB_0: 78 % in 3 h). $TgB_{1.0}$ sol has most been extended beyond 6 h with 32.6 % permeation in 1 h rather than other formulations. The order of amount permeated is mentioned as: $TgB_0 > TgB_{2.0} > TgB_{0.5} > TgB_{1.0}$. The interaction of TRZ bentonite nanoplatelets in the polymer matrix might have prolonged the corneal permeation following the similar mechanism as in in vitro release.

The kinetic models (Higuchi, Korsmeyer-Peppas, and Peppas-Sahlin models) were applied to estimate mechanism of TRZ release and corneal permeation of the sol formulation (Table 2). All formulations exhibited diffusion-controlled drug release as well as permeation as investigated using Higuchi model fitting ($r^2 = 0.901–0.986$). The release and permeation exponent as per Peppas model also justifies the same diffusion-controlled Fickian pattern ($n < 0.5$) without any erosion process ($n = 0.199–0.486$). According to the Peppas-Sahlin model k_1 is greater than k_2 demonstrating the release pattern of Fickian diffusion process.

Flux (J_s) was determined from the slope of the linear part of amount permeated per unit area vs. time plot. The permeability coefficient (Pgel) was evaluated from the steady state flux value and the TRZ concentration in the donor compartment ($Pgel = Js/C_{donor}$). Both the J_s

Table 4
Molecular docking study and interaction analysis of compex_1 (HPMC-B-TRZ-POL) and HPMC-TMZ-POL, in order to validate the drug delivery potency on a computational platform.

Sl. No.	Docking score of complexes (with and without Bentonite)	Some individual interactions	Docking score	Number of H-bonds (bond length (Å)
1	Complex_1 (HPMC-TRZ-B- POL) 5.13 kcal/mol	TRZ- B	−4.39	3 (2.14, 2.20, 2.23)
		B-HPMC	−3.48	2 (1.90, 2.01)
		B- POL	−1.81	1 (1.81)
2	Complex_2 (HPMC-TRZ- POL) -3.99 kcal/mol	TRZ- HPMC	−3.13	3 (1.84, 1.91, 1.95)
		TRZ- POL	−2.51	2 (1.91, 2.23)
		HPMC- POL	−0.41	1 (2.07)

and Pgel were decreased in presence of bentonite (Table 2).

Relationship of drug release and ocular tissue permeation exhibited a linear Level A correlation (Fig. 5C). A mean diagram of experiential vs. calculated permeability demonstrated the prediction's limitations depicted in Fig. 5D. Good linear correlation (r^2 = 0.9246 to 0.9972) warrants the reliability in ocular permeation. Permeation coefficients of $TgB_{0.5}$, $TgB_{2.0}$, and $TgB_{1.0}$ varied significantly from TgB_0 when compared pairwise by statistical testing (Table 3). The results indicated that the bentonite influenced a sustained effect on TRZ ocular delivery via sol-to-gel transformation.

3.9. In-vivo anti-inflammation study

Carrageenan is a well-known cytokine-mediated acute ocular inflammation model. Freund's adjuvant used to create chronic inflammation can persist up to fourteen days, but carrageenan-induced animal can be recovered in 24 h [29]. After 1 h of the injection of carrageenan in the eye of placebo group, watery eye with frequent lacrimation, swelling and reddening of the conjunctiva was observed (Fig. 6C). Normal eyes with no symptoms of inflammation were utilized as controls (Fig. 6B). After treatment with $TgB_{1.0}$ prophylactically in the test group (Fig. 6D) redness has very mildly observed and inflammation has almost been vanished within 2 h (Fig. 6E). Inflammatory markers such PDCD4, NF-kB, and TNF-α were shown to decrease by about 40 % after treatment with TRZ in the Guangzhou Bama miniature pig model of coronary artery micro embolism [47]. TRZ reduces the release of serum inflammatory mediators i.e., IL-1, IL-6, and also decreases the production of inflammatory cytokines during ischemia and inflammation [1,48]. In a report Wan et al. (2017) described that TRZ reduced caspase-8 dependent inflammatory reactions both in vivo and in vitro, which was studied by using ELISA and real time PCR [2]. Anti-inflammatory effect of drug was characterized by using rabbit eye model in many published reports [33,49,50]. Prophylactic treatment with TRZ has a significant role in decreasing inflammatory cytokine TNF-α, IL-1β and ROS production in the eye, and is likely the reason of reducing the course of ocular inflammation [2,5,51].

3.10. Docking

Bioinformatic tools are widely utilized by academic and industrial scientists to gain more fundamental knowledge as well as to reduce costs and experiments through early guidance. Based on docking results, complex_1 (HPMC-TRZ-B- POL) or formulation with bentonite showed stronger binding affinity (−5.13 kcal/mol) than complex_2 (HPMC-TRZ-POL) with docking scores of −3.99 kcal/mol or without bentonite formulation (Table 4). The individual interaction studies indicated that TRZ strongly interacted with bentonite (−4.39 kcal/mol) than B-HPMC (−3.39 kcal/mol) and B-POL (−1.81 kcal/mol) respectively (Table 4 and Fig. 7). POL exhibited the least interaction with TRZ with a score of −2.51 kcal/mol. Recorded docking score (−0.41 kcal/mol) indicated no significant interaction between HPMC-POL (Table 4).

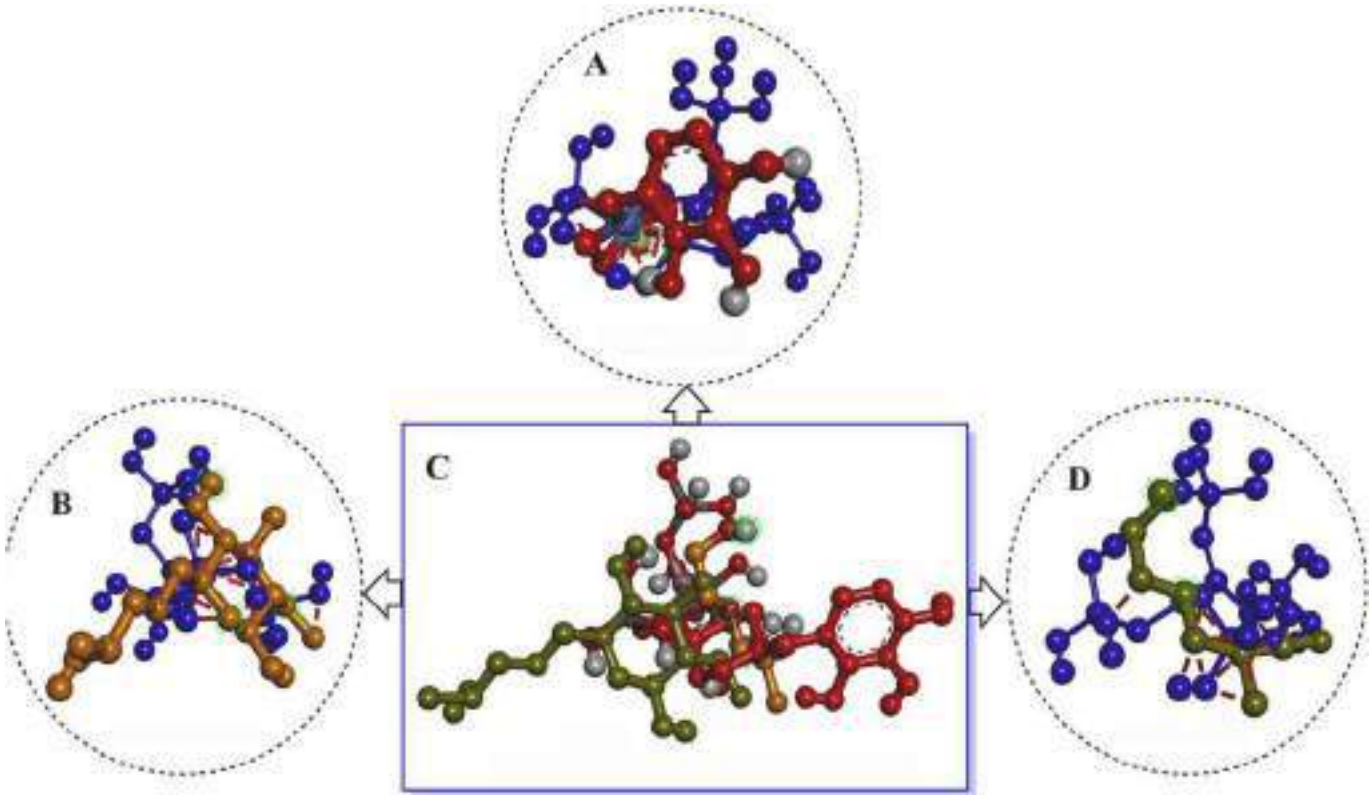

Fig. 7. Molecular docking interaction of complex_1 (HPMC-TRZ-B- POL) with individuals B-TRZ (A), B-HPMC (B), HPMC-TRZ-B- POL (C), B- POL (D) respectively. The image was generated by BIO-DSV software.

In summary, presence of bentonite provided more potential in sustaining the drug release from the sol-gel formulation. The computational analyses also supported the above results. Molecular docking study represented the interactions in a realistic manner with bioinformatic tools helping to elaborate in a theoretical perspective.

4. Conclusion

Bentonite clay incorporated hydroxypropyl methylcellulose-POL based topical delivery has been developed for studying the effect of bentonite on ophthalmic delivery of TRZ via sol-to-gel transformation and monitoring of anti inflammatory potential. The inclusion of HPMC in the composition lowered the concentration of POL, modulated the gelation temperature (33 °C) under physiological conditions, and also contributed to the formulations' viscoelastic performance. FTIR, DSC, and XRD studies confirmed the presence of TRZ in almost amorphous form of the drug in the in-situ gel formulation. $TgB_{1.0}$ sol containing TRZ: B ratio of 1:0.00001 showed 83 % of TRZ permeation across the cornea over a period of 6 h. Shear thinning and viscoelastic behavior of the formulation may facilitate smooth spreading on the epithelial surface and enhance precorneal residence time. Developed bentonite incorporated in-situ gel formulation could be utilized for the management of prevention of ocular inflammation.

CRediT authorship contribution statement

Rakesh Swain: Conceptualization, data curation, Investigation, Formal analysis, writing-original draft. **Souvik Nandi:** assisted during the in vivo, and ex vivo studies. **Shasank Sekhar Swain**: assisted in molecular docking study. **Krushna Prasad Pattanaik:** helped during the in vitro, and ex vivo studies. **Sujata mohapatra:** review and edit the manuscript. **Dhananjay Panigrahi:** assisted during the in vivo, ex vivo studies. **Subrata Mallick:** Conceptualization, Formal analysis, Writing-review & editing, Supervision. All authors have read and agreed to the final version of the manuscript.

Declaration of competing interest

The authors declare that they have no known competing financial interests or personal relationships that could have appeared to influence the work reported in this paper.

Acknowledgments

The authors are thankful to DST, New Delhi, for the award of Junior and Senior Research Fellowships to Rakesh Swain (IF 180581). The authors are acknowledging to the President, Siksha O Anusandhan (Deemed to be University) for support. Medley Pharmaceutical Ltd. and Ready's Laboratory are also gratefully acknowledged for gift sample of trimetazidine, and Poloxamer 407 & HPMC K15M respectively.

References

[1] X. Zhou, C. Li, W. Xu, J. Chen, Trimetazidine protects against smoking-induced left ventricular remodeling via attenuating oxidative stress, apoptosis, and inflammation, PloS one 7 (7) (2012) 40424.
[2] P. Wan, W. Su, Y. Zhang, Z. Li, C. Deng, Y. Zhuo, Trimetazidine protects retinal ganglion cells from acute glaucoma via the Nrf2/Ho-1 pathway, Clin. Sci. 131 (18) (2017) 2363–2375.
[3] A. Danikiewicz, J. Szkodziński, B. Hudzik, I. Korzonek-Szlacheta, M. Gąsior, B. Zubelewicz-Szkodzińska, Effects of trimetazidine on interleukin-2 and interleukin-8 concentrations in patients with coronary artery disease, Can. J. Physiol. Pharmacol. 95 (6) (2017) 759–762.
[4] F.M. Williams, K. Tanda, M. Kus, T.J. Williams, Trimetazidine inhibits neutrophil accumulation after myocardial ischaemia and reperfusion in rabbits, J. Cardiovasc. Pharmacol. 22 (6) (1993) 828–833.
[5] L. Argaud, L. Gomez, O. Gateau-Roesch, E. Couture-Lepetit, J. Loufouat, D. Robert, M. Ovize, Trimetazidine inhibits mitochondrial permeability transition pore opening and prevents lethal ischemia–reperfusion injury, J. Mol. Cell. Cardiol. 39 (6) (2005) 893–899.
[6] A. Özden, Z. Aybek, N. Saydam, N. Calli, O. Saydam, E. Düzcan, G. Güner, Cytoprotective effect of trimetazidine on 75 min warm renal ischemia-reperfusion injury in rats, Eur. Surg. Res. 30 (4) (1998) 227–234.
[7] C. Tetik, A. Özden, N. Çalli, A. Bilgihan, B. Bostanci, Ö. Yis, H. Bayramoğlu, Cytoprotective effect of trimetazidine on 60 minutes of intestinal ischemia-reperfusion injury in rats, Transpl. Int. 12 (2) (1999) 108–112.
[8] E.C. Tsimoyiannis, K.J. Moutesidou, C.M. Moschos, M. Karayianni, S. Karkabounas, O.B. Kotoulas, Trimetazidine for prevention of hepatic injury induced by ischaemia and reperfusion in rats, Eur. J. Surg. 159 (2) (1993) 89–93.
[9] P. Chrusciel, J. Rysz, M. Banach, Defining the role of trimetazidine in the treatment of cardiovascular disorders: some insights on its role in heart failure and peripheral artery disease, Drugs 74 (9) (2014) 971–980.
[10] S. Mohand-Said, A. Jacquet, A. Lucien, M.A. Espinasse-Berrod, M.F.C. De Silva, J. Sahel, Protective effect of trimetazidine in a model of ischemia-reperfusion in the rat retina, Ophthalmic Res. 34 (5) (2002) 300–305.
[11] K. Kaszuba-Bartkowiak, M.S. Nowak, P. Jurowski, R. Goś, The role of trimetazidine in the protection of the retina, Arch. Med. Sci. Spec.Issues 2007 (3) (2007), 66-66.
[12] Y. Mun, J.S. Hwang, Y.J. Shin, Role of neutrophils on the ocular surface, Int. J. Mol. Sci. 22 (19) (2021) 10386.
[13] S. Kumar, R. Karki, M. Meena, T. Prakash, T. Rajeswari, D. Goli, Reduction in drop size of ophthalmic topical drop preparations and the impact of treatment, J. Adv. Pharm. Technol. Res. 2 (3) (2011) 192.
[14] M.N. O'Brien Laramy, K. Nagapudi, Long-acting ocular drug delivery technologies with clinical precedent, Expert Opin. Drug Deliv. 19 (2022) 1285–1301.
[15] J.B. da Silva, M.T. Cook, M.L. Bruschi, Thermoresponsive systems composed of poloxamer 407 and HPMC or NaCMC: mechanical, rheological and sol-gel transition analysis, Carbohydr. Polym. 240 (2020), 116268.
[16] H. Almeida, M.H. Amaral, P. Lobão, J.M. Sousa Lobo, Applications of poloxamers in ophthalmic pharmaceutical formulations: an overview, Expert Opin. Drug Deliv. 10 (9) (2013) 1223–1237.
[17] A. Tatke, N. Dudhipala, K.Y. Janga, S.P. Balguri, B. Avula, M.M. Jablonski, S. Majumdar, In situ gel of triamcinolone acetonide-loaded solid lipid nanoparticles for improved topical ocular delivery: tear kinetics and ocular disposition studies, Nanomaterials 9 (1) (2018) 33.
[18] C. Jumelle, S. Gholizadeh, N. Annabi, R. Dana, Advances and limitations of drug delivery systems formulated as eye drops, J. Control. Release 321 (2020) 1–22.
[19] J. Chen, R. Zhou, L. Li, B. Li, X. Zhang, J. Su, Mechanical, rheological and release behaviors of a poloxamer 407/poloxamer 188/carbopol 940 thermosensitive composite hydrogel, Molecules 18 (10) (2013) 12415–12425.
[20] W. Wang, P.C. Hui, E. Wat, F.S. Ng, C.W. Kan, X. Wang, E.C. Wong, H. Hu, B. Chan, C.B. Lau, P.C. Leung, In vitro drug release and percutaneous behavior of poloxamer-based hydrogel formulation containing traditional Chinese medicine, Colloids Surf. B. 148 (2016) 526–532.
[21] X. Wang, X. Hou, P. Zou, A. Huang, M. Zhang, L. Ma, Cationic starch modified bentonite-alginate nanocomposites for highly controlled diffusion release of pesticides, Int. J. Biol. Macromol. 213 (2022) 123–133.
[22] H. Zhang, Y. Shi, X. Xu, M. Zhang, L. Ma, Structure regulation of bentonite-alginate nanocomposites for controlled release of imidacloprid, ACS Omega 5 (17) (2020) 10068–10076.
[23] X. Zheng, M. Xu, S. Yang, S. Omonov, S. Huang, J. Zhao, H. Ruan, M. Zeng, Novel bio-inspired three-dimensional nanocomposites based on montmorillonite and chitosan, Int. J. Biol. Macromol. 165 (2020) 2702–2710.
[24] A. Papagiannopoulos, S.P. Nikolakis, A. Pamvouxoglou, E. Koutsopoulou, Physicochemical properties of electrostatically crosslinked carrageenan/chitosan hydrogels and carrageenan/chitosan/Laponite nanocomposite hydrogels, Int. J. Biol. Macromol. 225 (2023) 565–573.
[25] D. Hou, R. Gui, S. Hu, Y. Huang, Z. Feng, Q. Ping, Preparation and characterization of novel drug-inserted-montmorillonite chitosan carriers for ocular drug delivery, Adv. Nano Res. 4 (03) (2015) 70.
[26] G.V. Joshi, B.D. Kevadiya, H.A. Patel, H.C. Bajaj, R.V. Jasra, Montmorillonite as a drug delivery system: intercalation and in vitro release of timolol maleate, Int. J. Pharm. 374 (1–2) (2009) 53–57.
[27] K.P. Behera, D. Qureshi, B. Mohanty, S.K. Habibullah, A. Anis, H. Shaikh, P. Sarkar, S. Verma, K. Pal, Bentonite increases the corneal permeation of the drug from the tamarind gum hydrogels, in: Food, Medical, And Environmental Applications of Polysaccharides, 2021, pp. 291–322.
[28] I.R. Schmolka, Artificial skin I. Preparation and properties of pluronic F-127 gels for treatment of burns, J. Biomed. Mater. Res. 6 (6) (1972) 571–582.
[29] S. Nandi, A. Ojha, A. Nanda, R.N. Sahoo, R. Swain, K.P. Pattnaik, S. Mallick, Vildagliptin plasticized hydrogel film in the control of ocular inflammation after topical application: study of hydration and erosion behavior, Z. Phys. Chem. 236 (2) (2022) 275–290.
[30] M.S. Shahab, M. Rizwanullah, S. Alshehri, S.S. Imam, Optimization to development of chitosan decorated polycaprolactone nanoparticles for improved ocular delivery of dorzolamide: in vitro, ex vivo and toxicity assessments, Int. J. Biol. Macromol. 163 (2020) 2392–2404.
[31] M.K. Pathak, G. Chhabra, K. Pathak, Design and development of a novel pH triggered nanoemulsified in-situ ophthalmic gel of fluconazole: ex-vivo transcorneal permeation, corneal toxicity and irritation testing, Drug Dev. Ind. Pharm. 39 (5) (2013) 780–790.
[32] A. Nanda, R.N. Sahoo, A. Pramanik, R. Mohapatra, S.K. Pradhan, A. Thirumurugan, D. Das, S. Mallick, Drug-in-mucoadhesive type film for ocular anti-inflammatory potential of amlodipine: effect of sulphobutyl-ether-beta-cyclodextrin on permeation and molecular docking characterization, Colloids Surf. B. 172 (2018) 555–564.

[33] A. Pramanik, R.N. Sahoo, A. Nanda, R. Mohapatra, R. Singh, S. Mallick, Ocular permeation and sustained anti-inflammatory activity of dexamethasone from kaolin nanodispersion hydrogel system, Curr. Eye Res. 43 (6) (2018) 828–838.
[34] E.H. Fini, B. Høgsaa, J.D.C. Christiansen, C.G. Sanporean, E.A. Jensen, M. Mousavi, F. Pahlavan, Multiscale investigation of a bioresidue as a novel intercalant for sodium montmorillonite, J. Phys. Chem. C 121 (3) (2017) 1794–1802.
[35] S.S. Swain, S.K. Paidesetty, B. Dehury, M. Das, S.C. Vedithi, R.N. Padhy, Computer-aided synthesis of dapsone-phytochemical conjugates against dapsone-resistant Mycobacterium leprae, Sci. Rep. 10 (1) (2020) 6839.
[36] N. Patel, V. Thakkar, V. Metalia, L. Baldaniya, T. Gandhi, M. Gohel, Formulation and development of ophthalmic in situ gel for the treatment ocular inflammation and infection using application of quality by design concept, Drug Dev. Ind. Pharm. 42 (9) (2016) 1406–1423.
[37] A. Chiş, I. Kacsó, G. Borodi, I. Bratu, Complexul de incluziune al trimetazidinei Cu β-cyclodextrina, Clujul Med. 84 (2) (2011) 184–187.
[38] S. Mandal, S.S. Kumar, B. Krishnamoorthy, S.K. Basu, Development and evaluation of calcium alginate beads prepared by sequential and simultaneous methods, Braz. J. Pharm. Sci. 46 (2010) 785–793.
[39] V.T. Farmer, J.D. Russell, The infra-red spectra of layer silicates, Spectrochim. Acta 20 (7) (1964) 1149–1173.
[40] M. Alshabanat, A. Al-Arrash, W. Mekhamer, Polystyrene/montmorillonite nanocomposites: study of the morphology and effects of sonication time on thermal stability, J. Nanomater. 2013 (2013), 9-9.
[41] H.M. El-Nahas, K.M. Hosny, Chitosan-based floating microspheres of trimetazidin dihydrochloride; preparation and in vitro characterization, Indian J. Pharm. Sci. 73 (4) (2011) 397.
[42] A.A. Matloub, M.M. AbouSamra, A.H. Salama, M.Z. Rizk, H.F. Aly, G.I. Fouad, Cubic liquid crystalline nanoparticles containing a polysaccharide from Ulva fasciata with potent antihyperlipidaemic activity, Saudi Pharm J. 26 (2) (2018) 224–231.
[43] J.B. Dressman, J. Krämer (Eds.), Pharmaceutical Dissolution Testing (No. 21892), Taylor & Francis, Boca Raton, FL, 2005, pp. 4–15.
[44] V. Gugleva, S. Titeva, N. Ermenlieva, S. Tsibranska, S. Tcholakova, S. Rangelov, D. Momekova, Development and evaluation of doxycycline niosomal thermoresponsive in situ gel for ophthalmic delivery, Int. J. Pharm. 591 (2020), 120010.
[45] P.H. Chang, W.T. Jiang, B. Sarkar, W. Wang, Z. Li, The triple mechanisms of atenolol adsorption on ca-montmorillonite: implication in pharmaceutical wastewater treatment, Materials 12 (18) (2019) 2858.
[46] S. Sengupta, P. Dhanapal, M. Nath, A. Haripriya, R. Venkatesh, Goat's eye integrated with a human cataractous lens: a training model for phacoemulsification, Indian J. Ophthalmol. 63 (3) (2015) 275.
[47] Q. Su, L. Li, J. Zhao, Y. Sun, H. Yang, Effects of trimetazidine on PDCD4/NF-κB/TNF-α pathway in coronary microembolization, Cell. Physiol. Biochem. 42 (2) (2017) 753–760.
[48] S. Balamurugan, D. Das, M. Hasanreisoglu, B.C. Toy, M. Akhter, V.K. Anuradha, E. Anthony, B. Gurnani, K. Kaur, Interleukins and cytokine biomarkers in uveitis, Indian J. Ophthalmol. 68 (9) (2020) 1750.
[49] P.M. Gaafar, O.Y. Abdallah, R.M. Farid, H. Abdelkader, Preparation, characterization and evaluation of novel elastic nano-sized niosomes (ethoniosomes) for ocular delivery of prednisolone, J. Liposome Res. 24 (3) (2014) 204–215.
[50] A. Nanda, S. Das, R.N. Sahoo, S. Nandi, R. Swain, S. Pattanaik, D. Das, S. Mallick, Aspirin–hydrogel ocular film for topical delivery and ophthalmic anti-inflammation, J. Serb. Chem. Soc. 87 (7–8) (2022) 829–843.
[51] G.D. Lopaschuk, R. Barr, P.D. Thomas, J.R. Dyck, Beneficial effects of trimetazidine in ex vivo working ischemic hearts are due to a stimulation of glucose oxidation secondary to inhibition of long-chain 3-ketoacyl coenzyme a thiolase, Circ. Res. 93 (3) (2003) 33–e37.

International Journal of Pharmaceutics 642 (2023) 123153

Contents lists available at ScienceDirect

International Journal of Pharmaceutics

journal homepage: www.elsevier.com/locate/ijpharm

Ocular delivery of felodipine for the management of intraocular pressure and inflammation: Effect of film plasticizer and in vitro in vivo evaluation

Rakesh Swain, Ankita Moharana, Sk Habibullah, Souvik Nandi, Anindya Bose, Sujata Mohapatra, Subrata Mallick *

Department of Pharmaceutics, School of Pharmaceutical Sciences, Siksha 'O' Anusandhan (Deemed to be University), Bhubaneswar, Odisha, India

ARTICLE INFO

Keywords:
Intraocular pressure
Glaucoma
Inflammation
Ocular delivery
In vitro in vivo correlation

ABSTRACT

Glaucoma may cause irreversible eyesight loss and damage to the optic nerve. Trabecular meshwork obstruction may raise intraocular pressure (IOP) in open-angle and/or closed-angle type inflammatory glaucoma. Ocular delivery of felodipine (FEL) has been undertaken for the management of intraocular pressure and inflammation. FEL film was formulated using different plasticizers, and IOP has been assessed using a normotensive rabbit eye model. Ocular acute inflammation induced by carrageenan has also been monitored. Drug release has been enhanced significantly (93.9 % in 7 h) in the presence of DMSO (FDM) as a plasticizer in the film compared to others (59.8 to 86.2 % in 7 h). The same film also exhibited the highest ocular permeation of 75.5 % rather than others (50.5 to 61.0 %) in 7 h. Decreased IOP was maintained up to 8 h after ocular application of FDM compared to the solution of FEL only up to 5 h. Ocular inflammation has almost been disappeared within 2 h of using the film (FDM), whereas inflammation has been continued even after 3 h of the induced rabbit without film. DMSO plasticized felodipine film could be used for the better management of IOP and associated inflammation.

1. Introduction

Glaucoma is a multifactorial neurodegenerative disorder with several forms that may cause irreversible eyesight loss and harm to both the optic nerve axons and retinal ganglion cells (Caprioli and Coleman, 2008; Holappa et al., 2020; Tabak et al., 2021a; Tham et al., 2014). Activation of the mineralocorticoid receptor (MR) can enhance the production of aqueous humor with trabecular meshwork cell swelling causing retention of aqueous humor and increasing IOP (May 2012; Mirshahi et al., 1997). Treatment in the right direction is known to be effective in slowing the progression of the disease. Spironolactone (MR antagonist) intra-vitreous administion has been experimented to decrease IOP in the aldosterone-induced rabbit eye model (Langman et al., 2005; Stárka et al., 1981). Trabecular meshwork might be blocked in uveitic glaucoma, causing pain and blurred vision (Hawkins; Tabak et al., 2021b). IOP may also be elevated due to trabecular dysfunction of open-angle and/or closed-angle type inflammatory glaucoma. Trabecular obstruction due to inflammatory debris may rise in IOP (Sundmacher and Neumann-Haefelin, 1979). Increased IOP has also been observed in trabeculitis with edema of the meshwork in simplex keratouveitis. Scleritis, a painful ocular inflammation, also shows elevation in IOP (Chen et al., 1982). Moreover, oxidative stress is a factor in the onset and development of eye diseases, including glaucoma (Tabak et al., 2021b).

Ca^{++} ion channels are abundantly present on the surface of the cornea, conjunctiva, and corneal nerve fiber (Comes et al., 2021; Yang et al., 2022). Transient receptor potential ankyrin 1 (TRPA1) ion channels present in ocular surface cells play a key role in the pathogenesis of acute inflammation. TRPA1 is a possible therapeutic target for inflammatory fibrosis-related corneal lesions and ocular infections, which may result in vision loss if left untreated (Okada et al., 2015; Okada et al., 2022). Increased interleukin-18 (IL-18), having pro-inflammatory properties, acts as an immunomodulatory agent in chronic inflammation.

Felodipine (FEL), dihydropyridine calcium channel blocker showed anti-inflammatory effect in rat with fructose-induced metabolic syndrome by down-regulating serum IL-18 levels (Bi et al., 2009). In some previous studies cardiovascular protection has been supported by FEL (Hishikawa and Lüscher, 1998; Sugawara et al., 1996). FEL also exhibited cardio-protective activity against doxorubicin-induced cardiotoxicity (Gandhi et al., 2013).

Felodipine, being a mineralocorticoid antagonist supposed to

* Corresponding author at: School of Pharmaceutical Sciences, Siksha O Anusandhan (Deemed to be University), Bhubaneswar 751003, Odisha, India.
E-mail addresses: subratamallick@soa.ac.in, profsmallick@gmail.com (S. Mallick).

https://doi.org/10.1016/j.ijpharm.2023.123153
Received 14 February 2023; Received in revised form 14 June 2023; Accepted 15 June 2023
Available online 18 June 2023

Table 1
Physicochemical properties of felodipine HPMC matrix films incorporating different plasticizers (mean ± sd; n ≥ 3).

Film code	Plasticizer (20 %)	Thickness (μm)	Folding endurance	Surface pH	Moisture Content (%)	Moisture uptake (%) at RH 75%	Felodipine content (%)
FTE	TEC	157.6 ± 6.6	>200	7.14 ± 0.04	4.12 ± 0.07	5.37 ± 0.56	9.13 ± 0.13
FTA	TA	177.6 ± 4.5	>200	7.14 ± 0.03	3.85 ± 0.43	6.07 ± 0.57	9.41 ± 0.22
FPG	PGD	150.3 ± 8.5	>200	7.23 ± 0.02	3.81 ± 0.64	6.58 ± 0.72	9.12 ± 0.18
FPE	PEG	159.3 ± 7.4	>200	7.11 ± 0.02	4.05 ± 0.27	7.80 ± 0.17	9.04 ± 0.14
FDM	DMSO	155.3 ± 8.4	>200	7.21 ± 0.03	5.38 ± 0.28	8.37 ± 0.56	9.50 ± 0.15

[a]FTE = [b]TEC; [a]FTA= [b]TA; [a]FPG= [b]PGD; [a]FPE =[b]PEG; [a]FDM= [b]DMSO, [a]Formulation code, [b]Used plasticize.

decrease not only the IOP but also ocular anti-inflammatory activity after topical application (Qi et al., 2017). Recently, the anti-inflammatory property of calcium channel blockers has been revealed by several studies (Ishida et al., 2010; Nanda et al., 2018). Ocular anti-inflammatory effect of HPMC-based amlodipine film has been studied after topical application (Nanda et al., 2018). Nilvadipine, a CCB, has inhibited the pathogenesis of ocular inflammation when given intra-peritoneal injection (Ishida et al., 2010). Li et al., 2021 developed a nimodipine micelle ophthalmic solution to treat glaucoma (Li et al., 2021). In another study by Maria et al., 2017 nimodipine topical ocular delivery was used successfully for the management of glaucoma (Maria et al., 2017). Topical administration of verapamil a CCB in to the human eye reported to show lowering of intraocular pressure (Shayegan et al., 2009). Hence, ocular delivery of FEL is supposed to be useful for simultaneously monitoring intraocular pressure and ocular inflammation.

FEL exhibits very low oral bioavailability of only 15 % due to poor water solubility and rapid hepatic first-pass metabolism. Several promising research reports are available for improving oral bioavailability of the drug (Luo et al., 2014; Sayed et al., 2018; Shah et al., 2014). The addition of plasticizer in many film-type delivery systems improved physicochemical properties and as-well-as bio-adhesion for better absorption potential (Ben-Yaakov, 2007). Triethyl citrate incorporation enhanced mechanical properties of the polymeric film along with drug release (Jennings et al., 2016). Triacetin incorporated poly (ethylene oxide) transmucosal film exhibited improved drug release (Thumma et al., 2008). Propylene glycol dicaprylate is reported as the skin penetration-enhancing agent (Matsui et al., 2015). PEG 600 in some polymer-based transdermal film is also known to increase the release of drug (Pivsa-Art et al., 2016). DMSO containing transdermal film, moreover showed improved drug release and skin permeation of valsartan (Luqman, 2012; Panda et al., 2020).

Ocular delivery of felodipine has been undertaken for monitoring of both intraocular pressure and carrageenan-induced ocular inflammation applying film formulation topically. The effect of triethyl citrate (TEC), triacetin (TA), propylene glycol dicaprylate (PGD), polyethylene glycol 600 (PEG), or dimethyl sulphoxide (DMSO) as plasticizer has also been studied. Ocular delivery of FEL film for simultaneous monitoring of intraocular pressure and ocular inflammation has rarely been reported earlier.

2. Materials

Felodipine was obtained from Dr. Reddy's Laboratories (Hyderabad, India). Hydroxypropyl methylcellulose K100M: 100,000 cPs (HPMC) was supplied by Burgoyne and Co (Mumbai, India). Triethyl citrate, triacetin, propylene glycol dicaprylate, polyethylene glycol 600 (PEG 600), PEG 6000, and di-methyl sulphoxide (DMSO) were purchased from Merk Pvt Ltd. (Mumbai, India). All the reagents used in the experiment were of analytical grade. Throughout the experiments, double distilled water was used.

2.1. Animals

Nine white New Zealand rabbits (sex: male; age: four to six months; weight: 2 to 2.5 kg) without any eye problems, including glaucoma, were identified for the present study. Rabbits were placed in a lab environment for one day before the start of the study. The animal experiment was carried out after being approved by the Institutional Animal Ethical Committee [IAEC/SPS/SOA/18/2020]. Guidelines were followed during the animal handling procedure made by CPCSEA (Committee for the Purpose of Control and Supervision of Experiments on Animals) and complied with the ARRIVE (Animal Research: Reporting of In Vivo Experiments) guiding principle. Animals were kept in 12 h light and dark circles with temperature of ~ 25 °C and ~ 50 % relative humidity giving free access to food and water (Hou et al., 2020).

2.2. Felodipine film preparation

Felodipine films were formulated using HPMC as the matrix polymer by solvent casting technique (Table 1). HPMC (1000 mg) was dispersed in 35 ml of water in one 100 ml beaker and, left for about 24 h at around 4–8 °C for hydration. Plasticizer (20 % w/w of HPMC) was then combined into the hydrated gel with constant stirring (40–50 rpm). Drug solution in ethanol (120 mg in 10 ml) was added to the polymeric mixture with continuous stirring magnetically (40–50 rpm) for 2–3 h at room temperature (25 – 30 °C). After that, the clear polymeric homogeneous jelly liquid was poured into the Petri dish and dried out at 40 °C till steady weight was achieved. The prepared film was protected inside an airtight closed glass container till further evaluation. The thickness of the film was calculated using a digital micrometer (Mitutoyo, Japan) at five different positions, and the mean value was calculated. Folding endurance was assessed by repeatedly folding a section of the film till it cracked at the point of folding or folded up to 200 times. A piece of the film (~2 cm × 2 cm) was positioned in a Petri dish and moistened with 1 ml of distilled H_2O for 10 min. The glass electrode was dipped into the swelled portion of the film formulation, and surface pH was noted.

2.3. Moisture content and moisture uptake

A small piece (~2 cm × 2 cm) of the prepared film was weighed (W_1) and positioned over the activated silica in a desiccator for 24 h or more until it showed a constant weight (W_2). Moisture content was evaluated by applying the equation:

$$\frac{(W_1 - W_2)}{W_2} * 100$$

Moisture uptake was investigated by the dried film was placed in a closed desiccator maintaining 75% relative humidity (maintained over sodium chloride supersaturated solution) until a constant weight was attained. The difference between final to initial weight divided by initial weight and multiplied by 100 was calculated and tabulated in Table 1.

2.4. Drug content determination

Exactly weighed film piece (25–41 mg) was dissolved in the volumetric flask containing 100 ml of phosphate buffer solution (pH 6.8 and Sodium lauryl sulfate (SLS) 0.5 %) with constant mechanical stirring and sonicated for an additional 1 h for complete extraction of drug. This test was repeated at least three times to get the mean value for each

formulation. The drug content of the filtered solution was analyzed using UV–Vis spectrophotometer (Shimadzu, 1900i, Japan) at 240 nm. Standard curve of felodipine in phosphate buffer solution (pH 6.8 and SLS 0.5 %) was prepared a serial concentration of 1 – 10 μg/ml. UV scanning of the drug solution at 200 to 400 nm was carried out in the same UV–Vis spectrophotometer. The λmax was noted as 240 nm and utilized for drug content estimation.

2.5. FTIR spectroscopy

FTIR study was executed to assess any possible interactions that might have occurred between the drugs with other components of the prepared films. Scanning was done using FTIR Spectrophotometer (JASCO FT/IR-4100, Japan) in frequency of the wave range from 600 to 4000 cm^{-1}.

2.6. Differential scanning calorimetry

Whole process of DSC (DSC-1, Mettler Toledo) was carried out in a nitrogen environment to ensure inertness between drug and excipients. Temperature range was fixed to 30–250 °C with a heating rate of 10 °C/min.

2.7. X-ray diffractometry

The powder XRD (Rigaku, Ultima IV) with a Cu X-ray supply emission range of 1.5406 was used to record the diffraction pattern of the felodipine films. A scan speed of 1° per minute was used for recording the diffraction (2θ) in the range of 5 to 50°.

2.8. SEM

Gold-coated formulation for SEM analysis was used by applying a voltage of 5–15 kv (ZEISS, GEMINI SEM 300), and the photomicrographs were captured.

2.9. Mechanical properties

Universal testing machine (Tinius Olsen H50KS) was used for determining mechanical properties of the films. Prepared films were uniformly sized and sliced into the dog bone shape, and average thickness was determined. Tensile strength, strain at break, % elongation, Young's modulus (elastic modulus), surface energy, toughness, and the ratio of tensile strength to Young's modulus were computed as the data generated by the machine till the film was broken. Elastic modulus was calculated from the linear regression slope of the stress vs strain curves. The maximum strength used to stretch before necking or rupture is recorded as tensile strength (MPa). Percentage of elongation (ε) is defined as the increase in length relative to the original length L_o.

$$\varepsilon = \frac{L - L_0}{L_0}$$

Where, L = length under a given tensile stress.

Surface energy is calculated by tensile strength divided by Young's modulus. The area under the stress–strain curve is the energy or work necessary to break the polymeric material, which is termed as toughness (Hota et al., 2022).

2.10. Swelling index

Initial clean and dry slide weight was taken. A small piece of accurately weighed film (~2cm × 2 cm) over a glass slide was placed inside the Petri plate containing buffer (25 ml, pH 6.8 (0.2 M, prepared with disodium hydrogen phosphate and potassium dihydrogen phosphate) at ambient temperature. At specified time points (60, 120, 180, 240, 300, 360, 420, 480, and 540 min) the slide containing the sample was removed and reweighed (W_t) after wiping it carefully to remove excess fluid with tissue paper on the swelled film surface. This process was repeated at least for 3 films of each formulation, and mean ± S.D was determined. The swelling index was evaluated using the bellow equation:

$$SwellingIndex(\%) = \frac{W_t - W_0}{W_0} * 100$$

W_t = Swollen film weight at time t.
W_o = Initial weight of the film.

2.11. In-Vitro mucoadhesion

Formulation's mucoadhesion was calculated by CTX texture analyzer (Ametek Brookfield, United States) using a cylindrical probe (35 mm diameter) and 5 kg load cell against set gelatin (6.67 % w/v) as the adhesive surface. Phosphate buffer solution (pH 6.8; 500 μL) was spread uniformly over the surface of the gelatin to simulate ocular mucosa before the film contacted the gelatin gel (Boateng and Popescu, 2016; Tighsazzadeh et al., 2019). Each film was cut into circular discs (35 mm dia) attached to the tip of the cylinder probe and moved towards the Petri dish containing the gelatin gel at a force of 0.5 N for 120 sec to ensure complete contact. The mucoadhesion parameters, such as peak adhesion force (PAF), total work of adhesion (TWA), and cohesiveness (distance travelled by probe before detachment) of the films, were collected from the software (Texture Pro).

2.12. In-vitro drug release

USP II (Electrolab, dissolution tester USP, TDT06L) dissolution apparatus was utilized for performing the release study. Release medium consisting of 200 ml of phosphate buffer of pH 6.8 (0.2 M, prepared with disodium hydrogen phosphate and potassium dihydrogen phosphate, Merck Life Science Private Limited) and 0.5 % SLS. Release studies were carried out at 34 ± 0.2 °C temperature with 50 rpm. A small piece of accurately weighed film (25–42 mg) was glued on top of the glass slide with cyanoacrylate adhesive and placed at the base of the dissolution vessel. At regular time points (30, 60, 90, 120, 180, 240, 300, 360, and 420 min) sample of 10 ml was withdrawn using a syringe-driven filter (Membrane filter, 0.45 μm). Same volume was replenished with fresh medium. Samples were analysed spectrophotometrically (Shimadzu, 1900i, Japan) at 240 nm. The ratio between the absorbance and the slope obtained from the linear regression equation of the standard curve was calculated as FEL concentration.

2.13. Corneal permeation study

Within one hour of the sacrifice, the complete goat eyeballs were collected in the glass beaker filled with saline from the slaughterhouse and carefully cleaned with distilled H_2O, followed by phosphate buffer solution (PBS, pH 6.8). The cornea with the 5–6 mm of scleral tissue around the eyeball was carefully removed using forceps and scissors. It was then rinsed with enough phosphate buffer to remove all proteins and unnecessary tissues from the washings. Modified Franz diffusion apparatus was utilized for the process of permeation. Precisely measured quantity of film formulation (30–40 mg) was positioned such that the epithelial surface faced the donor compartment to allow the drug to permeate into the medium with an effective surface area of 1.56 cm^2. Simulated tear fluid (few ml) was added to the donor chamber to equilibrate the cornea for 10 min before starting the permeation experiment, and the equilibrium media was then removed from the chamber (Mehra et al., 2021). The receiver chamber was filled with 200 ml of PBS (pH 6.8) and 0.5 % SLS and was maintained at temperature of 34 ± 0.2 °C under the steady stirring rate of fifty rpm. At predetermined time points (30, 60, 90, 10, 180, 240, 300, 360, and 420 min) the sample of 10 ml was withdrawn by a syringe-driven filter (Membrane filter,

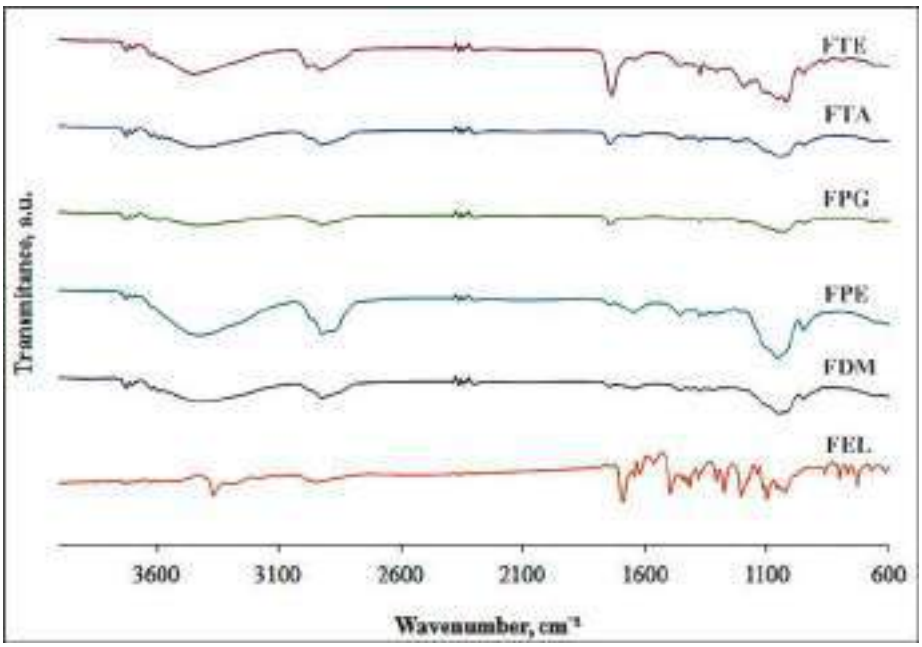

Fig. 1. FTIR spectrograms of pure drug and film formulations.

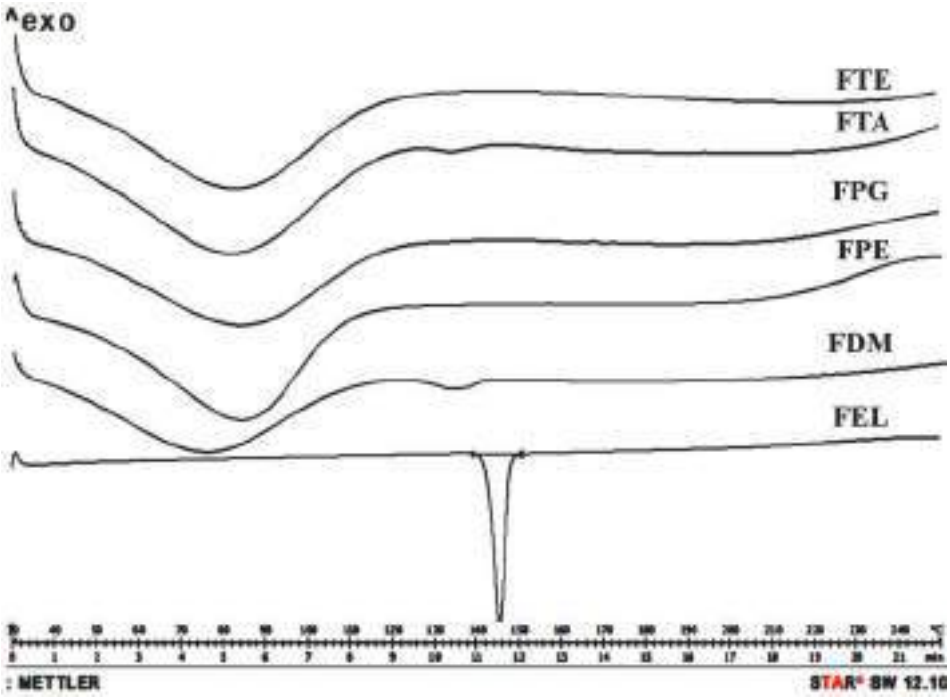

Fig. 2. DSC thermogram of pure drug (FEL) and formulated films.

0.45 μm) and replenished with an equal volume of fresh PBS. Then spectrophotometric analysis of the samples was carried out. A blank experiment was performed to eradicate any interference from the tissue. The experiment was performed 3 or more times, and the mean ± SD was recorded.

2.14. Kinetics

To determine the release and permeation mechanism of drug, Higuchi, Korsmeyer-Peppas model, and the Peppas-Sahlin model applied the *in-vitro* drug release and *ex-vivo* permeation data. The drug release kinetics by taking the linear relationship between the square root of time plot and the cumulative percent drug release was described by Higuchi. Peppas Sahlin model enables the evaluation of mathematical modelling (M) of each of the drug release mechanism through the constants k_1 and k_2. If $k_1 > k_2$, then the drug release follows Fickian diffusion. However, when k2 is greater than k1, the polymer chains relax first (Swain et al., 2023).

Higuchi Model:.$C = K\sqrt{t}$

C = Cumulative amount of drug release or permeation per unit area of the film; K = Higuchi release or permeation rate constant.

Korsmeyer- Peppas Model:

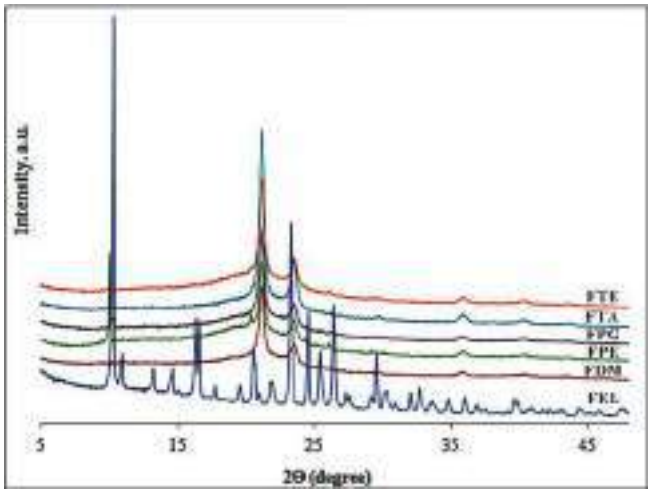

Fig. 3. XRD pattern of felodipine crystalline drug (FEL), and the plasticized film formulation.

$$\frac{C_t}{C_\infty} = Kt^n$$

C_t/C_∞ = at time t amount of drug release/permeation; k = Peppas release/permeation rate constant; n = exponent of release/permeation.

Peppas Sahlin model:

$$\frac{M_t}{M_\infty} = k_1 t^m + k_2 t^{2m}$$

M_t/M_∞ = Fraction dissolved, %; k_1 = Fickian kinetics constant; k_2 = Case-II relaxation kinetic constant; m = exponent of the diffusion.

2.15. Corneal hydration

The hydration levels of the cornea (HLC, %) were utilized to evaluate the corneal integrity throughout the study. Following completing the *ex-vivo* study, each cornel sample was removed from the sclera ring and weighed (W_w). Then the corneal selection was dried at 100 °C for six h to calculate the dry weight (W_d).

$$HLC(\%) = \left(1 - \frac{W_d}{W_w}\right) * 100$$

2.16. Ocular irritation test

In vivo, ocular irritation of film formulation was assessed in the rabbit eye model. The film was applied directly into the lower conjunctival sac. Fluorescein staining was used to examine the corneal epithelium's structural integrity at different time intervals (6 h, and 24 h) after the application of the film (Fang et al., 2021).

2.17. IOp

For the purpose of measuring the intraocular pressure of felodipine film formulation, the rabbits were divided into two groups, each with three rabbits. Proparacaine hydrochloride (Two drops, 0.5 % w/v, Alcaine) ophthalmic solution USP was used for local anaesthesia before 5 min of the study. Felodipine solution (0.5 %) was prepared in PEG 6000 solution (20 %) using sterile water for injection and terminally sterilized by filtration (Nylon-66, 0.2 μm, HIMEDIA, India) just before instillation (Bhole and Patil, 2009). A few ml of drug solution has been passed through the filter and discarded to equilibrate any possible retention before sterilization of felodipine solution. Sterilized felodipine solution (one drop) was instilled in the rabbit eye at 0, 10, and 20 min consecutively in Group I (control). In Group II (test) FDM formulation of ~ 10 mg (4 mm × 12 mm) containing ~ 1 mg of the drug was applied topically in the *cul de sac* of the rabbit eye. The film was sterilized using U.V. radiation for 10 mins at 25 cm height on both the sides just before application to rabbit eye. Ocular pressure was measured using Schiotz Tonometer (Riester, Germany) at 30 min before dosing, and 0.5, 1, 1.5, 2, 3, 4, 5, 6, 7, and 8 h after the dosing of the film. The test was repeated 3 times and recorded as mean ± standard error. Finally, rabbit eyes were carefully swabbed and cleaned with sterile saline solution, and Moxifloxacin eye drops IP, 0.5 % (MOXI TOR) was instilled for quick recovery of any possible infection. Finally, rabbits were rehabilitated in the animal house for further studies.

2.18. Correlation study

Level A correlation has been examined using MS excel-office 7 between (i) *in-vitro* release vs. swelling index, (ii) *ex-vivo* permeation vs. swelling index, (iii) permeation vs. release, and finally, (iv) area under the decreased IOP (AUDC) vs. *ex-vivo* permeation to understand the relationship and predictability.

2.19. In-vivo anti-inflammation study

For the anti-inflammation study, male New Zealand rabbits were categorized into three classes containing three rabbits each. Group-I (test group with formulation) received carrageenan injection (200 μL; 2 % w/v) into the sub-conjunctival region of the rabbit eye, followed by topically applied one piece of film (sterilized by UV exposure at distance 25 cm for 10 min) in the lower cul-de-sac after 1 h. Group-II (+ve control) was induced with carrageenan injection only. Group-III was the –ve control of normal healthy rabbits without any treatment. Proparacaine hydrochloride 0.5 % ophthalmic solution USP was instilled in the eye for local anaesthesia in this study. Lastly, Moxifloxacin eye drops IP, 0.5 % (MOXI TOR) was used for quick recovery.

2.20. Computational analysis

Computational analysis was carried out in DELL Inspiron 14 with intel core i5 processor, 4 GB RAM and 500 GB hard disk capacity. The software used were MGL Tools1.5.4, Autodock Vina (version 1.1.2), Discovery Studio Visualizer 2017 R2 (version 17.2.0, 16349), and Open Babel (Version 2.4.1). The crystal structure of mineralocorticoid (PDB ID: 2A3i) and TRPA1 ion channel (PDB ID: 3J9P) were retrieved from the RCSB Protein Data Bank. After removing the ligand and water molecules, the structure of the enzyme was saved in the PDB format. 3-D structure of the test ligand felodipine and gingerol (standard TRPA1 ion inhibitor) were downloaded from PubChem (SDF format) were first converted to the PDB format by the use of Discovery Studio Visualizer. An AutoDock Tool grid-box covered the whole binding site of the protein. Docking analysis between FEL with mineralocorticoid, and TRPA1 receptor is done by Auto dock Vina software (v. 1.2. 0). The macromolecules were remained rigid throughout the docking, whereas the ligand molecules were flexible. The binding affinities of the optimum binding configurations to the target protein were measured in Kcal/mol.

3. Results and discussion

3.1. Physicochemical characterisation of film

Table-1 summarizes the physicochemical results for the plasticized felodipine film formulations for ocular application. Transparent and colorless film produced with a thickness of 150.3 ± 8.5 to 177.6 ± 4.5 μm could be favourable for eye delivery. All films demonstrated excellent folding endurance of more than 200, which were sufficiently flexible, tough, and not brittle enough for ocular use. The film surface pH (7.14 ± 0.03 to 7.23 ± 0.02) was supposed to be compatible for ocular administration. The moisture content value was varied from 3.81 ± 0.64

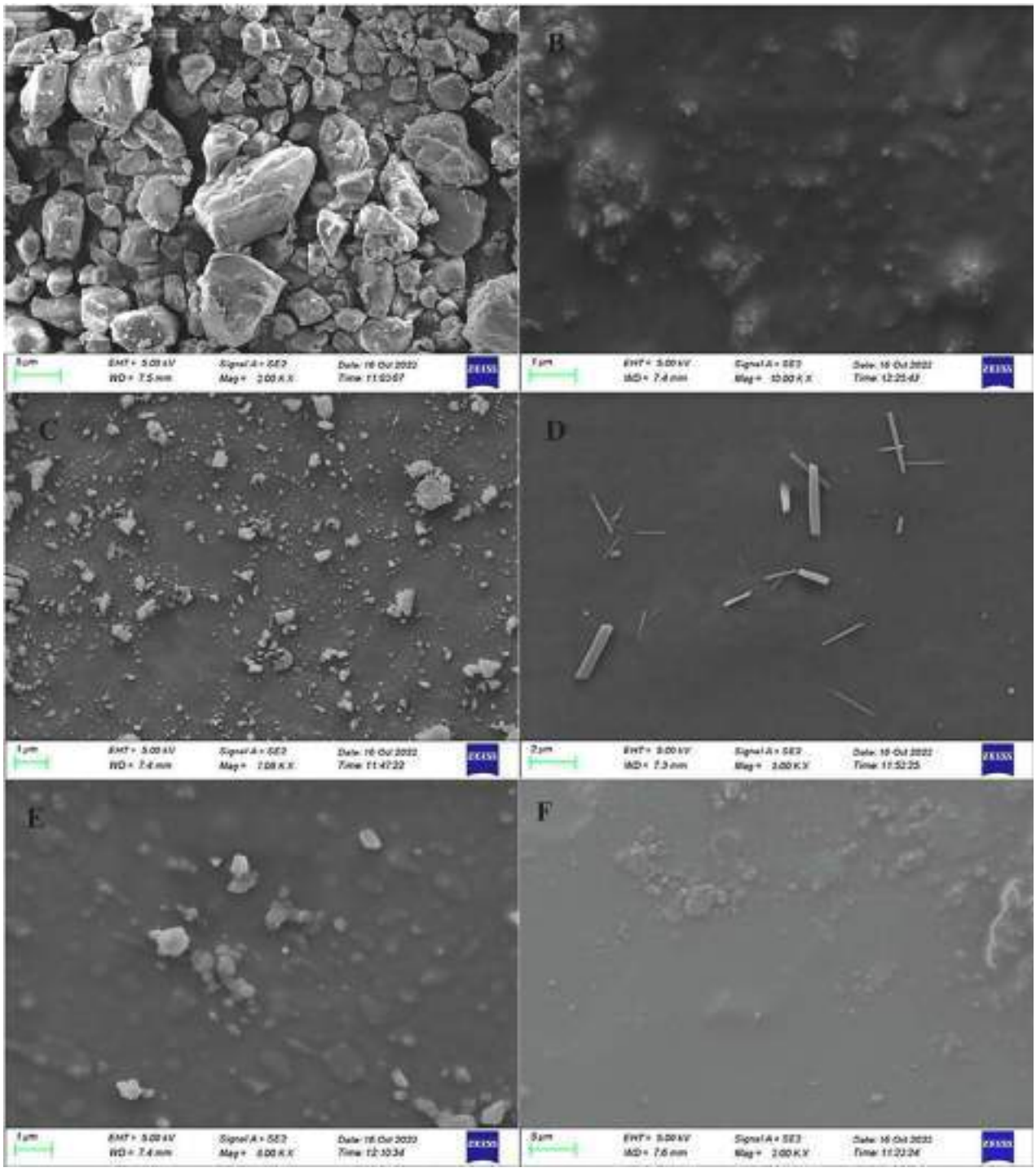

Fig. 4. Surface morphology of the formulation by SEM microscope (A) FEL, (B) FTE, (C) FTA, (D) FPG, (E) FPE, (F) FDM.

to 5.38 ± 0.28 whereas for moisture uptake 6.07 ± 0.57 to 8.37 ± 0.56 % at relative humidity (RH) 75 %. It was found that the amount of drug content ranged between 9.04 ± 0.14 to 9.50 ± 0.15 %. Previously developed HPMC films have already been reported for ocular drug delivery of similar thickness, flexibility, and film surface pH (Nanda et al., 2018; Nandi et al. 2022b; Swain et al. 2022). The amount of felodipine added during film preparation by solvent casting technique has totally been loaded in the film, and the amount appropriately chosen for ocular delivery.

3.2. FTIr

FTIR of felodipine and the formulations are depicted in Fig. 1. In IR spectra of pure drug bands at 3370, 2948, 1687, and 1644 cm^{-1} indicate the existence of NH stretching, CH3 group, C = O stretching, and NH bending, respectively. Peaks at 1621, 1495 and 1460 cm^{-1} are due to the C = C bond of benzene ring stretching, and 1099 cm^{-1} is due to C-O-C stretching vibration of ester (Hariprasanna et al., 2010; Jana et al., 2014; Noor and Khalil, 2015). Band broadening at the range of 3200–3500 cm^{-1} has been noted in all the films. In comparison to FTE, FTA, FPG and FDM, the degree of broadening is comparatively greater in the case of

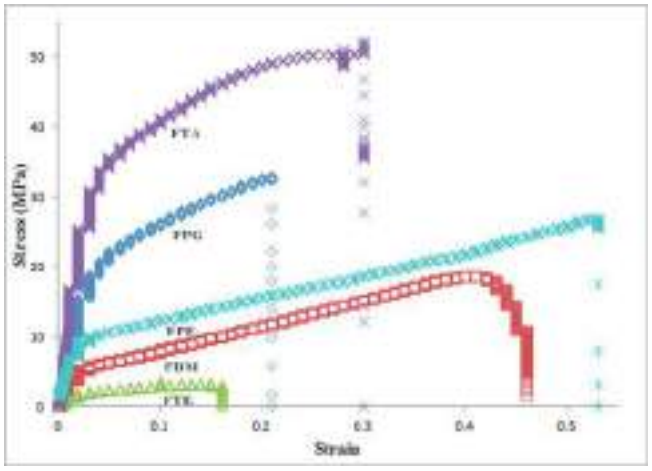

Fig. 5. Mechanical strength (Stress–strain plot) by Tinius Olsen.

FPE. FPE might have masked the NH group of FEL to a larger extent (Nanda et al., 2018). FTIR spectrum of all film formulations exhibited a substantial shift in the –NH stretch towards a lower wave number. The downward shifting of N–H bond may be due to the involvement in hydrogen bonding. The –NH group of FEL probably made stronger hydrogen bonds with the acceptor groups of polymer in film formulation (Tang et al., 2002).

3.3. Differential scanning calorimetry

DSC analysis was carried out for pure felodipine and film formulations to recognize the thermal behaviour and physical state of the drug (crystalline/amorphous) in the formulation through characteristic melting points. In Fig. 2 endothermic peak at 145.22 °C for pure FEL indicates the crystallinity of drug. Film formulations showed a wide range (60–100 °C) of endothermic shouldering because of evaporation of water from the HPMC polymeric matrix. Disappearance of endothermic melting peak of FEL in all the films indicates clearly the conversion of crystalline form of drug to the amorphous state. This may be due to the dispersion and stabilization of drug in their amorphous state in polymeric carrier (Senceroglu et al., 2022).

3.4. X-ray diffractometry

By using XRD, the FEL crystal structure was confirmed, as shown in Fig. 3, with distinctive peaks at 10.21°, 10.89°, 16.30°, 16.50°, 20.41°, 23.14°, 24.47°, 26.34°, and 29.5° (Zhang et al., 2020). Because of hydroxypropyl methylcellulose was present, the XRD patterns of the films that included various types of plasticizer showed dramatically decreased reflections of the drug. Because of the presence of HPMC and plasticizer, the XRD patterns of the films showed dramatically decreased reflections of the drug. All the formulations have almost the same pattern. DMSO doesn't contain any hydrogen bond donor, which facilitated drug to be accommodated more easily in DMSO than in water. The interaction between felodipine and DMSO is favourable due to DMSO's high dielectric constant. Additionally, the literature review

Table 2
Effect of plasticizer on mechanical and mucoadhesion properties of film formulation.

Film code	Tensile strength (MPa)	Elongation at break (%)	Elastic modulus (MPa)	Surface energy	Toughness (MPa)	PAF (N)	TWA (N/s)	Cohesiveness (mm)
FTE	3.40	9.64	20.70	0.16	0.406	0.571	6.6	1.4
FTA	52.3	30.2	365.41	0.14	12.54	0.730	6.6	1.5
FPG	32.9	20.7	202.39	0.16	5.17	0.457	6.3	1.0
FPE	26.9	53.2	59.44	0.45	13.95	0.302	1.8	0.7
FDM	18.6	40.5	44.04	0.42	5.56	1.129	9.9	1.1

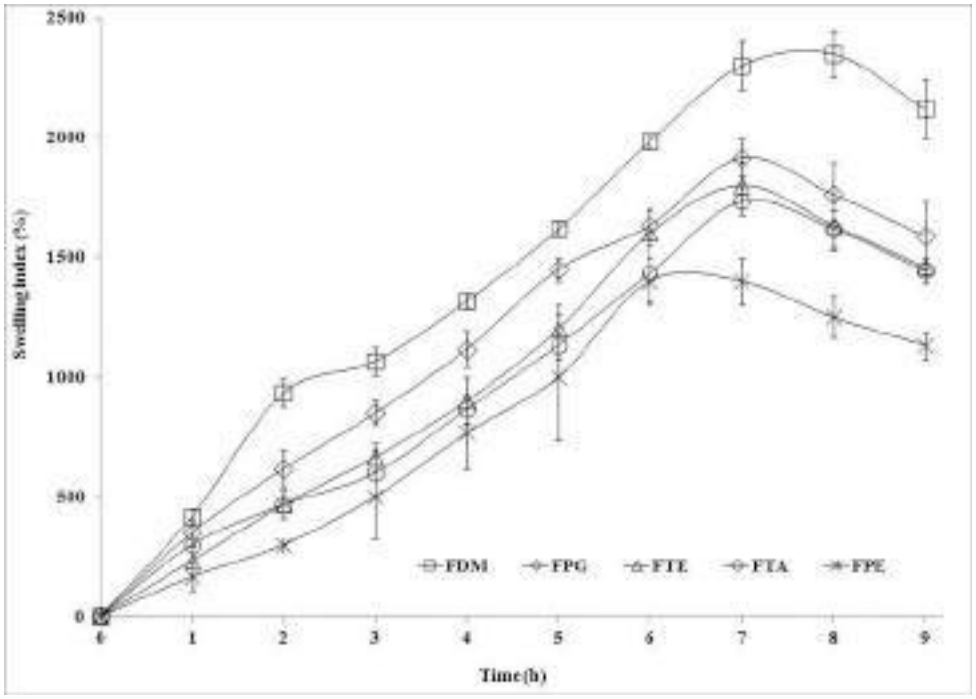

Fig. 6. Swelling index (mean ± SD; n = 3) of HPMC matrixes as a function of plasticizer content.

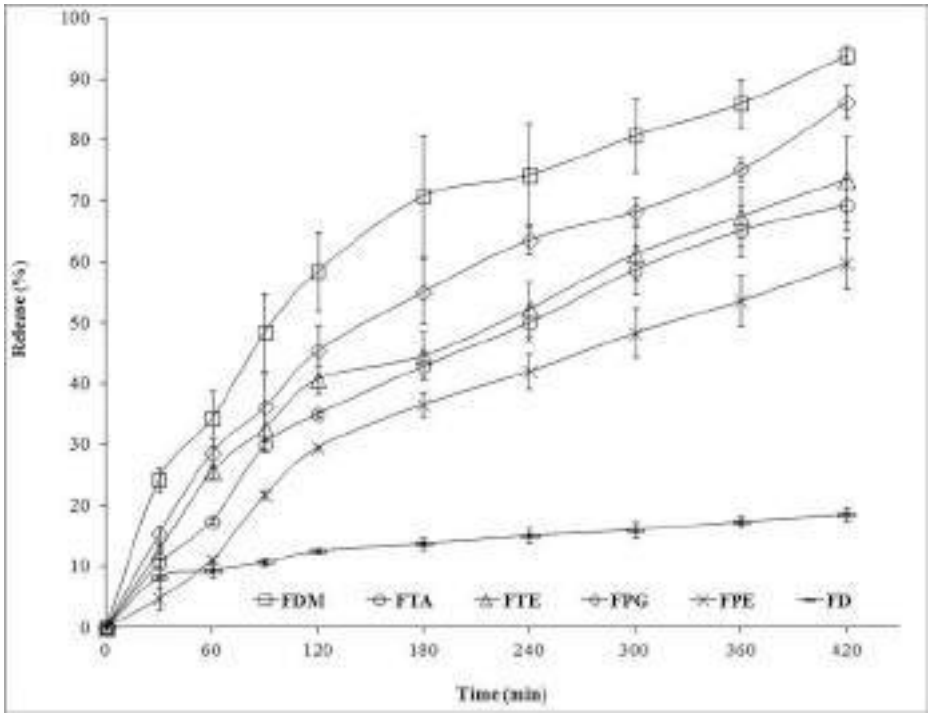

Fig. 7. In vitro dissolution study of film formulation as function of plasticizer content.

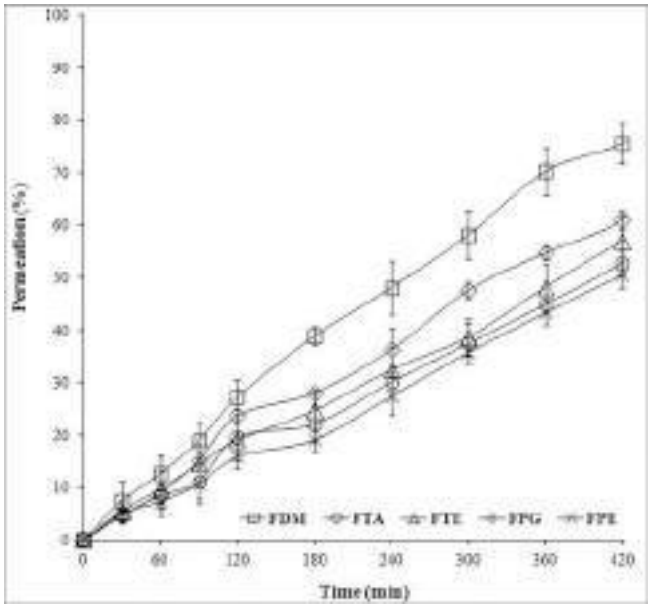

Fig. 8. Corneal permeation study of all plasticized film formulations.

demonstrated that PEG had a greater impact on the reduction in crystallinity than polypropylene glycol when used as a plasticizer (Kulinski et al., 2006).

Table 4
Correlation study between swelling index vs invitro drug release, swelling index vs ex-vivo permeation and in vitro-ex vivo correlation.

Film	Swelling vs. release		Swelling vs. permeation		Release vs. permeation	
	r^2	Trendline equation	r^2	Trendline equation	r^2	Trendline equation
FTE	0.941	y = 0.0324x + 11.746	0.984	Y = 0.0263x-0.2954	0.957	Y = 0.8578x-11.389
FTA	0.930	y = 0.0373x + 5.0951	0.972	Y = 0.0274x-1.7232	0.955	Y = 0.7947x-7.7616
FPG	0.957	Y = 0.0377x + 7.48	0.979	Y = 0.0326x-7.7827	0.965	Y = 0.8549x-13.918
FPE	0.919	Y = 0.0354x + 4.323	0.967	Y = 0.028x-0.1873	0.925	Y = 0.8268x-4.3596
FDM	0.873	Y = 0.0343x + 14.154	0.964	Y = 0.0353x-11.062	0.938	Y = 1.0137x-24.679

Table 3
Kinetic study of in vitro release and ex vivo permeation of film formulations.

Film	In-vitro drug release							Corneal permeation						
	Higuchi		Peppas		Peppas Sahlin			Higuchi		Peppas		Peppas Sahlin		
	k	r^2	n	r^2	K1	K2	m	k	r^2	n	r^2	K1	K2	m
FTE	3.615	0.971	0.501	0.989	2.112	0.013	0.647	2.571	0.900	0.316	0.999	0.672	0.010	0.557
FTA	3.117	0.969	0.558	0.974	1.488	0.006	0.685	2.377	0.900	0.294	0.996	0.562	0.005	0.751
FPG	4.231	0.987	0.499	0.976	3.096	0.018	0.525	2.780	0.906	0.334	0.994	1.157	0.726	0.385
FPE	2.561	0.961	0.542	0.974	49.956	32.103	0.139	1.976	0.900	0.202	0.991	0.789	0.228	0.463
FDM	4.852	0.985	0.432	0.973	2.752	0.021	0.683	3.596	0.928	0.490	0.993	10.440	4.875	0.270

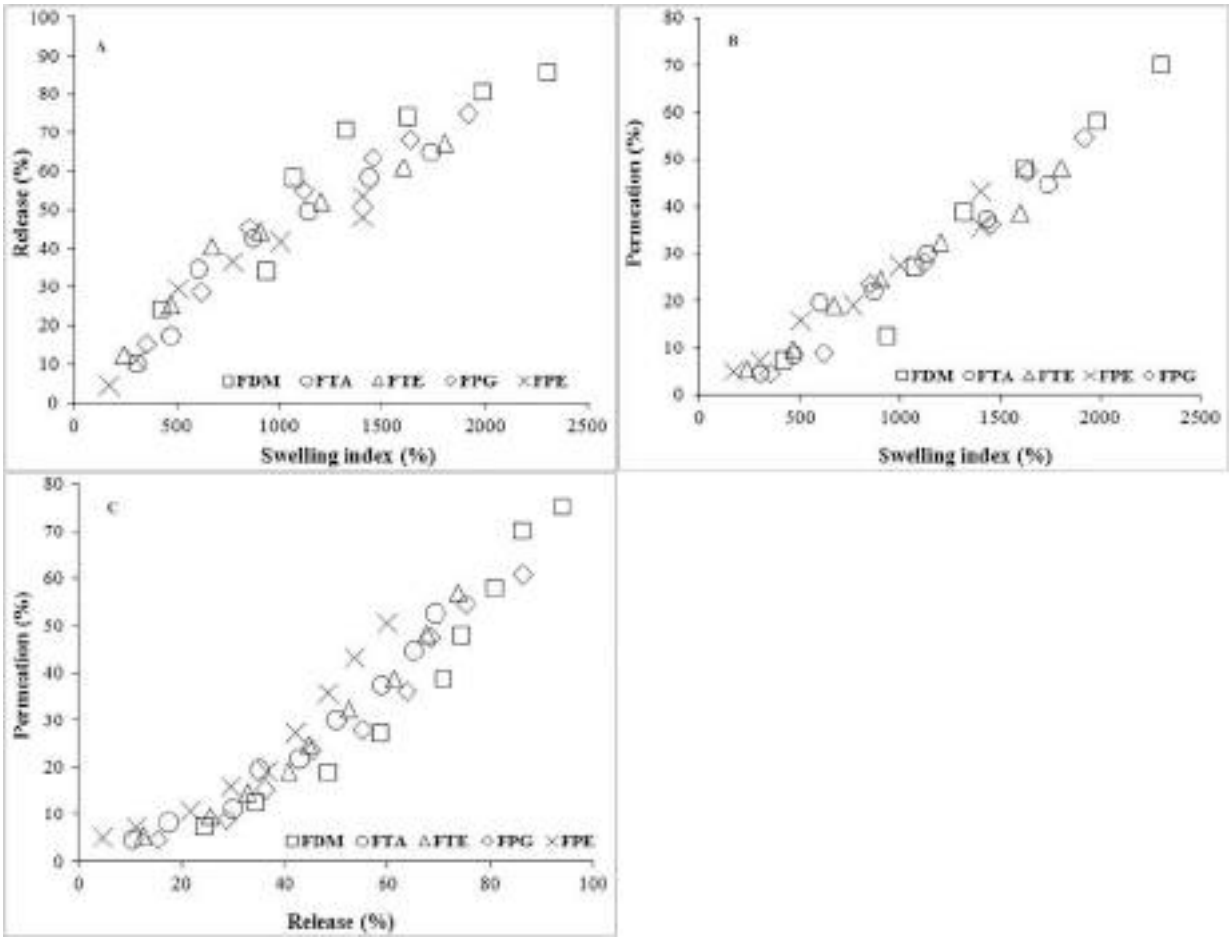

Fig. 9. (A) Correlation study between Swelling index vs invitro drug release, (B) Swelling index vs ex-vivo permeation, (C) In vitro and Ex vivo permeation.

3.5. SEm

Drug crystal nature, its distribution and surface morphology of the film observed by SEM analysis has been shown in Fig. 4. Distinct crystal geometry of pure FEL was clearly observed in Fig. 4A. Microparticulate crystals with lack of definite shape were spreading on the surface of the polymeric matrix films (Fig. 4B-F). The presence of different plasticizers in HPMC matrix influenced the drug particle morphology and surface texture diversely. Overall, photomicrographs resulted good drug dispersion, efficient wetting of drug by the polymer, and strong adhesion between drug and polymer. Appearance of particle was very much affected in the formulation FDM compared to other formulations. Higher dielectric constant of DMSO in FDM might have affected drug crystallinity to the greatest extent compared to others.

3.6. Mechanical properties

Due to the weak intermolecular interactions and branching fundamental structure, polymers are brittle by nature. Plasticizers' main purpose is to make polymers more flexible and processable by lowering intermolecular tensions, decreasing the inflexibility of the film structure, and increases polymeric chain mobility (Fundo et al., 2015; Vieira et al., 2011). The stress–strain profile was shown in Fig. 5 and the mechanical properties of the prepared formulations were calculated and tabulated in Table 2. These properties were related to the microstructure of the films and hydrogen bonding within the components of the formulations. From the above formulations, film containing triethyl citrate has a low tensile strength (3.40 MPa) whereas tricetin showed the highest tensile strength (52.3 MPa). Recently Shinde et al. reported that they prepared the transdermal film by using triethyl citrate as a plasticizer and obtained tensile strength value of 5.486 MPa (Shinde et al., 2008). All the rest formulations show tensile strength values between 18.6 and 32.9 MPa. According to the finding, it was established that tensile strength and elongation at break of many biopolymers can be enhanced in presemnce of PEG (Jimenez Bartolome et al., 2020). PEG600 (10%) containing formulation not only shows a tensile strength close to the tabulated value but also exhibits the same elongation of break (Jimenez Bartolome et al., 2020).

Another crucial factor in film characterization is elongation. Elongation gives a sense of mechanical robustness, flexibility, and film deformation properties. Low levels of elongation at break served as a sign of the film's instability. A good film should be flexible and have a high elongation at break to resist forces acting on it (Liew et al., 2014; Macleod et al., 1997). The prepared formulation containing plasticizer PEG 600 shows the highest elongation of break. Bartolome et al. also reported that PEG-containing plasticizer shows the highest elongation of break (Jimenez Bartolome et al., 2020). Among all the formulations triethyl citrate shows less elongation of break, which means brittleness in the film was more than other formulations. The rest of the formulation shows the elongation of the break between the 20 to 40 %. Elongation at break and flexibility are expected to increase with the addition of a plasticizer. A strong yet brittle film is formed without the use of an appropriate plasticizer. High brittleness indicates that even little external pressures, such as bending, peeling, or tensile, may cause a film to break. It has been observed that adding of plasticizer in a polymeric film resulted in considerable ductility and sufficient flexibility. Transdermal drug delivery films also use plasticizer in the formulation to meet better patient compliance (Cheng et al., 2006; Nandi et al., 2022a;

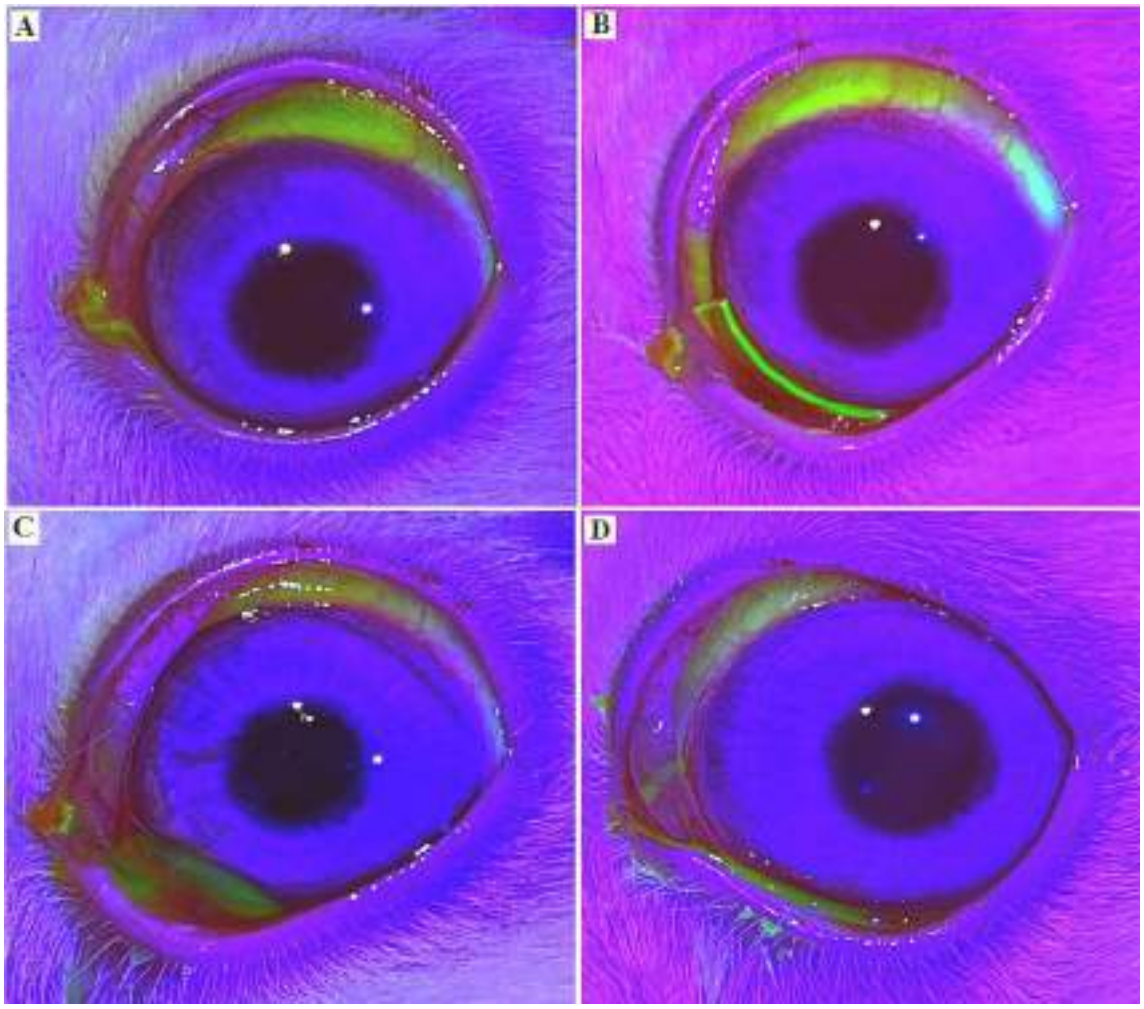

Fig. 10. Fluorescein staining before starting experiment (A), Initial of film application (B), after 6 h of film application (C), 24 h of post application (D).

Suyatma et al., 2005; Swain et al., 2022).

3.7. Swelling study

The swelling profile of hydrophilic polymeric film was determined by measuring increased weight due to swelling after predetermined time. Hydration after 9 h of swelling has been exhibited in Fig. 6. Polymer's ability to swell was essential for it to function as a bioadhesive nature. The adhesion will increase with the degree of hydration up to a certain point; excessive hydration causes an abrupt decline in adhesive strength owing to disentanglement at the polymer/tissue interface. The presence of DMSO exhibited a maximum swelling rate 289.5 min^{-1} compared to other formulations (262.3 min^{-1}, 264.7 min^{-1}, 226.6 min^{-1}, 243.8 min^{-1}). The swelling rates of the prepared film showed in the order: FDM > FPG > FTE > FTA > FPE.

3.8. In-vitro muco-adhesion

Mucoadhesion parameters of the formulations are depicted in Table 2. The mucoadhesive force as expressed PAF for all the films is higher (0.302 to 1.129 N) than the force required by the eyelids to blink (0.2 N), concluding that the films are not easily displaced by blinking (Tighsazzadeh et al., 2019). The Film containing DMSO (FDM) showed the highest both of PAF and TWA values indicating the greatest stickiness and work done of detaching two adherent surfaces compared to all other films (1.129 N and 9.9 N/s respectively). PEG containing film (FPE) showed the lowest mucoadhesion and cohesiveness (0.7 mm) among all the films. This is fascinating and appears to support the findings of the swelling capacity test. Presence of the mucosal layer in the mucous membrane resulted in polymer hydration and swelling. That led to physical entanglement between the polymeric chains and the mucosal substrate by formation of hydrogen bonding and electrostatic interaction. Hydrogel-forming polymer, HPMC, promoted quick hydration and swelling and led to enhanced mucoadhesion.

3.9. In vitro drug release study

Plasticized HPMC film delivery plays a vital function in FEL release control from the formulation. Fig. 7 is depicted the release patterns of the different felodipine film formulations. The drug dissolution has been improved to a great extent (93.9 % in 7 h) in presence of DMSO compared to the least by PEG 600 (59.8 % in 7 h). The order of drug release was found as: FDM > FPG > FTE > FTA > FPE. Significantly reduced intensity of drug crystallinity in the film formulation has further been validated by SEM, XRD, DSC analysis. Patterned release of drug from the plasticized HPMC film plays a vital role in the intensity of therapeutic effect. Improved drug release is supposed to exhibit more intensed therapeutic effect and that have been proved by in vivo experiment. Felodipine film formulation (FDM) exhibited much more improved pharmacodynamic bioavailability compared to felodipine only solution. Loss of mass of the film occurs during the release experiment due to mass of drug release and erosion of polymer, and the film gradually disappears. Hydrogel forming polymer (HPMC) matrix film is actually non disintegrating type because of hydration and swelling of the

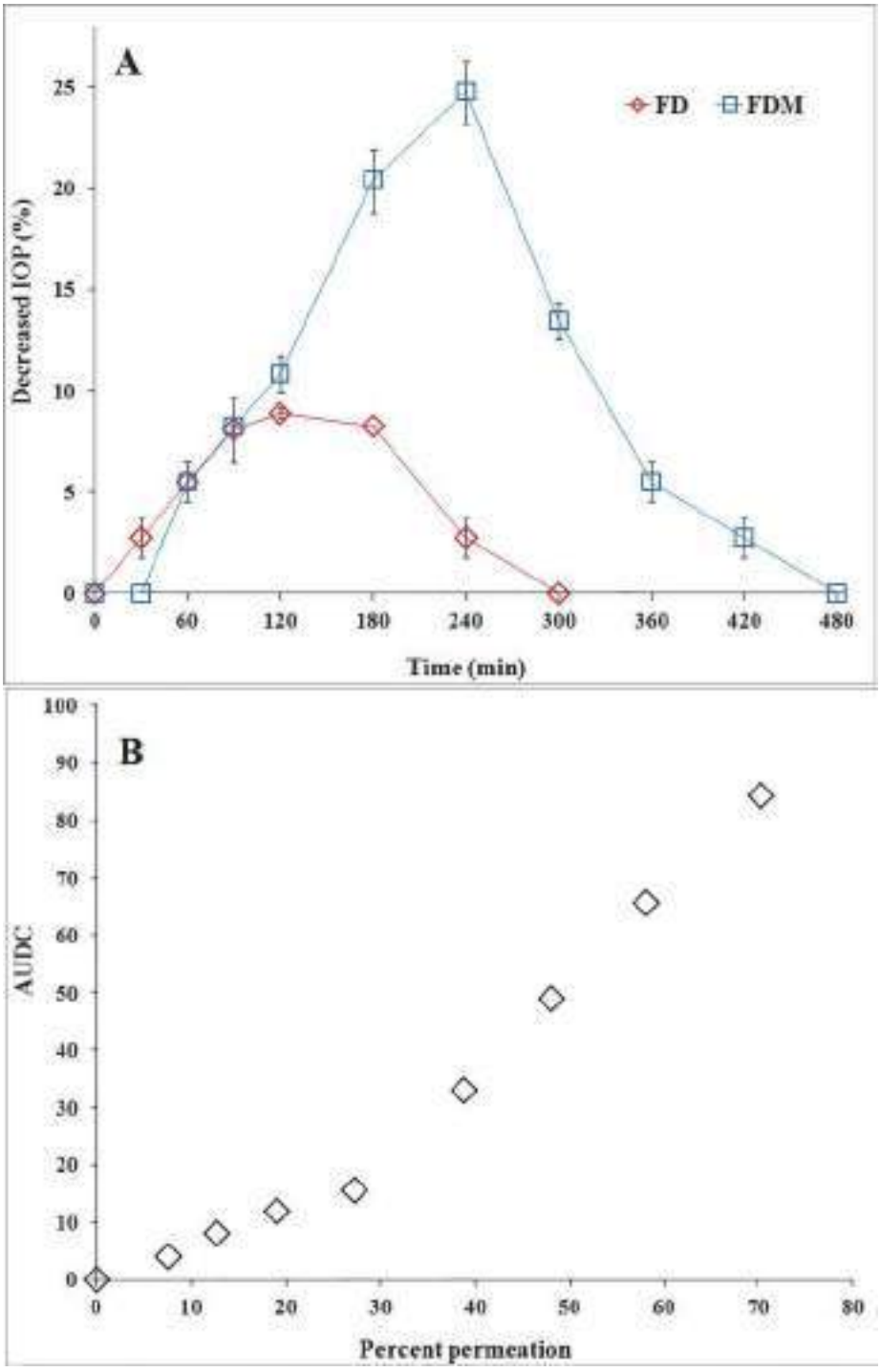

Fig. 11. Percent decrease in IOP by application of felodipine film (FDM) & eye drop (FD), (B) Correlation study between Percent permeation and area under decreased IOP curve (AUDC).

film.

3.10. *Ex vivo permeation study*

Plasticizer incorporation modifies the water absorption behavior, mechanical properties and mucoadhesive properties of the HPMC films. These factors have an effect on the integrity and strength of the polymeric film, which also impacts the drug release (Lin et al., 2000). The present study aimed to understand how the used plasticizer influences the permeation of FEL from HPMC polymer matrices. A comparison study between the drug permeation in accordance with the type of plasticizer was illustrated in Fig. 8. The rate of permeation of the film containing DMSO was faster (75.5 % in 7 h) as compared to the PEG 600 (55.5% in 7 h). According to the result, drug permeation amount in film formulations was in following order FDM > FPG > FTE > FTA > FPE. These results suggest that higher water solubility plasticizers may affect drug release more than lower water solubility plasticizers. This behavior may be caused by the fact that water soluble plasticizer does not hinder the flow of water molecules inside the polymeric matrix when the release media diffuses into it (Chun et al., 2003). In another study water soluble plasticizers often leach out and create pores that allow faster drug release when expose to dissolution medium (Khatri et al., 2018).

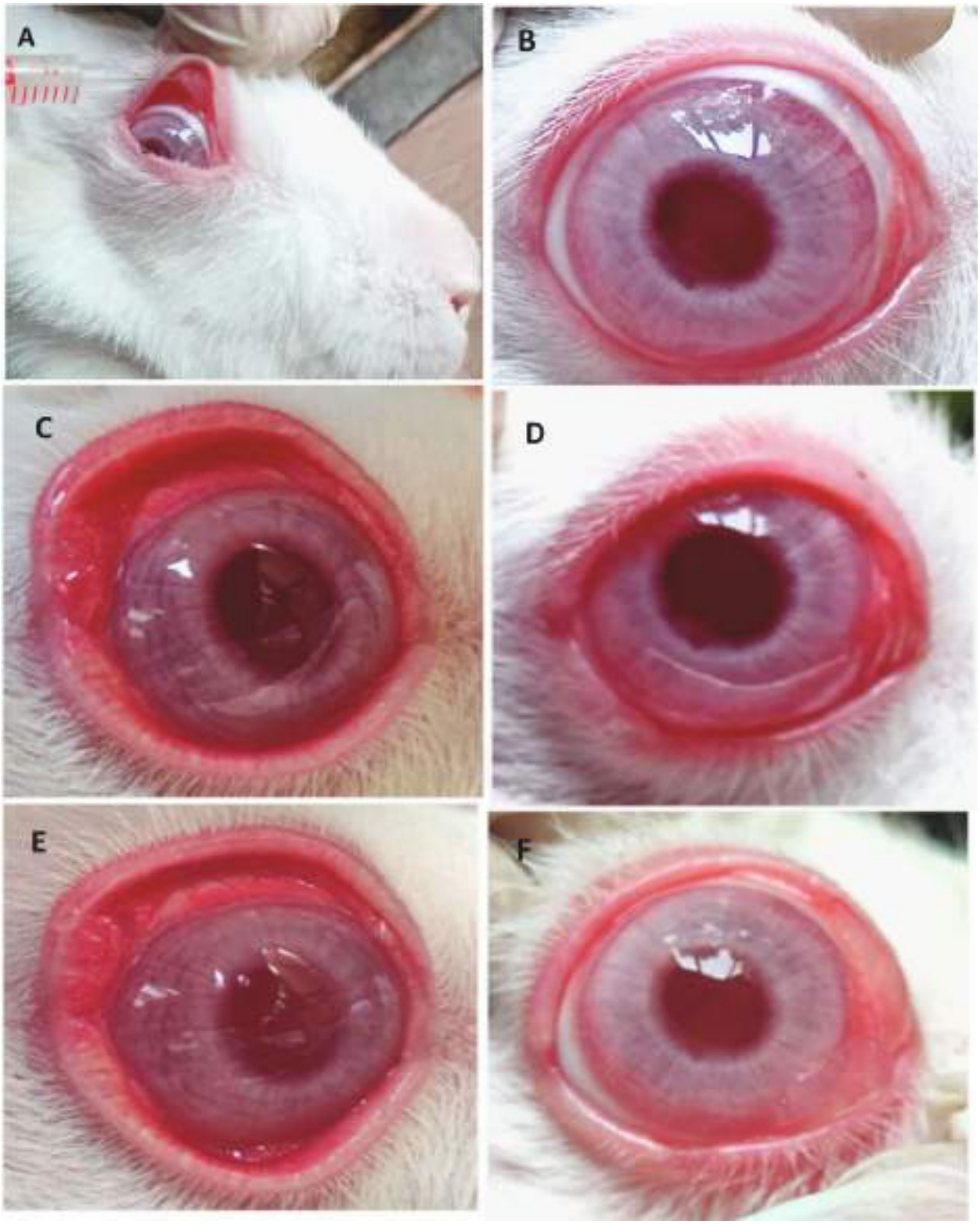

Fig. 12. (A) Carrageenan injection into the rabbit eye, (B) Normal rabbit eye, (C) Conjunctival redness and swelling after 30 min of carrageenan injection, (D) application of film film just after inflammation induction, (E) inflammation continued even after 3 h of the induced rabbit without film, (F) After two hours of using the film, the inflammation has almost been disappeared, the film has partially swollen and degraded.

The permeation kinetic was studied using Higuchi, Korsmeyer-Peppas and Peppas Sahlin, and illustrated in Table 3. All formulations have a Peppas permeation exponent (n) value in the range of 0.20–0.49 (<0.5) representing that the permeation mechanism was diffusion-controlled (r^2 = 0.991–0.999). According to the Peppas-Sahlin model, both drug release and permeation follow Fickian diffusion mechanism ($k_1 > k_2$). A point-to-point "Level A" correlation was observed between the swelling vs. release, *in-vitro* and *ex-vivo* permeation (0.873 to 0.984). The adoption of the linear regression equation might provide uniformity from batch to batch (Table 4). In a similar manner, a "Level A" correlation (r^2

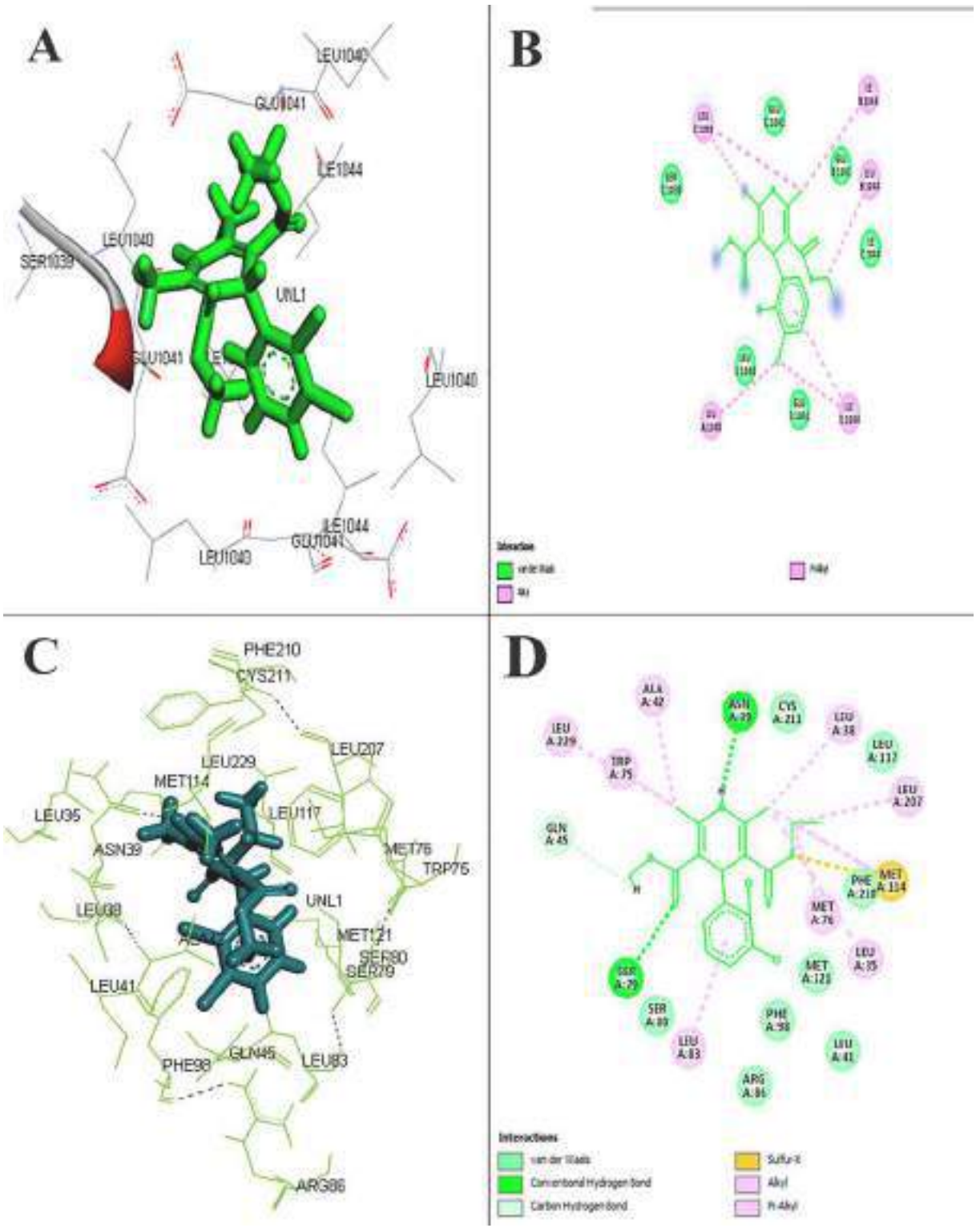

Fig. 13. Molecular docking study of drug (A) mineralocorticoid receptor, (B) TRPA1.

= 0.925 to 0.965) was also observed between *in and vitro* drug release and *ex-vivo* permeability Fig. 9.

3.11. Corneal hydration

Estimation of the hydration levels of the cornea was evaluated the corneal integrity during the entire experiment. Normal corneal hydration ranges from 76 to 80%, while a level exceeding 83% indicates endothelial and/or epithelial damage to the corneal tissue (Pramanik et al., 2020). The HLC treated with different plasticized film formulations was found to be 77.9–81.6 %. This indicated that the polymeric film could maintain safe corneal hydration and remain intact during the procedure.

3.12. Ocular irritation test

Normal corneal epithelium cannot be stained with fluorescein, while damaged epithelium is colored green. Fig. 10 is depicted the corneal epithelial photographs at different time intervals. Following each film formulation treatment, there was no inflammatory reaction and no visible damage to the corneal epithelium.

3.13. IOp

Results of the intraocular pressure profile after installation of felodipine solution (ocular drop form (0.5 %) and film formulation (FDM) in normotensive rabbit eye have been depicted in Fig. 11 (A). Mean IOP of 20.4 ± 0.4 mm Hg has been recorded as the control before drug administration. FEL solution exhibited the peak % decrease of IOP of 8.8 ± 0.2 at 2 h after instillation whereas, the peak value as 24.7 ± 1.5 at 4 h after application of the film (FDM). IOP lowering effect by FDM has been controlled for 8 h compared to only 5 h by the drug solution. Sustained release of drug from FDM could able to maintain the controlled IOP lowering effect more powerfully rather than the solution probably due to nasolacrimal drainage. FEL solution has short precorneal residence time because of tear turnover, reflex blinking and nasolacrimal drainage resulting in poor ocular bioavailability. Many recent reports are available as hydrogel forming (e.g., HPMC) ocular medication delivery systems. The delivery systems provide a continuous drug reservoir at the application site as soon as they come into contact with the aqueous biological fluid in a sustained manner. In our present study, HPMC used as a polymer, can adhere to the conjunctival mucosa for improving bioavailability by extending ocular residence time (Nanda et al., 2018; Swain et al., 2022).

3.14. In vivo anti-inflammation study

Stages of the anti-inflammation after injection of carrageenan in the eye are shown in Fig. 12(A-F). Following the carrageenan injection (A), when compared with the normal eye (B) symptoms of acute inflammation including conjunctival redness and watery eyes were visible after one hour (C). Acute inflammation stage after induction (C), application of film (FDM) at acute inflammation stage (D) and without film application after 2 h (E) are almost similar in inflammation. Whereas, inflammation has almost been disappeared after 2 h of film application (F) are clearly visible when compared through without film application (E).

3.15. Docking study

Felodipine is a widely used dihydropyridine class drug that inhibits aldosterone-induced mineralocorticoid receptor activation. Mineralocorticoid is present in ocular tissue, including pigment epithelium, ciliary epithelium, lens, and cornea which activation can cause elevation of intra-ocular pressure. Current study FEL has shown a favourable docking score of −5.2 Kcal/mol with mineralocorticoid receptor. TRPA1 antagonist clearly inhibits the development of carrageenan-induced paw edema in mouse (Moilanen et al., 2012). It was found that FEL interacts efficiently with TRPA1 of docking score −5.3 Kcal/mol. Fig. 13 (A & B) and 13 (C & D) depicted drug binding with mineralocorticoid receptor and TRPA1, respectively.

4. Conclusion

HPMC-based flexible swellable film has been developed successfully incorporating plasticizer for controlled ocular delivery of felodipine. HPMC matrix polymer inhibited the drug crystal growth in the presence of plasticizer in the film and facilitated the release and permeation of drug. The obtained results indicated that both drug release and corneal permeation are diffusion controlled as the pattern: FDM > FPG > FTE > FTA > FPE. The presence of DMSO as the plasticizer improved the release of drug together with permeation significantly compared to others. Controlled lowering effect of IOP has been noticed for 8 h more strongly compared to only 5 h by the drug solution, possibly due to nasolacrimal drainage. A good correlation was perceived between swelling vs. drug release, drug release vs. permeation, and permeation vs. AUDC. After two hours of applying film at the acute inflammation stage, the inflammation has almost been disappeared compared to inflammation without film. FEL was found to form a stable interaction with mineralocorticoid and TRPA1 receptors with docking scores of −5.2 and −5.3 Kcal/mol, respectively. Felodipine film plasticized by DMSO could be used for the better management and control of intraocular pressure and associated inflammation.

Institutional Review Board Statement

This work was approved by the institutional animal ethical committee of the School of Pharmaceutical Sciences, S'O'A University, India [IAEC/SPS/SOA/18/2020], and complied with the ARRIVE guidelines.

Informed Consent Statement.

Not applicable.

Data Availability Statement.

Not applicable.

CRediT authorship contribution statement

Rakesh Swain: Conceptualization, Data curation, Methodology, Writing – original draft, Writing – review & editing. **Ankita Moharana:** Data curation, Methodology, Formal analysis. **Sk Habibullah:** Methodology, Data curation. **Souvik Nandi:** Methodology. **Anindya Bose:** Software. **Sujata Mohapatra:** Writing – review & editing. **Subrata Mallick:** Conceptualization, Supervision, Writing – review & editing.

Declaration of Competing Interest

The authors declare the following financial interests/personal relationships which may be considered as potential competing interests: Subrata Mallick reports was provided by Siksha O Anusandhan University School of Pharmaceutical Sciences. Subrata Mallick reports a relationship with Siksha O Anusandhan University School of Pharmaceutical Sciences that includes:. Subrata Mallick has patent NA pending to NA. NA.

Data availability

Data will be made available on request.

Acknowledgement

The authors are thankful to DST, New Delhi, for the award of Junior and Senior Research Fellowships to Rakesh Swain (IF 180581). The authors are acknowledges to the President, Siksha O Anusandhan (Deemed to be University) for support. Medley Pharmaceutical Ltd. and Ready's Laboratory are also gratefully acknowledged.

Funding

This research received no external funding.

References

Ben-Yaakov, A., 2007. title., M. Sc. Thesis.

Bhole, P.G., Patil, V.R., 2009. Enhancement of water solubility of felodipine by preparing solid dispersion using poly-ethylene glycol 6000 and poly-vinyl alcohol. Asian Journal of Pharmaceutics (AJP) 3 (3), 240.

Bi, X.P., Tan, H.W., Xing, S.S., Zhong, M., Zhang, Y., Zhang, W., 2009. Felodipine downregulates serum interleukin-18 levels in rats with fructose-induced metabolic syndrome. J. Endocrinol. Invest. 32 (4), 303–307.

Boateng, J., Popescu, A., 2016. Composite bi-layered erodible films for potential ocular drug delivery. Colloids Surf. B Biointerfaces 145, 353–361.

Caprioli, J., Coleman, A.L., 2008. Intraocular pressure fluctuation: a risk factor for visual field progression at low intraocular pressures in the Advanced Glaucoma Intervention Study. Ophthalmology 115 (7), 1123–1129.
Chen, C., Harisdangkul, V., Parker, L., 1982. Transient glaucoma associated with anterior diffuse scleritis in relapsing polychondritis. Glaucoma 4, 109.
Cheng, L.H., Karim, A.A., Seow, C.C., 2006. Effects of water-glycerol and water-sorbitol interactions on the physical properties of konjac glucomannan films. J. Food Sci. 71, E62–E67.
Chun, M.-K., Kwak, B.-T., Choi, H.-K., 2003. Preparation of buccal patch composed of carbopol, poloxamer and hydroxypropyl methylcellulose. Arch. Pharm. Res. 26 (11), 973–978.
Comes, N., Gasull, X., Callejo, G., 2021. Proton sensing on the ocular surface: Implications in eye pain. Front. Pharmacol. 3409.
Fang, G., Wang, Q., Yang, X., Qian, Y.u., Zhang, G., Zhu, Q., Tang, B.o., 2021. Vesicular phospholipid gels as topical ocular delivery system for treatment of anterior uveitis. Colloids Surf A Physicochem Eng Asp 627, 127187.
Fundo, J.F., Galvis-Sanchez, A.C., Delgadillo, I., Silva, C.L.M., Quintas, M.A.C., 2015. The effect of polymer/plasticiser ratio in film forming solutions on the properties of chitosan films. Food Biophys. 10 (3), 324–333.
Gandhi, H., Patel, V.B., Mistry, N., Patni, N., Nandania, J., Balaraman, R., 2013. Doxorubicin mediated cardiotoxicity in rats: Protective role of felodipine on cardiac indices. Environ. Toxicol. Pharmacol. 36 (3), 787–795.
Hariprasanna, R., Kulkarni, U., Ahmad, Q., Gururaj, S., Srinath, B., 2010. A study on formulation and processing factor influencing the release of Felodipine. Int. J. Curr. Pharm. Res. 2, 86–89.
Hawkins, A.S., Intraocular Inflammation and Glaucoma, Glaucoma. Oxford University Press.
Hishikawa, K., Lüscher, T.F., 1998. Felodipine inhibits free-radical production by cytokines and glucose in human smooth muscle cells. Hypertension 32 (6), 1011–1015.
Holappa, M., Vapaatalo, H., Vaajanen, A., 2020. Local ocular renin–angiotensin–aldosterone system: any connection with intraocular pressure? A comprehensive review. Ann. Med. 52 (5), 191–206.
Hota, S.S., Nandi, S., Mallick, S., 2022. Efecto del surfactante en hidratación y tensión-deformación en la formación de película de hipromelosa. Rev. Cuba. Farm. 55.
Hou, B., Wang, F., Ye, Z., Jin, X., Fu, Y., Li, Z., 2020. Study of minimally invasive radiofrequency ablation of the ciliary body for the treatment of glaucoma in rabbits. Mol. Med. Rep. 21, 1071–1076.
Ishida, S., Koto, T., Nagai, N., Oike, Y., 2010. Calcium channel blocker nilvadipine, but not diltiazem, inhibits ocular inflammation in endotoxin-induced uveitis. Jpn. J. Ophthalmol. 54 (6), 594–601.
Jana, U., Mohanty, A.K., Pal, S.L., Manna, P.K., Mohanta, G.P., 2014. Felodipine loaded PLGA nanoparticles: preparation, physicochemical characterization and in vivo toxicity study. Nano Convergence 1, 1–10.
Jennings, C.L., Dziubla, T.D., Puleo, D.A., 2016. Combined effects of drugs and plasticizers on the properties of drug delivery films. J. Bioact. Compat. Polym. 31 (4), 323–333.
Jimenez Bartolome, M., Bischof, S., Pellis, A., Konnerth, J., Wimmer, R., Weber, H., Schwaiger, N., Guebitz, G.M., Nyanhongo, G.S., 2020. Enzymatic synthesis and tailoring lignin properties: A systematic study on the effects of plasticizers. Polymer 202, 122725.
Khatri, P., Desai, D., Shelke, N., Minko, T., 2018. Role of plasticizer in membrane coated extended release oral drug delivery system. J. Drug Delivery Sci. Technol. 44, 231–243.
Kulinski, Z., Piorkowska, E., Gadzinowska, K., Stasiak, M., 2006. Plasticization of poly (L-lactide) with poly (propylene glycol). Biomacromolecules 7, 2128–2135.
Langman, M., Lancashire, R., Cheng, K., Stewart, P., 2005. Systemic hypertension and glaucoma: mechanisms in common and co-occurrence. Br. J. Ophthalmol. 89, 960–963.
Li, X., Fang, J., Xin, M., Li, Q., Wang, J., Yang, H., Wu, X., 2021. Rebaudioside A/TPGS mixed nanomicelles as promising nanocarriers for nimodipine ocular delivery. Drug Deliv. Transl. Res. 11 (3), 1119–1132.
Liew, K.B., Tan, Y.T.F., Peh, K.-K., 2014. Effect of polymer, plasticizer and filler on orally disintegrating film. Drug Dev. Ind. Pharm. 40 (1), 110–119.
Lin, S.-Y., Chen, K.-S., Run-Chu, L., 2000. Organic esters of plasticizers affecting the water absorption, adhesive property, glass transition temperature and plasticizer permanence of Eudragit acrylic films. J. Control. Release 68 (3), 343–350.
Luo, C., Li, Y., Sun, J., Zhang, Y., Chen, Q., Liu, X., He, Z., 2014. Felodipine nanosuspension: a faster in vitro dissolution rate and higher oral absorption efficiency. J. Drug Delivery Sci. Technol. 24 (2), 173–177.
Luqman, M., 2012. Recent advances in plasticizers. BoD–Books on Demand.
Macleod, G.S., Fell, J.T., Collett, J.H., 1997. Studies on the physical properties of mixed pectin/ethylcellulose films intended for colonic drug delivery. Int. J. Pharm. 157 (1), 53–60.
Maria, D.N., Abd-Elgawad, A.-E., Soliman, O.-E., El-dahan, M.S., Jablonski, M.M., 2017. Nimodipine ophthalmic formulations for management of glaucoma. Pharm. Res. 34 (4), 809–824.
Matsui, R., Ueda, O., Uchida, S., Namiki, N., 2015. Transdermal absorption of natural progesterone from alcoholic gel formulations with hydrophilic surfactant. Drug Dev. Ind. Pharm. 41 (6), 1026–1029.
May, C.A., 2012. Could mineralocorticoids play a role in the pathophysiology of open angle glaucoma? J. Ophthalmol. 2012, 1–5.
Mehra, N., Aqil, M., Sultana, Y., 2021. A grafted copolymer-based nanomicelles for topical ocular delivery of everolimus: Formulation, characterization, ex-vivo permeation, in-vitro ocular toxicity, and stability study. Eur. J. Pharm. Sci. 159, 105735.
Mirshahi, M., Mirshahi, A., Sedighian, R., Hecquet, C., Faure, J.P., Agarwal, M.K., 1997. Immunochemical demonstration of the mineralocorticoid receptor in ocular tissues. Neuroendocrinology 65, 70–78.
Moilanen, L.J., Laavola, M., Kukkonen, M., Korhonen, R., Leppänen, T., Högestätt, E.D., Zygmunt, P.M., Nieminen, R.M., Moilanen, E., 2012. TRPA1 contributes to the acute inflammatory response and mediates carrageenan-induced paw edema in the mouse. Sci. Rep. 2, 1–6.
Nanda, A., Sahoo, R.N., Pramanik, A., Mohapatra, R., Pradhan, S.K., Thirumurugan, A., Das, D., Mallick, S., 2018. Drug-in-mucoadhesive type film for ocular anti-inflammatory potential of amlodipine: Effect of sulphobutyl-ether-beta-cyclodextrin on permeation and molecular docking characterization. Colloids Surf. B Biointerfaces 172, 555–564.
Nandi, S., Nanda, A., Sahoo, R.N., Swain, R., Mallick, S., 2022a. Formulation and administration of ramipril prodrug for improving bioactivity significantly: In vitro and in vivo correlation. J. Drug Delivery Sci. Technol. 74, 103597.
Nandi, S., Ojha, A., Nanda, A., Sahoo, R.N., Swain, R., Pattnaik, K.P., Mallick, S., 2022b. Vildagliptin plasticized hydrogel film in the control of ocular inflammation after topical application: study of hydration and erosion behaviour. Z. Phys. Chem. 236, 275–290.
Noor, A.H., Khalil, Y.I., 2015. Formulation and evaluation of felodipine orodispersible films. Pharmacie Globale 6, 1.
Okada, Y., Reinach, P.S., Shirai, K., Kitano-Izutani, A., Miyajima, M., Yamanaka, O., Sumioka, T., Saika, S., 2015. Transient receptor potential channels and corneal stromal inflammation. Cornea 34, S136–S141.
Okada, Y., Sumioka, T., Reinach, P.S., Miyajima, M., Saika, S., 2022. Roles of epithelial and mesenchymal TRP channels in mediating inflammatory fibrosis. Front. Immunol. 12, 5682.
Panda, B.B., Chatterjee, A., Sahoo, R.N., Mallick, S., 2020. Effect of plasticizer on delivery of valsartan from tamarind gel based transdermal film formulation. Ind. J. Pharmaceut. Educ. Res. 54 (3s), s485–s491.
Pivsa-Art, W., Fujii, K., Nomura, K., Aso, Y., Ohara, H., Yamane, H., 2016. The effect of poly (ethylene glycol) as plasticizer in blends of poly (lactic acid) and poly (butylene succinate). J. Appl. Polym. Sci. 133 (8).
Pramanik, A., Sahoo, R., Nanda, A., Pattnaik, K., Mallick, S., 2020. Swelling kinetics and corneal hydration level of Kaolinin-HPMC hydrogel film. Indian J. Pharm. Sci. 82, 306–314.
Qi, J., Zheng, J.B., Ai, W.T., Yao, X.W., Liang, L., Cheng, G., Shou, X.L., Sun, C.F., 2017. Felodipine inhibits ox-LDL-induced reactive oxygen species production and inflammation in human umbilical vein endothelial cells. Mol. Med. Rep. 16, 4871–4878.
Sayed, S., Habib, B.A., Elsayed, G.M., 2018. Tri-block co-polymer nanocarriers for enhancement of oral delivery of felodipine: preparation, in vitro characterization and ex vivo permeation. J. Liposome Res. 28 (3), 182–192.
Senceroglu, S., Ayari, M.A., Rezaei, T., Faress, F., Khandakar, A., Chowdhury, M.E., Jawhar, Z.H., 2022. Constructing an Intelligent Model Based on Support Vector Regression to Simulate the Solubility of Drugs in Polymeric Media. Pharmaceuticals 15, 1405.
Shah, U., Joshi, G., Sawant, K., 2014. Improvement in antihypertensive and antianginal effects of felodipine by enhanced absorption from PLGA nanoparticles optimized by factorial design. Mater. Sci. Eng. C 35, 153–163.
Shayegan, M.R., Boloorian, A.A., Kianoush, S., 2009. Comparative study of topical application of timolol and verapamil in patients with glaucoma within 6 months. J. Ocul. Pharmacol. Ther. 25 (6), 551–554.
Shinde, AnilJ, Garala, KevinC, More, HarinathN, 2008. Development and characterization of transdermal therapeutics system of tramadol hydrochloride. Asian Journal of Pharmaceutics (AJP) 2 (4), 265.
Stárka, L., Obenberger, J., Louženský, G., 1981. Effect of aldactone administration into the rabbit eye. Ophthalmic Res. 13 (3), 160–164.
Sugawara, H., Tobise, K., Kikuchi, K., 1996. Antioxidant effects of calcium antagonists on rat myocardial membrane lipid peroxidation. Hypertens. Res. 19 (4), 223–228.
Sundmacher, R., Neumann-Haefelin, D., 1979. Herpes simplex virus isolations from the aqueous humor of patients suffering from focal iritis, endotheliitis, and prolonged disciform keratitis with glaucoma (author's transl). Klin. Monatsbl. Augenheilkd. 175, 488–501.
Suyatma, N.E., Tighzert, L., Copinet, A., Coma, V., 2005. Effects of hydrophilic plasticizers on mechanical, thermal, and surface properties of chitosan films. J. Agric. Food Chem. 53 (10), 3950–3957.
Swain, R., Nandi, S., Sahoo, R.N., Swain, S.S., Mohapatra, S., Mallick, S., 2022. Bentonite clay incorporated topical film formulation for delivery of trimetazidine: Control of ocular pressure and in vitro-in vivo correlation. J. Drug Delivery Sci. Technol. 67, 102956.
Swain, R., Nandi, S., Swain, S.S., Pattanaik, K.P., Mohapatra, S., Panigrahi, D., Mallick, S., 2023. Bentonite-in hypromellose-poloxamer sol-gel for corneal application of trimetazidine: Study of rheology and ocular anti inflammatory potential. Int. J. Biol. Macromol. 242, 124628.
Tabak, S., Feinshtein, V., Schreiber-Avissar, S., Beit-Yannai, E., 2021a. Non-pigmented ciliary epithelium-derived extracellular vesicles loaded with SMAD7 siRNA attenuate Wnt signaling in trabecular meshwork cells in vitro. Pharmaceuticals 14, 858.
Tabak, S., Schreiber-Avissar, S., Beit-Yannai, E., 2021b. Crosstalk between MicroRNA and oxidative stress in primary open-angle glaucoma. Int. J. Mol. Sci. 22, 2421.
Tang, X.C., Pikal, M.J., Taylor, L.S., 2002. A spectroscopic investigation of hydrogen bond patterns in crystalline and amorphous phases in dihydropyridine calcium channel blockers. Pharm. Res. 19, 477–483.

Tham, Y.-C., Li, X., Wong, T.Y., Quigley, H.A., Aung, T., Cheng, C.-Y., 2014. Global prevalence of glaucoma and projections of glaucoma burden through 2040: a systematic review and meta-analysis. Ophthalmology 121 (11), 2081–2090.

Thumma, S., ElSohly, M.A., Zhang, S.-Q., Gul, W., Repka, M.A., 2008. Influence of plasticizers on the stability and release of a prodrug of Δ9-tetrahydrocannabinol incorporated in poly (ethylene oxide) matrices. Eur. J. Pharm. Biopharm. 70 (2), 605–614.

Tighsazzadeh, M., Mitchell, J.C., Boateng, J.S., 2019. Development and evaluation of performance characteristics of timolol-loaded composite ocular films as potential delivery platforms for treatment of glaucoma. Int. J. Pharm. 566, 111–125.

Vieira, M.G.A., da Silva, M.A., dos Santos, L.O., Beppu, M.M., 2011. Natural-based plasticizers and biopolymer films: A review. Eur. Polym. J. 47 (3), 254–263.

Yang, S., Wu, Y., X. Jin, ChunYang Wang, 2022. Ocular surface ion-channels are closely related to dry eye Front. Med. 9.

Zhang, H., Liu, X., Ma, X., 2020. The preparation of felodipine/zein amorphous solid dispersions and in vitro evaluation using a dynamic gastrointestinal system. Pharm. Dev. Technol. 25, 1226–1237.